

Chalk facies and its petrophysical expression from core and wireline data, North Sea Basin, the Netherlands.

ERWIN VAN WINGERDEN

Author: Erwin van Wingerden

Student Number: 2507713

Date: August 2016

Course: "Master Thesis Solid Earth"

Course Code: AM_450199

Supervisors VU: Prof. Dr. J.J.G. Reijmer and Dr. B. Andeweg

Supervisor EBN: L.J. Heijnen MSc. and J. Lutgert MSc.

Commissioned by: EBN B.V. and VU Amsterdam



The logo for EBN, consisting of the lowercase letters 'ebn' in a white, sans-serif font, centered within a dark blue square.

Copyright

© Copyright by EBN B.V. and the VU Amsterdam

This publication may not be altered or reproduced in any form or by any means without permission of the company, the university and the author. Requests for obtaining the right to reproduce or utilize parts of this publication should be addressed to:

L.J. Heijnen MSc., EBN B.V., Technology Departement, Daalsesingel 1, 3511 SV Utrecht, The Netherlands, E.: nora.heijnen@ebn.nl T.: +31 30 233 9001.

Thesis

This thesis is part of the curriculum of the master Earth Sciences, specialization Solid Earth, and necessary for the author to obtain a Master of Science degree at the VU University Amsterdam.

0. Abstract

With new hydrocarbon discoveries in the Chalk Group in the North Sea Basin, questions rise regarding the predictability and geological controls of possible reservoir units. This thesis captures all the core and wireline data from the cored Chalk intervals in the Netherlands to date, in order to find the influence of facies on the petrophysical signature. Existing facies model from GEUS has been generalized and combined with other facies core reports and literature, where after the facies of the cores have been reinterpreted. It was found that marly, glauconitic and siliciclastic content have lowering impact on the porosity in comparison to homogeneous chalk. Bioclast content was found to increase porosity. Secondary alteration in the chalk is has a negative impact on the reservoir properties due to diagenetic processes as cementation and recrystallization. Pelagic chalk is most prospective in middle to late Maastrichtian and Danian without intercalations of hemipelagic clay. Detrital clay is found to have relative higher permeabilities than clean chalk. It is furthermore suggested that inversion and salt movement may have enhanced the porosity and permeability of the system. Danian chalk is found to have different characteristics than Maastrichtian or older chalk, depicted from its deviations from the wireline logs. Sonic depth trends for pelagic chalk, except for chalk with high bioclast content is found to behave in a linear relation with depth.

Contents

0.	Abstract	3
1.	Introduction.....	5
1.1	Chalk.....	5
1.2	Aim and outline of this thesis	6
1.3	Study area	6
2.	Geological setting	8
2.1	Chalk.....	8
2.2	Tectonic setting.....	11
2.3	Climatic influence.....	13
3.	Methodology	14
3.1	Chalk facies model	14
3.2	Core measurements.....	14
3.3	Wireline measurements.....	14
3.4	Sonic velocity trends	16
4.	Results	17
4.1	Chalk facies	17
4.2	Core measurements.....	22
4.3	Facies influence on wireline measurements.....	29
4.4	Log calculated porosity	34
4.5	Depth trends in sonic velocity.....	Error! Bookmark not defined.
5.	Discussion	50
5.1	Improved facies model	50
5.2	Chalk facies petrophysics	51
5.3	Facies influence on wireline data.....	53
5.4	Depth trends in sonic velocity.....	Error! Bookmark not defined.
6.	Conclusion	58
7.	Acknowledgement.....	60
8.	References.....	61
	Appendix I	64
	Appendix II	67
	Appendix III	68
	Appendix IV	69
	Appendix V	70
	Appendix VI	71

1. Introduction

1.1 Chalk

From the Late Cretaceous up to the Early Paleogene, the Chalk Group accumulated in the North Sea Basin. Post-rift subsidence persisted throughout the Jurassic, creating significant accommodation space in the basin. In addition, sea levels were rising rapidly with maxima in the Turonian and Campanian, being approximately 250 meters higher than present-day sea level. This sea level rise is believed to be induced by the accelerated formation of oceanic crust ([Hays & Pitman, 1973](#)). Combined, the Late Cretaceous creates unique conditions for the deposition of the lithology chalk. Chalk is a carbonate rock which mainly consists of coccolithophores exoskeleton platelets; coccoliths. These nannoplanktonic algae grew in warm seas, where they will eventually disintegrate and fall out, forming pelagic sediment accumulations on the sea floor. No present day equivalent of chalk depositional environment is found.

Several phases influenced and interrupted the deposition of chalk in the North Sea basin, namely salt diapirism and inversion tectonics. Inversion tectonics occur in two phases i.e. the Mid-Campanian Sub-Hercynian and the Late Danian Laramide inversion. These two phases eroded most of the earlier deposited sediments in the inverted basins. In the vicinity of these inverted basins, as well as in the vicinity of salt tectonics, clastic input and unconsolidated chalk, redeposited as turbidites and slumps, dominate the sediment record. A regression in the Danian Paleogene ended the deposition of the Chalk Group. As a result, the Chalk Group is distributed in highly variable thicknesses throughout the North Sea basin, as illustrated on Figure 1.1.

The Chalk Group is found extensively throughout the subsurface of the North Sea Basin and therefore, it has been the subject of various studies. Most authors focus on the seismic character of the chalk ([van der Molen, 2004](#), [Gennaro et al., 2013a](#)), whilst others concentrate on the biostratigraphy ([Bailey et al., 1984](#)). However, not all aspects of the Chalk have been studied extensively. Only a few reports have addressed the facies model and development of the Chalk Group and their impact on hydrocarbon exploration. Recent studies focus mainly on the depositional setting and their accompanied products ([Brasher et al., 1996](#), [Gennaro et al., 2013b](#)). The majority of the reports have reviewed present-day outcrops in for instance the United Kingdom, France and Denmark. However, the Chalk in the North Sea basin is buried up to 3500 meters depth, which is of significant influence on hydrocarbon potential. Knowledge of the Chalk Group is relevant for hydrocarbon exploration. In the Netherlands, only a few oil and gas field in the Chalk Group have been found; the Hanze, Harlingen, Rembrandt and Vermeer fields. In Denmark however, multiple Chalk fields like the Ekofisk, Eldfisk, Kraka, Dan and Half-Dan fields have been found. A characteristic for most of these fields is the salt-induced doming underneath, creating reservoir potential in the Chalk Group above.

Velocity predictions of the Chalk Group are of great importance for the depth estimation of the stratigraphy underneath. Present day depth estimates and true depths can vary significantly due to the poor relationship between velocity and depth in the in the Chalk over greater lateral extent.

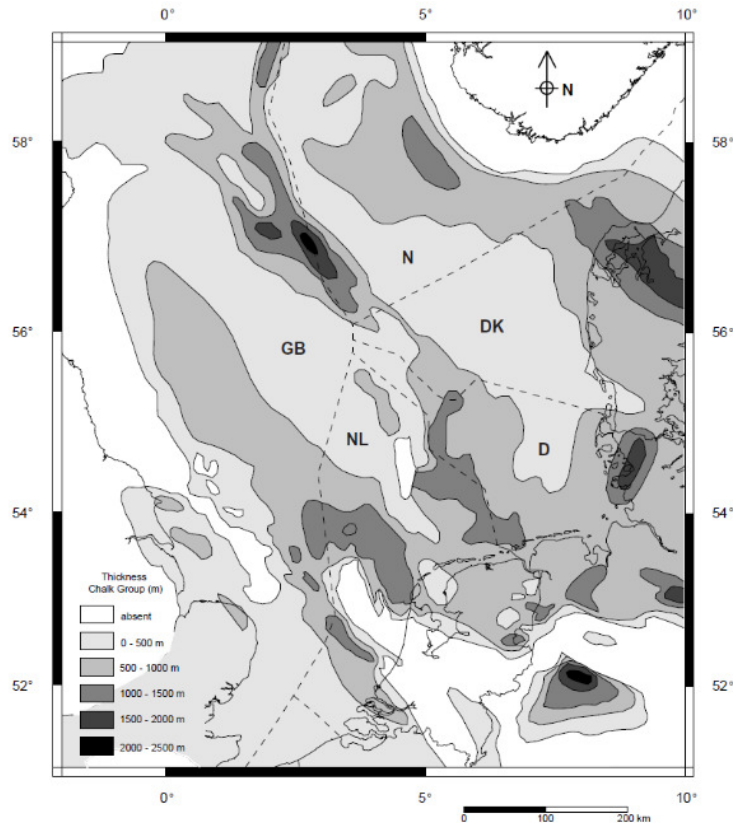


Figure 1.1 - Thickness of the Chalk Group in the North Sea Basin from [van der Molen, 2004](#). Offshore sectors indicated by the dashed lines and the country abbreviations.

1.2 Aim and outline of this thesis

The aim of this thesis is to combine previous chalk facies research with present-day core data reports and core analysis to make an improved chalk facies model for the Dutch North Sea Basin. This model will be applied to several Dutch offshore wells and compared to the wireline logs, to see if facies can be determined based on wireline logs. Other chalk subdivision will be made on the basis of biostratigraphy, well position, regional inversion grade and bioturbation grade, which will also be compared to the wireline logs. This comparison is a convenient way to link up the chalk subdivisions with the physical and petrophysical properties in order to improve the knowledge of chalk petrophysics and sonic with depth predictions.

1.3 Study area

The study area of this thesis focusses on the Dutch North Sea basin and part of the Danish North Sea basin. Most Chalk Group cores in Dutch offshore wells are taken in the Northern and Western part of the North Sea, focusing on the offshore with 24 wells spread out over the A, B, E, F, K and L blocks, with the addition of four onshore wells: Franeker-01-S1, Den Burg-01, Harlingen-02 and Ried-02. The position of the wells is indicated in Figure 1.2.

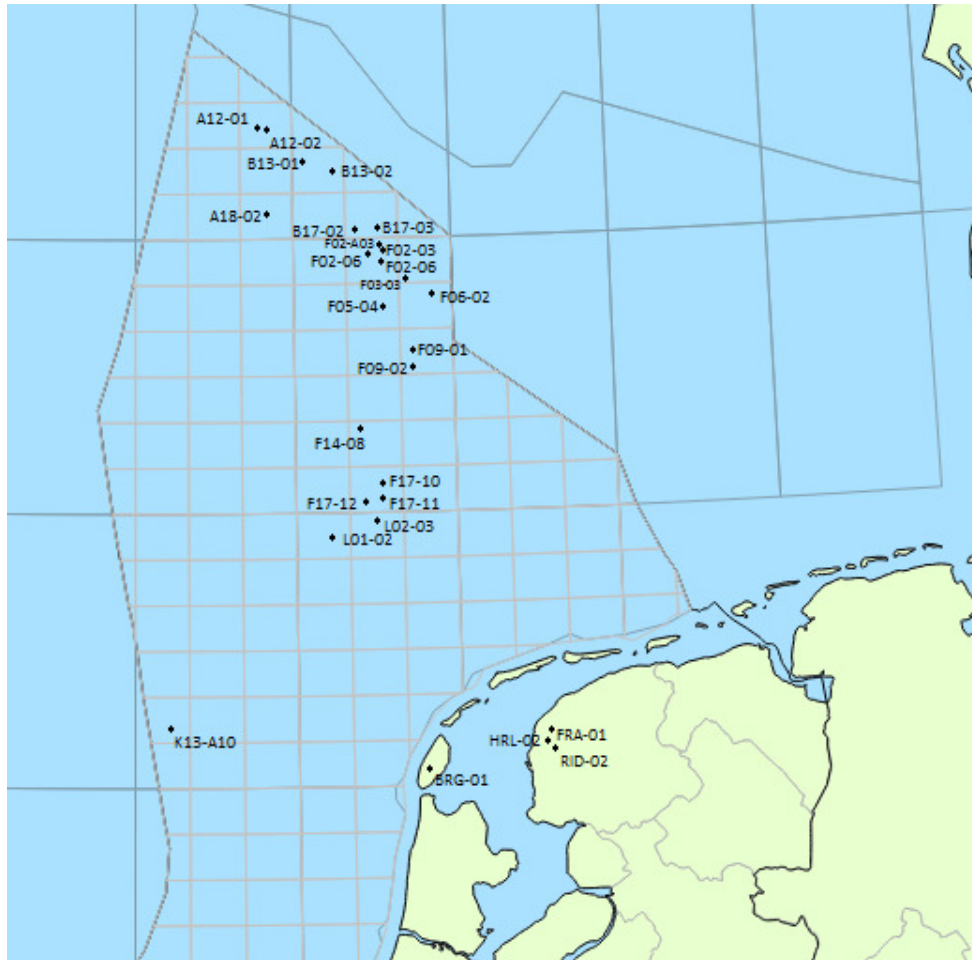


Figure 1.2 – Position of the wells, with their abbreviations, used for either facies analysis or facies quality checks.

2. Geological setting

2.1 Chalk

2.1.1 Chalk composition

Chalk is the name for a carbonate limestone which consist mainly of coccoliths, platelets from eukaryotic phytoplanktonic coccolithophores. The coccolithophores with the individual coccoliths stacked are illustrated in Figure 2.1. Coccolithophores live in the open marine domain and their exoskeleton is made up of primarily calcium carbonate. During favourable conditions coccolithophores tend to overproduce ([Paasche, 2002](#)), leading to their platelets falling off; coccoliths. The coccoliths have a diameter of approximately 0.5 to 20 μm .

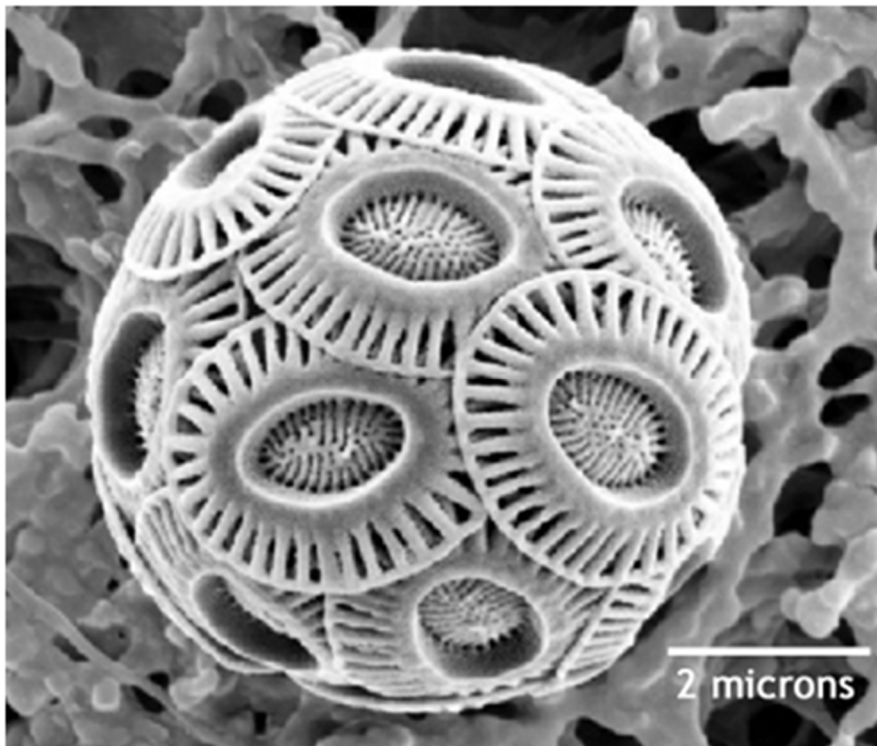


Figure 2.1 – Coccolithophore *Emiliana Huxleyi* under a SEM, consist of coccolith platelets build-up. Photo credit: [University of California San Diego](#).

Intermingling of other bioclasts is common in the North Sea Chalk. These bioclasts are mainly bivalves, sponge spicules, echinoids and bryozoa and can occur as in place bioclasts on the continental outer shelf to slope or as redeposited bioclasts on the slope or basin floor. Planktonic foraminifera are also commonly found in the chalk deposits. The presence of bioturbation is a characteristic for some of the chalk lithologies. These bioturbations are occasionally preserved in the rock record, leading to the identification of the ichnofossils. Most frequent ichnofossils are *Thalassinoides* and *Zoophycos* with minor presence of *Planolites*, *Chondrites*, *Taenidium* and *Paleophycus*. Generally, the *Thalassinoides* are believed to be shallow water fabric, whilst the *Zoophycos* are believed to be deeper water fabric. On the other hand, bioturbation can also be problematic for the preservation of primary structures in the chalk, therefore making it impossible to interpret the depositional environment of the particular chalk layers.

Two other lithologies interfere with the deposition of chalk, namely sand and clay. In proximal parts and around structural highs, the influx of sand and clay is recognized, leaving the chalk to be either sandy or marly. In places, sandstone with over 50% quartz content is recognized.

2.1.2 Chalk depositional mechanisms

Chalk deposition, described as above is primarily a pelagic sediment; falling out of coccoliths as coccolithophores overproduce and disintegrate. These platelets accumulate at the sea floor forming homogenous chalk. Homogenous chalk is often referred to as autochthonous pelagic chalk. At some places, influx of detrital material is common. This detrital material primarily consists of quartz and clay. Homogenous chalk is generally deposited in large spatial areas as the coccolithophores bloom in the photic zone of warm seas (Kennedy, 1987, van der Molen, 2004). During the beginning of the Late Cretaceous, steady subsidence persisted and sufficient accommodation space was created for the deposition of homogenous chalk. This makes the homogeneous chalk a major component of the Chalk Group in the North Sea basin.

Sedimentary features in the chalk suggest redeposition has occurred extensively throughout the North Sea basin. Laminations, debris of skeletal grains and shear deformation (Anderskov et al., 2011) are indicators of redeposition in the chalk. Mechanisms for this redeposition are slides, slumps, turbidites, mud-flows and mud-clouds (Kennedy, 1987). These depositional products can be from millimetre to meter scale, depending on the process. It is therefore complex to prove that some layers are redepositional features. Redepositional chalk is often referred to as allochthonous chalk.

Redepositional chalk can be deposited during tectonic quiescence or be induced by tectonic movement. Main tectonic processes influencing the Chalk Group in the North Sea basin are salt diapirism and tectonic inversion. It is thought that the chalk, during redeposition, is not fully lithified but somewhat dewatered, so that it enters a firm state (Mallon & Swarbrick, 2002). Figure 2.2 illustrates a simplistic visualization on the different depositional mechanisms and their spatial occurrence.

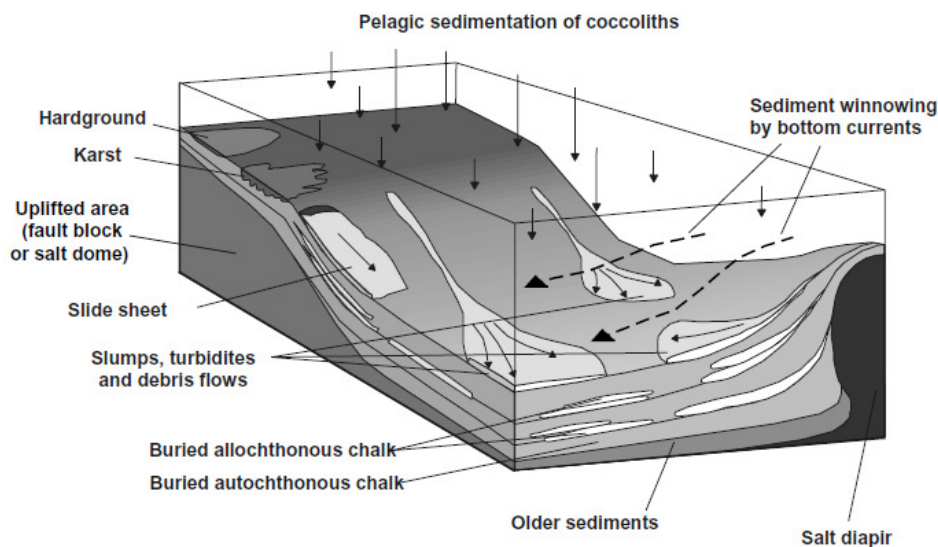


Figure 2.2 – Depositional processes of chalk. After van der Molen, 2004.

After deposition, either autochthonous or allochthonous, diagenetic processes occur in the chalk. Different diagenetic processes are hardground formation, density differentiation, current winnowing, karstification and recrystallization. These processes create alternating products as: flint, hardgrounds, glauconite and conglomerates. Flint layers form due to density differentiation and can occur as nodules in between chalk. The flint layers are composed of silica which comes from detrital material such as sponge spicules.

Hardgrounds and glauconite are products of very slow to non-sedimentation periods, combined with cementation and recrystallization processes. Conglomerates can form through various process as erosion and cementation, density differentiation but also as debris flows ([Kennedy, 1987](#)).

During the Late Cretaceous and Danian time periods, volcanic activity increased. This volcanic activity led to the deposition of volcanic ash and clay layers, sometimes found in the sedimentary record as for instance in the F06-02 well.

2.1.3 Stratigraphy

In the Netherlands, the Chalk Group is subdivided in 3 main units, the Texel Formation (from here on Fm.), the Ommelanden Fm. and the Ekofisk Fm. The Texel Fm. roughly equals the Cenomanian time period, the Ommelanden Fm. comprises the Turonian up to the Maastrichtian and the Ekofisk Fm. was deposited in the Danian. Figure 2.3 provides the lithostratigraphic subdivision of the Chalk Group in the Netherlands, Norway and Denmark, showing that more differentiation in the Netherlands is possible.

SYSTEM	STAGES (Hardenbol et al., 1998)	LITHOSTRATIGRAPHIC UNITS		
		Netherlands (van Adrichem Boogaert & Kouwe, 1994)	Southern Norway (Oakman & Partington, 1998)	Offshore Denmark (Oakman & Partington, 1998)
Paleo- cene Late Cretaceous	60.9 Ma. — Danian 65	Ekofisk Fm.	Ekofisk Fm.	Chalk-6
	Maastrichtian 71.3	Chalk Group Ommelanden Fm.	Tor Fm.	Chalk-5
	Campanian		Shetland (Chalk) Group Hod Fm. — Middle — Upper Hod Fm. — Lower — Middle — Upper	Chalk-4
	83.5 — Santonian 85.8 — Coniacian 89			Chalk-3
	Turonian 93.5		Blødøks Fm.	Chalk-2
	Cenomanian 98.9	Plenus Marl Mb. Texel Fm.	Plenus Marl Mb. Hidra Fm.	Turonian Shale Plenus Marl Mb. Chalk-1

Figure 2.3 - Lithostratigraphic division of the Chalk in the Netherlands, Norway and Denmark. After: [van der Molen, 2004](#).

The Texel Fm. includes limestones, chalk and glauconitic sands. It lays between the Lower Cretaceous Holland Fm. and the overlying Ommelanden Fm. and is characterized by the low gamma ray response in respect to the neighbouring members. The formation comprises the Texel Greensand, Texel Marlstone and Plenus Marl members. The Texel Greensand Member is the basal part of the formation, composed of glauconitic sandstones and is limited to the margins of the Western Netherlands Basin.

The Texel Marlstone member consist of limestones and (marly) chinks and is deposited in a marine environment. The Plenus Marl member is a dark grey to black claystone which probably represents an ocean anoxic event ([Schlanger et al., 1987](#)).

The Ommelanden Fm. comprises approximately 28 Ma of the Chalk Group interval, from 93.5 to 65 Ma. Chalk and limestone are the dominant lithology types with occasional intercalations of sand, marl or flint layers. This formation is also the thickest member of the three, but not intact in all places due to inversion phases or periods of non-deposition.

The Ekofisk Fm. is the only Paleogene formation within the Chalk Group and named after the Danian Ekofisk field. The Ekofisk Fm. consist of white chalky limestones to chalk with interbedded flint layers. The above described formation names are introduced by [Adrichem Boogaert & Kouwe \(1994\)](#).

2.2 Tectonic setting

2.2.1 Pre-Cretaceous

In the Permian, significant salt accumulations of the Zechstein Group were deposited in the Southern Permian Basin, where the study area is situated. This led to complete infill of the basin, exposure and thus a minor hiatus between Permian and Triassic times. After the hiatus, fluvial to marine sandstones and lacustrine claystone were deposited known as the Lower Germanic Triassic Group. Simultaneously, the salt of the Zechstein Group began to move as a result of the sedimentary loading on top and onset of tectonic activity ([Remmelts, 1995, 1996](#)). During the middle Triassic times, periods of uplift occurred in the Southern Permian Basin, mainly focused on the Texel-IJsselmeer High.

A rifting phase began in Late Triassic, breaking up the continent of Pangaea. This led to thermal subsidence of the basin and the creation of an Early Jurassic epicontinental sea. This is also the period in which the Posidonia Shale Formation, known for its source rock capacities, was deposited. Uplift occurred due to the thermal Central North Sea Dome, e.g. [Hallam and Sellwood \(1976\)](#), affecting part of the basins. Salt movement of the Zechstein Group still persisted throughout this period.

During the Middle Jurassic, rifting in the North Sea Basin accelerated which continued into the Early Cretaceous. Uplift of platforms combined with a low sea-level resulted in the Late Cimmerian unconformity.

2.2.2 Cretaceous

Opening of the North Atlantic Ocean in the Early Cretaceous led to a further extensional regime in the North Sea Basin with subsidence as result. This subsidence combined with the influx of clastic sediments resulted in the accumulation of the Rijnland Group. At the end of the Cretaceous, the extensional regime had shifted towards the north, leaving the North Sea basin to subside as a result of thermal relaxation. Combined with a sea level rise and the stop of clastic influx it were the ultimate conditions for the deposition of the Chalk Group.

During the Late Cretaceous, the onset for the Alpine orogeny changed the tectonic regime to a compressional state in the North Sea basin. This led to the inversion of former basins, indicated in blue on the left image of Figure 2.4 below. In the right image, the degree of inversion is illustrated.

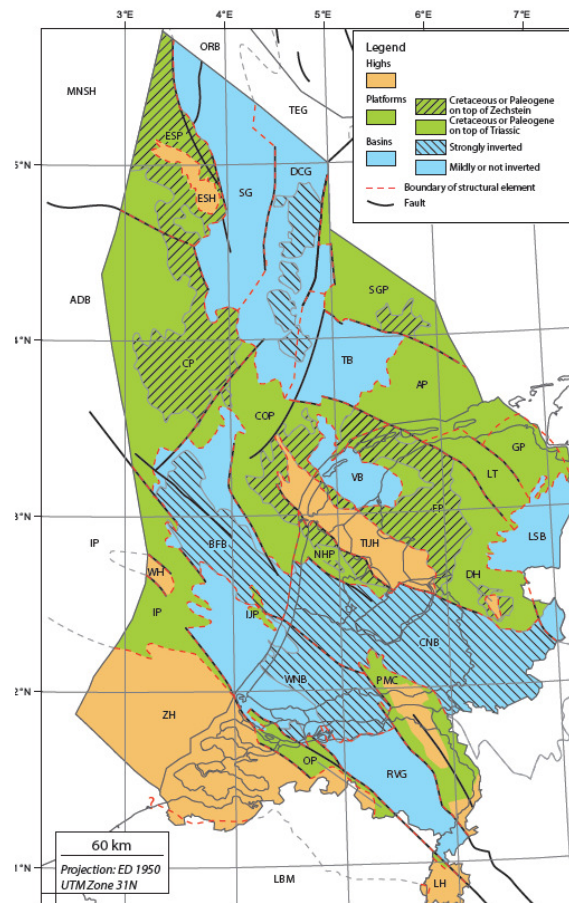


Figure 2.4 – Structural setting at the Late Cretaceous with different basins and highs indicated, as well as inversion areas and inversion grades (dashed areas). From [Kombrink et al., 2012](#).

The inversion in the Late Cretaceous persisted into the Paleogene and occurred in different pulses. The main pulses which are relevant for the North Sea basin are the Mid-Campanian inversion Sub-Hercynian inversion and the Late Danian Laramide inversion. The latter resulted in the end of the Chalk Group deposition as substantial amounts of fluvial material was transported into the basin. The inversion phases coincide with sub aerial exposure and erosion of the Chalk group. This is also visible on the thickness map of the Chalk Group on Figure 2.5. Another factor which influences the thickness of the Chalk Group is the ongoing movement of the Zechstein salt underneath during and after deposition. This salt movement had influence on both basin inversion and Chalk deposition.

2.2.3 Cenozoic

During the Cenozoic, one major and one minor inversion phases took place. These phases are called respectively the Pyrenean phase at the end of the Eocene and the Savian phase at the end of the Oligocene. The Alpine Orogenesis continued, affecting the structural elements in the southern Netherlands. The Cenozoic deposits are thinnest towards the southern Netherlands and gradually thicken towards the offshore. Figure 2.5 provides the present day thickness of the Chalk Group (left) and the Cenozoic deposits (right).

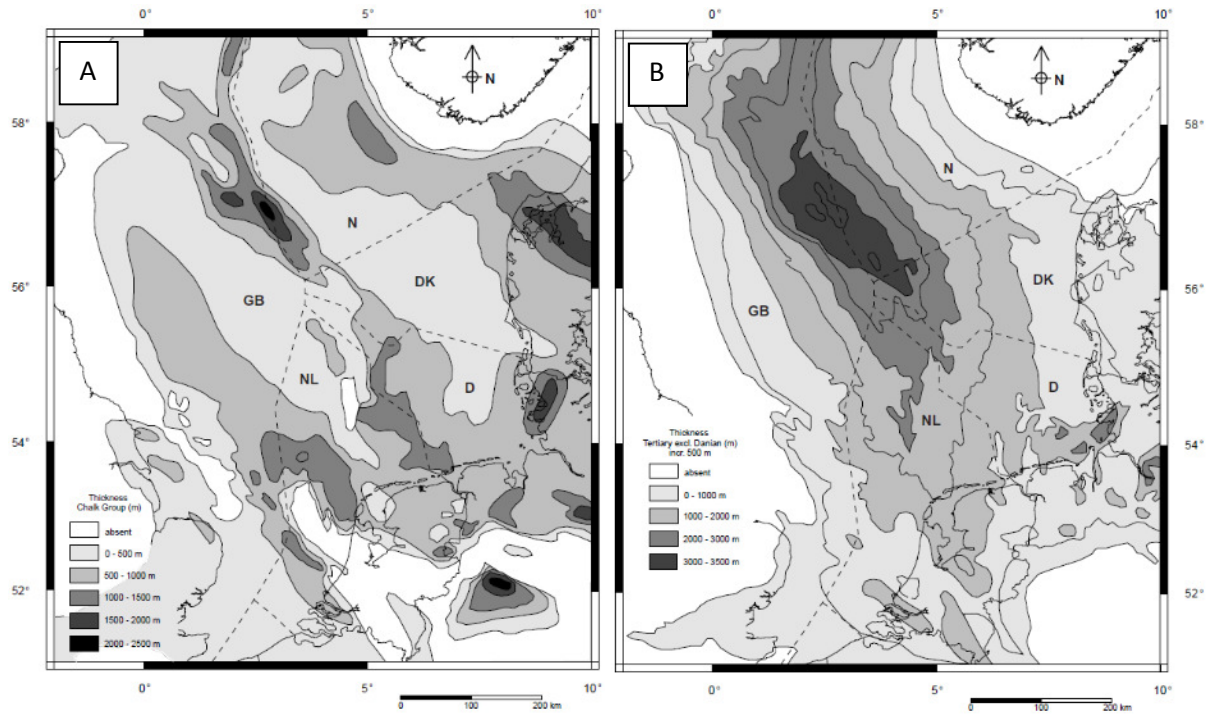


Figure 2.5 – Thicknesses of the Chalk Group incl. Danian (A) and of the overlying Tertiary succession (B). After [van der Molen, 2004](#).

2.3 Climatic influence

2.3.1 Pre-Cretaceous

The Triassic is characterized by a transition from arid to sub-tropical latitudes. In the first stages of the Triassic, the Southern North Sea Basin was submerged. Thermal doming led to exposure where after continental clastic sediments were deposited in a hot and arid climate. A gradual shift from an arid to a sub-tropical climate occurred during the Anisian. Across the Triassic, a relative low sea level curve was maintained.

The warm and moist climate of the Middle to Late Triassic persisted into the Jurassic, but in the Late Jurassic, a sudden drop in global average temperature was observed, suggesting an onset for transgressions and anoxic events. The sea level was fluctuating in the Jurassic, but had a generally increasing trend towards the end of the Jurassic.

2.3.2 Cretaceous

The Early Cretaceous started with a rapid temperature increase which stagnated shortly after. Enormous CO₂ release due to volcanism contributed to this warming ([Caldeira et al., 1991](#)). Multiple transgressional phases led to a global rising sea level. These transgression phases persisted into the Late Cretaceous.

2.3.3 Cenozoic

The transgression phases in the Cretaceous continue into the Danian. At the end of the Danian, a major regression led to the end of the Chalk Group deposition. Both the global temperature and the overall sea level decreased towards the end of the Cenozoic.

3. Methodology

3.1 Chalk facies model

A facies report from the Geological Survey of Denmark and Greenland (GEUS) and Wintershall ([Ineson et al., 2014](#)) was used as the basis of this master thesis. The report introduces different individual facies and facies associations in the chalk lithology based on 20 Dutch offshore wells and 2 Dutch onshore wells. The individual facies were first combined with individual well reports: F06-02 (Total), F14-08, F17-11 and F17-12 (Wintershall) and literature. These scientific reports that were used to determine a final facies model are: [Kennedy \(1987\)](#), [Brasher & Vagle \(1996\)](#), [Bramwell et al. \(1999\)](#), [Anderskov & Surlyk \(2011\)](#), and [Gennaro et al. \(2013b\)](#). The individual facies of each of the reports and papers were combined, generalized and separated in order to propose a new facies model for the chalk in the North Sea Basin. Observations of three cores, F06-02, HRL-02 and RID-02 were used as a quality check for the facies model even though the latter two are not included in the model itself.

3.2 Core measurements

The core data was provided from either [NLOG](#) (public) or EBN (confidential). Multiple types of core measurement techniques are used in this report including conventional core analysis, special core analysis, x-ray diffraction and thin section point counting. Not all techniques were available for each well. An overview of all core measurements and core lengths is found in Appendix I. These analysis result in porosity, permeability, grain density and rock and mineral composition measurements.

3.3 Wireline measurements

Wireline logs were also collected for the whole Chalk Group from either [NLOG](#) (public) or EBN (confidential) from the selected wells. These well log curves include measurements such as gamma ray, sonic velocity, neutron, bulk density, resistivity and caliper data. Caliper and bit size logs are used as a quality check of the reliability of the measurements.

All data regarding the wells were gathered and stored in an Excel database. The database includes 4338 wireline log data points from 26 wells with their accompanied wireline measurements. This means that the database only comprises the cored chalk interval and they do not comprise the whole chalk interval in these wells. Appendix II represents the available wireline logs per well.

Porosity

Interactive Petrophysics (IP) is used for the calculation of porosity from wireline logs, based on the available logs from each well. First the amount of clay in the system is calculated via the gamma ray wireline log, which measures the natural radioactivity in a sample. Values for the gamma ray of clean chalk and for clay were assigned per well and average respectively around 10 API and 120 API.

The clay volume is one of the input curves used for the porosity and water saturation calculations. The calculation uses a neutron density model, where available, to build the porosity log with the help of the [Archie \(1952\)](#) saturation equation. If neutron and density logs are missing from a well or an interval, the porosity will be calculated by neutron-sonic, density, neutron or sonic in this specific order. A temperature curve was calculated for each well via a gradient of 3.3°C per 100 meters with a surface temperature of 12°C ([KNMI](#)).

The parameters were optimized for the individual wells. Wet clay values were determined by Lower Cretaceous clay response. If the member is absent, approximate values are taken for the wet clay parameters determined from other wells in the vicinity. Water resistivity was determined by cross plotting resistivity and total porosity, while the mud resistivity was taken from the drilling data. Core data helped determining the minimum, average and maximum density values for the chalk. The [Raymer \(Hunt-Gardner, 1980\)](#) model is used for porosity determination from the sonic. The parameters that were assumed are shown in Table 3.1.

<i>Parameter</i>	<i>Value</i>	<i>Remarks</i>
Clay Porosity (fraction)	0.10	Assumed an approximate clay porosity which is taken into account.
Phi maximum (fraction)	0.40	Maximum porosity for the chalk, confirmed by core measurements.
Phi delta (max)	0.05	Maximum porosity difference between two measurements. This to limit erroneous measurements.
Cementation exponent m	2.00	Standard input, close to SCAL data.
Saturation exponent n	2.00	Standard input, checked with SCAL data.

Table 3.1 – Made assumptions for porosity calculations in IP.

The input curves were used to calculate the porosity with Interactive Petrophysics (IP). The depth error of the wireline logs is less than the depth error of the retrieved cores, therefore depth shifts are needed to combine the core data with the wireline logs. An example is illustrated in Figure 3.1, where the core porosity is shifted to match the patterns as recognized from the porosity curve. Normally the gamma ray log from the core are compared to those of the log, however no gamma ray log of these cores are currently available. Not all cores needed shifting or had too few data measurements and therefore the depth shift was not applied. This latter is also an uncertainty in the data that need to be held in mind. The depth shifts are located in Appendix IV.

These depth shifts were quality checked by cross plotting the total porosity versus the core porosity on forehand and after the depth shift. The ideal regression line between these two factors is linear through the points [0.0, 0.0], [0.1, 0.1] etc. If the regression line of the cores coincides or best approaches this ideal linear trend, the depth shift is assumed to be correct.

The core data can then be coupled with the wireline log data at the correct depth. All the data was gathered in an Excel database and visualized in Tibco Spotfire in order to visualize and interpret trends in the data.

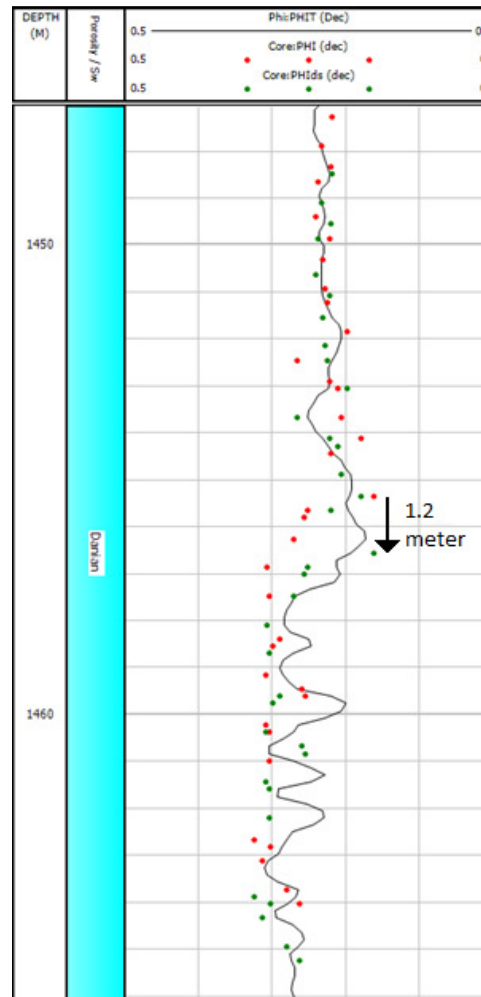


Figure 3.1 – Depth shift for the F06-02 core to match the total porosity calculations. Red dots are uncorrected core porosity measurements while green are corrected, black line is the calculated total porosity. Applied depth shift is 1.2 meters.

Most of the core vs. log cross plot correlations were statistically checked by releasing an RMA function on the dataset to incorporate the uncertainties of both parameters. This was done with help of the programs from [Lutgert \(2016\)](#) and [Bohonak \(2004\)](#). If only one of the two parameters is expected to have uncertainties, than a linear regression with X on Y or Y on X, has been applied.

In order to utilize the data as efficient as possible, the dataset was tested with neural networking and fuzzy logic toolboxes, incorporated in IP. The toolboxes were used to predict the facies based on the gamma ray, sonic and neutron wireline log.

3.4 Sonic velocity trends

The sonic measurements were compared to depositional facies, lithofacies, chronostratigraphy and acoustic facies in order to observe correlations and trends in sonic.

4. Results

4.1 Chalk facies

4.1.1 Improved chalk facies model

As the basis of this report, the GEUS chalk facies study ([Ineson et al., 2014](#)) is used, which describes 21 different facies in the chalk. The findings of the individual well reports of the F17-11 and F17-12 (Wintershall) and F06-02 (Total) were compared with and added to the existing model. The updated model was then compared with several literature chalk facies studies in order to check consistencies or differences.

Several facies were grouped together on the basis of lithology, mineralogical composition, bioclastic abundance and depositional processes. The improved facies model is stated below; fourteen individual facies, which can be grouped in five associations, are distinguished. The association names as listed below are named after their accompanied depositional mechanism or mineralogical composition. Described clay compositions in this model are based on mineralogy rather than grain size.

Pelagic Association	
	This association is deposited as the low energetic carbonate fall. Clay and marly content are thought to origin as hemipelagic content or by cyclic changes in sediment supply. Variable bioturbation grades in the chalk layers indicate varying oxygenated bottom waters, with thorough bioturbation representing high oxygenation levels. Episodic nutrient supply is believed to coincide with skeletal lithoclasts. Pelagic chalk is often referred to as autochthonous chalk. The siliciclastic content of pelagic chalk is between 0 and 10%.
1	<p>Marly chalk</p> <p>Consists of all chalk that have any marly and clayey content in the chalk, typically mudstones to wackestones. Marl and clay can occur in solution seams, primary laminations and in the matrix. Low skeletal content, limited to sponge spicules and small inoceramid fragments. Bioturbation is common and dominated by <i>Zoophycos</i>, <i>Chondrites</i> and <i>Planolites</i>, <i>Taenidium</i>, <i>Thalassinoides</i>. Styrolites and solution seams are common.</p> <p>Type locality: A12-01, 2058.9 – 2108.8 meter MD.</p>
2	<p>Homogenous chalk</p> <p>Clean chalk mudstone to wackestone regardless of bioturbation or stylolitization grade. Can often appear as structureless due to limited primary depositional features or thorough bioturbation, mainly focused on <i>Zoophycos</i> and <i>Thalassinoides</i> and less common <i>Planolites</i>, <i>Chondrites</i>, <i>Taenidium</i> and <i>Palaeophycus</i>. Skeletal grains as sponge spicules, inoceramid, echinoderms and bryozoa are found.</p> <p>Type locality: F17-11, 1432.5 – 1463.2 meter MD.</p>
3	<p>Skeletal chalk</p> <p>This chalk is very similar to the previous two facies classes but can be distinguished based on skeletal content. The accompanying Dunham classification is packstone, grainstone, floatstone, rudstones and boundstones. The chalk matrix is locally bioturbated and densely cemented, whilst the lithoclasts are (partly) recrystallized. Skeletal clasts persist in a wide range,</p>

		bryozoa, sponge spicules, inoceramid fragments, bivalves, echinoderms and corals.
Type locality: F17-11, 1419.9 – 1432.1 meter MD.		
Redepositional Association		
		The redepositional chalk association is represented by chalk which is removed from its original position and redeposited at a new position. This movement can be accommodated by either gravitational flows, currents, storm currents, turbidites and slumps. Redepositional chalk can consist of all other individual facies or as a mix of different facies. Useful indicators for redeposition are broken lithoclasts and secondary laminations. One exception of redeposition is the shear deformed chalk mentioned below, which can be either in place deformation or deformed during movement. Different lithologies are present in this association, where chalk remains the major component, however minor amount of clay has been found. Redepositional chalk is often referred to as allochthonous chalk.
4	Laminated chalk	Laminated chalk facies consist of interbedded chalk mudstone with different chalk units as for instance marly chalk. Slight variation in content of skeletal grains can occur. Bioturbation is seen locally, e.g. <i>Chondrites</i> , however not thoroughly, otherwise the laminations are not preserved.
Type locality: B13-02, 1621.8 – 1622.2 meter MD.		
5	Skeletal chalk (debris)	Close to laminated chalk, but defined by higher skeletal content, which may be scattered through the layers or focussed in specific parts. Associated Dunham classifications are wackestone, packstone and grainstone. Bioturbation is locally found and the burrows are generally filled in with bioclasts, chalk or flint. Beds are usually thicker than laminated chalk, ranging up to tens of centimetres.
Type locality: F03-03, 1653.2 – 1653.7 meter MD.		
6	Shear deformed chalk ¹	Shear deformed chalk is recognized by several authors in previous studies. This particular facies can be folded or convoluted from in place deformation, or during the movement of chalk. These processes can have led to the banding of chalk layers.
Type locality: F02-03, 1534.6 meter MD.		
Secondary Alteration Association		
		In the secondary alteration association are facies that have been altered after the deposition in of one of the other facies associations. Processes leading to alteration of the chalk are (re)crystallization, diagenesis, winnowing, karstification and brecciation.
7	Flint layers/nodules	By some classified as belonging in the homogenous - or marly chalk facies, here separated due to its probable impact on petrophysics. Generally thought to originate from void filling fluids and crystallization (e.g. Maliva et al, 1989). Siliceous content originates from bioclasts as sponge spicule accumulations. Siliclastic input into the chalk does not seem to be coupled to the formation flint, even though that the input is rich in silica.
Type locality: F06-02, +- 1456.7 meter MD.		

8	Hardground	Hardground formation is the processes which forms layers of densely cemented chalk. The formation occurs during periods of low to non-deposition, at which cementation of the top of chalk layers takes place. Hardground formation can coincide with glauconite formation, facies 9, and therefore the chalk layers can be impregnated with a glauconitic layer. Hardground formation is defined as a period of low or non-deposition while authors as Hancock (1993) present that similar processes after 30 centimetres of burial can also occur, resulting in physical compaction and the formation of nodular chalk.
Type locality: F02-A-03, 1658.9 – 1659.0 meter MD.		
9	Glauconitic chalk	Glauconitic chalk is distinguished on its glauconite content. The mineral glauconite forms during periods of low to non-deposition and is formed by diagenetic processes. The Dunham classification ranges from wackestone to grainstone depending on the size of the glauconite grains and their abundance. The matrix of this rock is homogenous or marly chalk.
Type locality: F05-04, 1360.4 – 1362.3 meter MD.		
10	Chalk conglomerate	Chalk conglomerate is believed to form from diagenetic processes including cementation, erosion and debris flow differentiation. Chalk clasts with mudstone to wackestone textures float in a matrix of more bioclast rich wackestone to packstone. Dissolution can occur along clast boundaries.
Type locality: F02-A-03, 1658.0 – 1658.4 meter MD.		
11	Sandy/ Glauconitic chalk conglomerate	This facies differs from the chalk conglomerate in its silica and/or glauconitic content. Whilst the clasts mainly consist of pelagic chalk, the matrix is rich in either quartz or glauconite. Bioturbation can distort the quartz distribution.
Type locality: F02-05, 1453.1 – 1453.3 meter MD.		
Siliciclastic Association		
This association is similar to pelagic chalk with the only exception of more siliciclastic input. Bioturbation probably linked to sedimentation rate. The sandstone found in this association is believed to be of marine origin. This silica input, most probably, is the erosional product of continent or nearby islands.		
12	Sandy chalk	Defined as the chalk with a SiO ₂ content between 10% and 50%. This chalk can be bioturbated and stylolitized. Silica rich event beds, due to their silica content, will be associated with this facies.
Type locality: F17-12, 1424.9 – 1433.7 meter MD.		
13	Sandstone	The sandstone facies is defined to have a SiO ₂ content of more than 50%. In between the quartz grains, chalk still persists. Coarse bioclasts are usually found in this facies, even as thorough bioturbation.
Type locality: F17-12, 1435.7 – 1450.8 meter MD.		
Volcanic Association		
The volcanic association consist of one facies and is only found in well F06-02 were it is interpreted as a volcanic clay. This volcanic activity is believed to have stopped the carbonate factory for a short period of time.		

14

Red clay²

This red coloured clay is siliciclastic red clays without any chalk. The facies is rich in arenaceous foraminiferas.

Type locality: F06-02, 1462.0 meter MD.

¹: From [Gennaro et al., 2013b](#).

²: From [Biondi, 1998](#).

Several generalizations were made with the improved facies model, due to the fact that no overlap between the facies occurs. A more generalized facies model has the advantage that misinterpretation of certain layers becomes less likely. Figure 4.1 presents an overview of the different facies from the GEUS Wintershall reports from well F17-11, F17-12 ([Ineson et al., 2014](#)) and the F06-02 core reports ([Biondi, 1998](#)) and how their facies fit in the new improved facies model.

van Wingerden, 2016	Geus Wintershall rapport	F17-11 & F17-12	F06-02
1 Marly Chalk	F Slightly Marly chalk mudstone G Marly Chalk mudstone H (Chalky) Marl	9 Cenomanian marly Chalk	
2 Homogenous Chalk	A Homogenous chalk mudstone B Biomottled chalk mudstone	1a Structureless clean chalk 1b Bioturbated clean chalk 1c Styolitic and bioturbated chall 1d Styolitic chalk 8 Cenomanian bioturbated chalk	3 Bioturbated Chalk mudstone 6 Stylolized chalk
3 Skeletal Chalk	J Skeletal Wackestone P Coral Floatstone Q Skeletal Coral Wackestone		
4 Laminated Chalk	C Laminated chalk mudstone		4 Laminated chalk
5 Skeletal Chalk (debris)	D Skeletal-intraclastic Wacke/Mud E Skeletal-intraclastic Wacke/Pack I Marly chalk Wacke/Pack/Grain K Skeletal Packstone		1 Allochthonous skeletal 1 2 Allochthonous skeletal 2
6 Shear deformed Chalk			
7 Flint layers/nodules			5 Flint
8 Hardground	R Hardground		
9 Glauconitic Chalk	M Glauconitic Skeletal Packstone N Glauconitic Skeletal Grainstone		
10 Chalk conglomerate	S Chalk Conglomerate T Chalk Breccia	3 Chalk matrix-supp conglomerate 4 Clast supported conglomerate	
11 Sandy/ Glauconitic Chalk Conglomerate	U Quartz Pebble Conglomerate V Matrix-supp. glc Conglomerate	5 Sand-supported conglomerate	
12 Sandy Chalk		2a Bioturbated sandy chalk 2b Bioturbated and styolitic sandy chalk	
13 Sandstone	X Sandstone	6 Glauconitic Sandstone 7 Bioturbated Sandstone	
14 Red clays			7 Red Clays

Figure 4.1 – Overview of the different facies used for the new facies model and their position inside this new model, indicated in the left column.

The abundance of each of the facies as found by the wireline data points is displayed in Figure 4.2. The three pelagic facies have the highest abundance, together comprising 84.92 % of the total cored chalk interval. The redepositional association comprises 4.84 % of the data, redepositional 6.27% and siliciclastic 3.97 %. The red clay facies is only found in the F06-02 well but no wireline measurements accompanying this depth are found due the limited resolution of the logs.

4.1.2 Facies model validity

To quality check for the new proposed facies model, observation from the cores HRL-02, RID-02 and F06-02 were compared with the new facies model.

Dark contrast layers in between the chalk facies can be observed which provide evidence of redeposition. An example is presented in Figure 4.3. The evidence for redeposition is the turbulent deposition patterns which are found in the layers and the macro fossil debris in the layers as indicated by the red circles in the figure. The majority of these layers have been described in the GEUS reports as being a marly solution seam in between the pelagic chalk. However, these descriptions do not match the observations and therefore the layers are interpreted as skeletal chalk debris layers in this report. This interpretation was then integrated into the existing facies analysis from the cores by looking at visual representations of these layers in core photographs. If abundant, approximately 50% or more dark contrast layers are found over an interval of minimum 10 centimetres, the interval was interpreted as skeletal chalk (debris) facies.

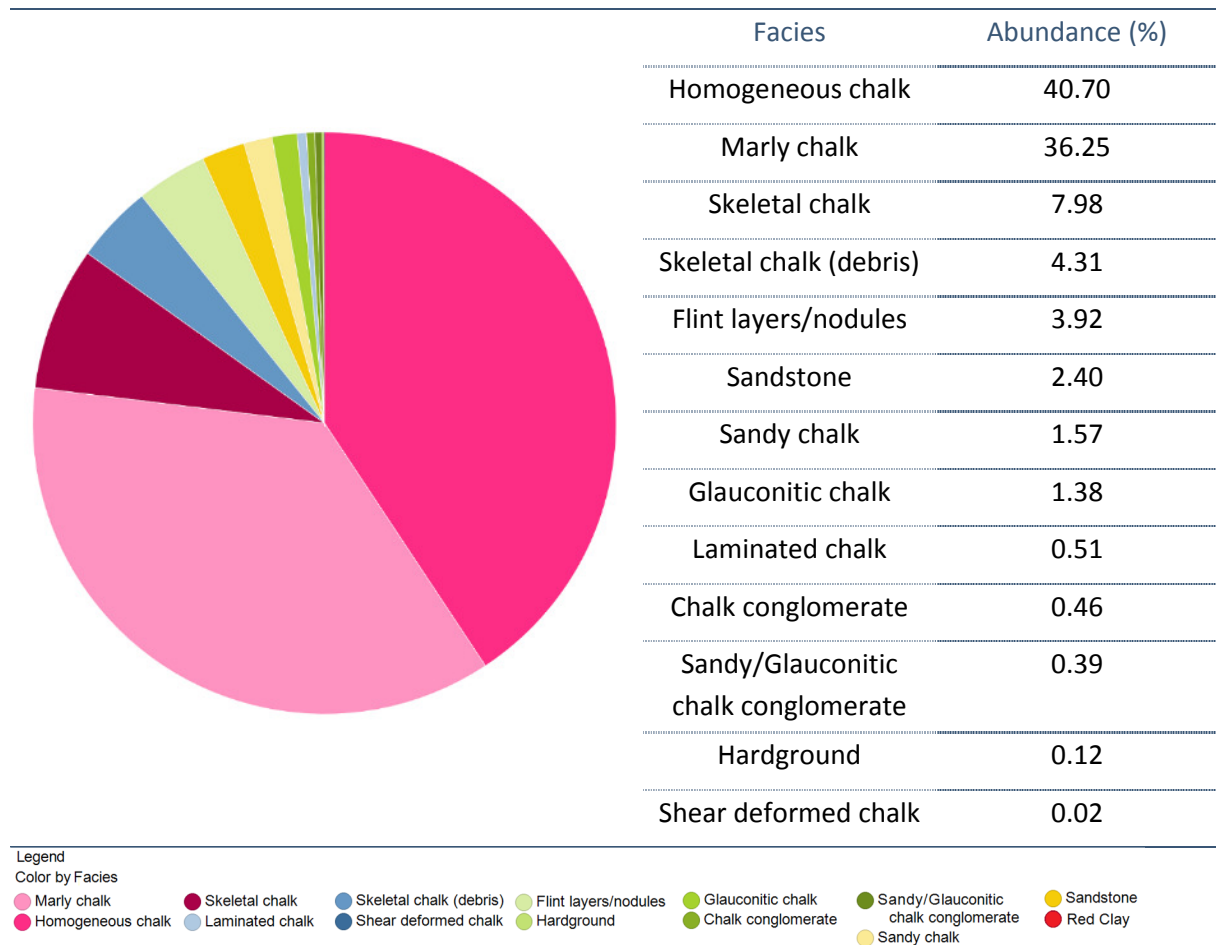


Figure 4.2 – Relative abundance of the facies in the cored Chalk sections of the wells. Abundance is based on measurement point instead of layer thickness. Note that the facies order in the table on the right of the figure is sorted by abundance rather than association.

The influence of flint layers and/or nodules in the system is significant in the observations of the F06-02 well. The core illustrates an oil up to contact at the exact position where a flint layer is seen in the core, as presented in the right image of Figure 4.3. Above the flint layer, the chalk is not oil stained, therefore suggesting that the flint layers can act as impermeable layers throughout the chalk and therefore can be of significant lateral extent.

Another important core observation is the presence of shear deformed chalk. Figure 4.4 illustrates the interpreted situated of a sigmoidal bioclast, outlined by the white line, being possibly shear deformed

by deformation of the chalk or by an overriding layer. The directions of the interpreted shear deformation are also indicated by the isolated white arrows above and below the structure.



Figure 4.3 – **Left:** Homogeneous chalk (A) with a dark contrast clay wavy layer (B) in between from HRL-02 core, top depth 1078.6 meter. Red circles indicate macro fossil debris in the dark contrast layers. **Right:** Oil up to contact in the F06-02 well, where the lower part of the image is oil stained homogeneous chalk and the top part is a flint nodule/layer.

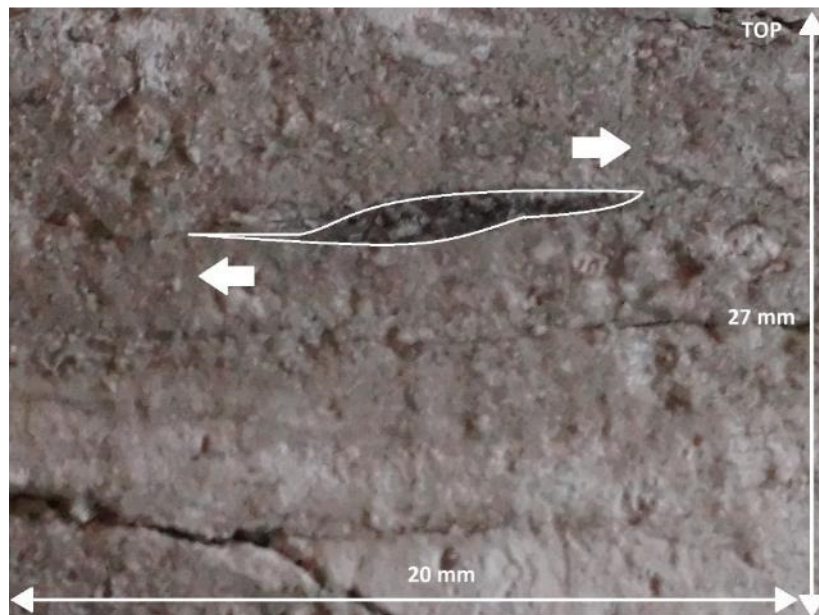


Figure 4.4 – Indications of shear deformation in redeposited chalk layers, HRL-02 core, 1078.7 meters measured depth.

4.2 Core measurements

Core data was gathered in a database and visualized in Spotfire. An overview of the gathered data and the minimum, maximum and averages for each of the facies per measurement are provided in Appendix I. The porosity, permeability and density are analysed and plotted in distribution diagrams in the following sub-paragraphs.

4.2.1 Porosity

The porosity distribution in Figure 4.5 reveals an average porosity of 27%, with a standard deviation of 6%. The minimum values are found in 2 flint layers with respective porosity values of 0 and 2%. The maximum porosity values are found in homogeneous chalk in the K13-A-10, F17-12 and B13-01 wells and range between 40 and 43 %.

Skeletal and homogeneous chalk facies have generally higher porosities than marly chalk facies. The most significant marly chalk sediment abundancies are accumulated in basins as for instance the Step Graben (A12-01, A12-02, B13-01 and A18-02-S1), Vlieland Basin (FRA-01-S1) and Texel IJselmeer High (BRG-01), while the homogeneous chalk is found throughout all structural units. The skeletal chalk facies is focussed in the Dutch Central Graben.

In the wells F02-A-03, F02-03, F02-06 and F17-11, it is found that the skeletal chalk has slightly higher porosities than the homogeneous chalk. This relation is however not found in all wells, as for instance in the F05-04, F06-02, F09-02. Here the skeletal chalk reveals lower porosity values than the homogeneous chalk of the surroundings. In these wells the skeletal chalk facies indicates significant redepositional intercalations in between the skeletal chalk. Bioturbation might influence in porosity if surrounding layers are intermingled with the skeletal chalk.

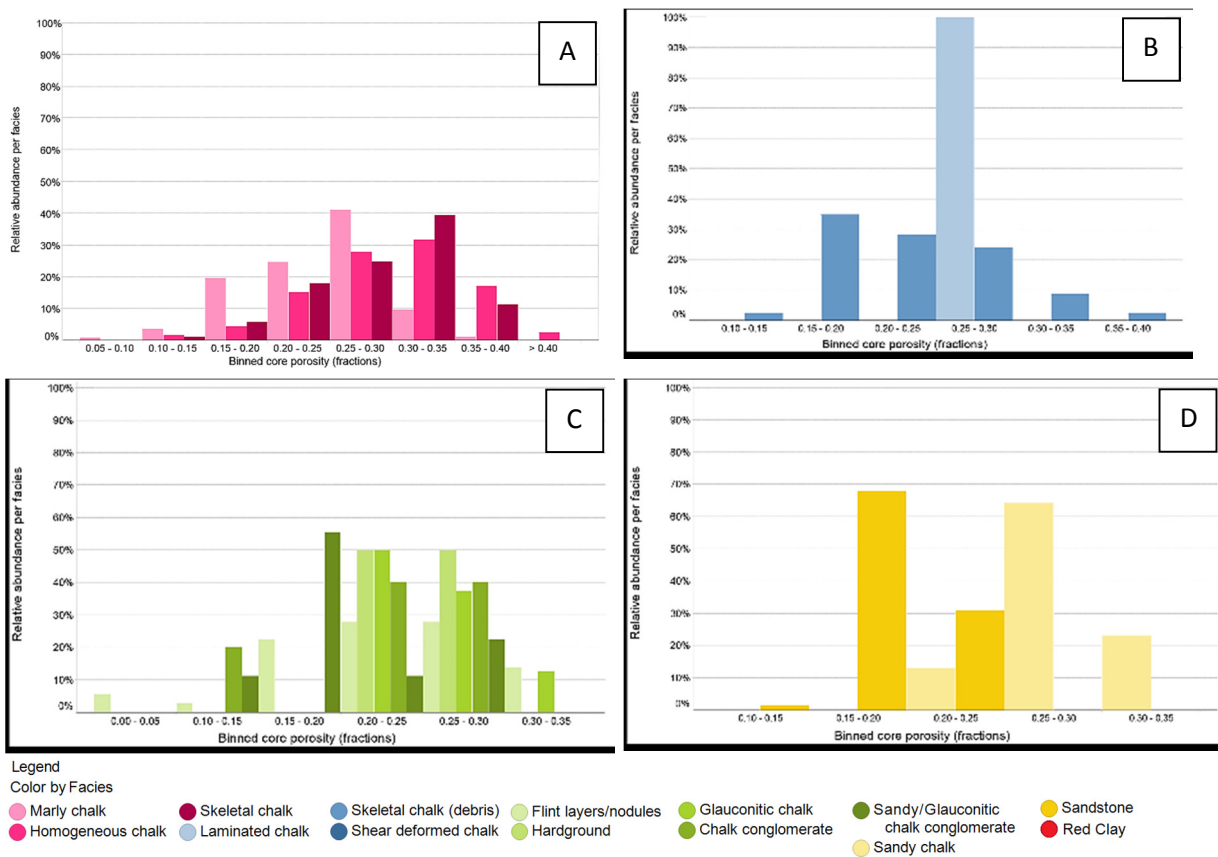


Figure 4.5 – Relative porosity distribution (fractions) per facies of all core measurements. Bins of porosity per 5 percent, note the x-axis scale is not the same for all trellises. Trellis per association; A: pelagic, B: redepositional, C: secondary alteration and D: siliclastic. Note that the laminated chalk facies has only 2 measurements, therefore the relative abundance is 100% in one bin.

The redepositional association illustrates porosity values between 12% and 34%. However, the majority of the measurements in these bins are found to be between 15 to 20%, which is generally lower than the pelagic association. The laminated chalk peaks in the 25 to 30% ranges, however only two measurements in this facies occur.

The secondary alteration facies, except for the flint layers/nodules, reveal porosities up to 28%, which is lower than the pelagic association. The lowest porosity values are found in flint layers/nodules, being 0 and 2 %. The figure indicates that the majority of porosities in this association occur between 20 and 30%. Sandy and glauconitic chalk conglomerate facies occur on the low side of the porosity spectrum while the chalk conglomerate and glauconitic chalk facies focus on the high side.

Sandstone facies does not exceed 25% porosity. The thin sections from well F17-11 and F17-12 reveal that the sandstones are still limestone rich (Petrea, 2015 and 2016). Sandy chalk reveals the same porosity relation as the sandstone, only having less than 50% SiO₂. Therefore, there is more space for chalk in the sandy chalk, which results in that the sandy chalk behaves in between the sandstone facies and the pelagic association.

4.2.2 Permeability

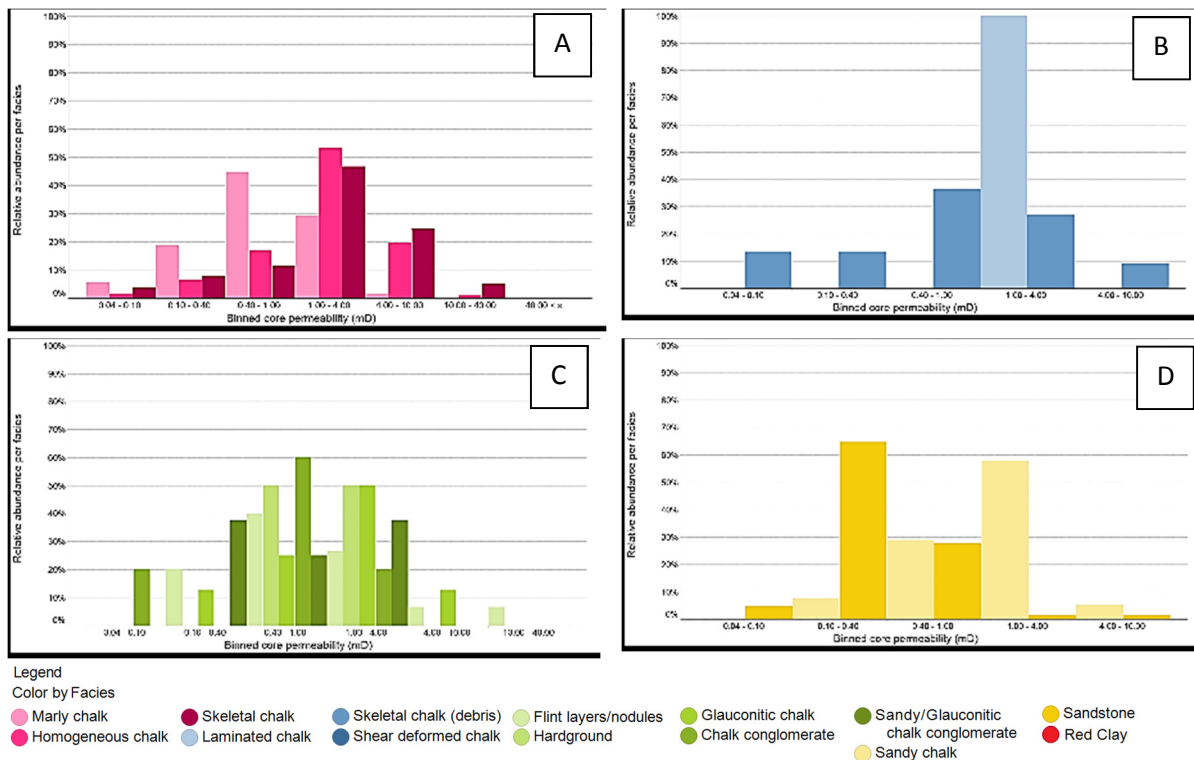


Figure 4.6 – Relative permeability distribution (mD) per facies of all core measurements. Note the x-axis scale is not the same for all trellises. Trellis per association; A: pelagic, B: redepositional, C: secondary alteration and D: siliclastic.

The distribution of 829 horizontal permeability measurements is illustrated in Figure 4.6. The permeability is displayed on the x-axis with a random chosen bin interval. The permeability ranges from 0.05 mD to 42.76 mD with an average of 2.09 mD and a standard deviation of 3.09 mD. The majority of measurements is found in the low permeability ranges of several milli-Darcys. The values

higher than 23 mD are homogeneous chalk and skeletal chalk facies from the F02-05, F02-06 and the F06-02 wells.

For the pelagic association, the permeability distribution reveals the same relative patterns as the porosity distribution. The marly chalk facies peaks in the lower 0.4 - 1 mD permeability while the homogeneous and skeletal chalk facies peak in the slightly higher 1 - 4 mD range. In wells where both marly chalk and homogeneous or skeletal chalk occur, the marly chalk provides consistently lower permeability while the porosity of the facies is approximately the same as for instance in the FRA-01-S1 well.

Redepositional association exhibits a wide range in permeabilities which is closely linked to the pelagic association. The skeletal chalk (debris) facies peaks in between the homogeneous/skeletal chalk facies and the marly chalk facies. The laminated chalk has limited samples and concentrates in the same bin as the homogeneous and skeletal chalk facies.

The secondary alteration association reveals a large variance in the permeabilities, with an average permeability of approximately 2 mD. All of the facies peak in the 0.4 – 1 mD range except for the glauconitic chalk and hardground facies, which both peak in the 1 – 4 mD range. The flint layer/nodules facies peak at the lower end of the spectrum, suggesting flint has significant impact on the porosity of the system, which is also confirmed by the flint layer acting as intra chalk seal in the F06-02 well as described in section 4.1.2. Not all flint is recognized to have such low permeabilities. The thickness of these flint layers and nodules might be a factor which might account for this distortion.

The siliciclastic association demonstrates the lowest permeabilities of all associations; an average of 0.83 mD. The two separate facies illustrate that the average permeability and the range for the sandy chalk is higher than for the sandstone. Furthermore, the sandstone reveals lower average permeability than the sandy chalk, ranging up to a log factor.

Porosity-permeability relationship

The porosity-permeability relation is illustrated in Figure 4.7. Ideally this would be a trend where low porosities equals low permeabilities and vice versa. The data cloud reveals that this is not the case for the chalk in whole, however some minor trend can be observed in the data when looking at facies individually. Horizontal and vertical permeabilities are grouped together due to the limiting amount of vertical permeability measurements.

The marly chalk facies features low permeability in comparison to the overall chalk trend, however a large spread of the data is found. The lowest permeabilities in the marly chalk are from the deep marly A12-01 well. The homogeneous chalk focusses in the middle to top part of the cloud with the approximate same distribution ranges than marly chalk. The skeletal chalk is mainly found on the top side of the diagram, relative higher permeabilities with approximate same porosities. However, some significant lower permeability values have been found for the skeletal chalk in well F06-02, where it is intermingled with skeletal chalk debris.

The porosity and the permeability of the redepositional features are found to be close to the surrounding pelagic chalk. However, the porosity data has limiting values while the permeability seem

to be persistent throughout the higher intervals. The secondary alteration association also reflects the pelagic association due to the limited thickness and possible pattern distortion through bioturbation. The facies conglomeratic and brecciated chalk focusses on the lower part of the porosity range, even though permeability is sustained. The number of measurements in this facies are however limited. Flint layers are generally found to have lower permeabilities than the surrounding rock.

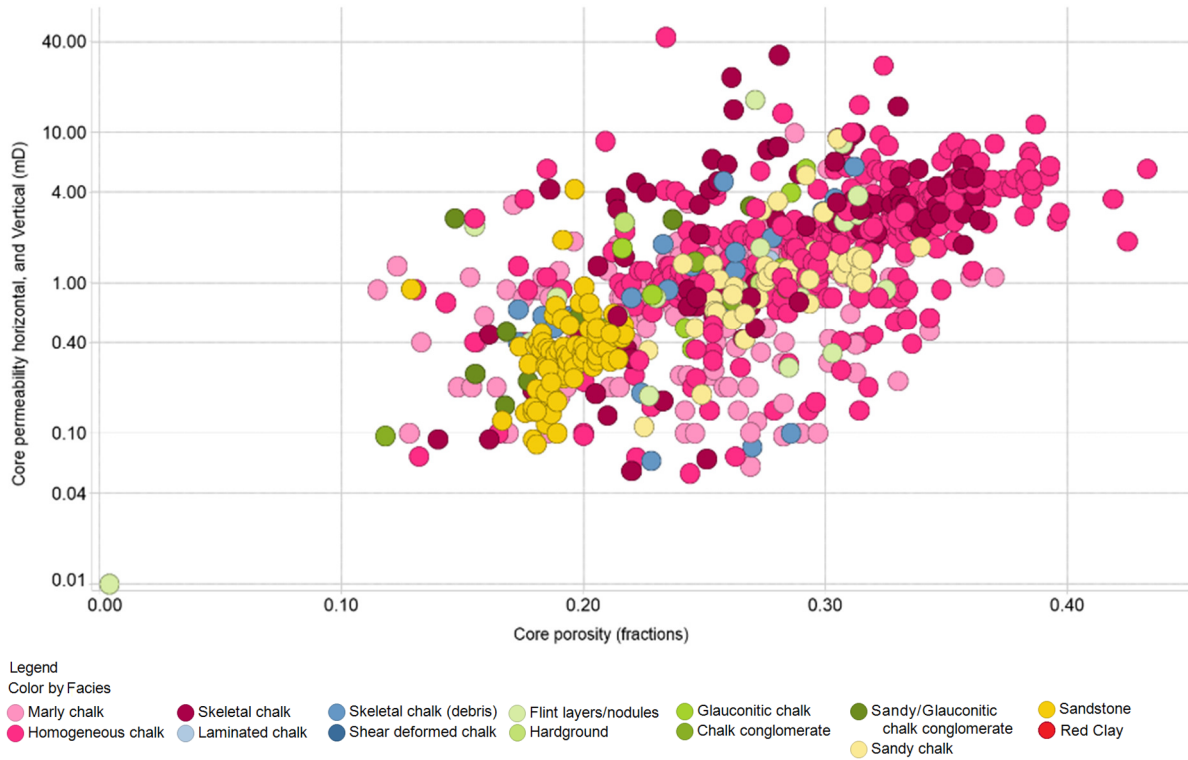


Figure 4.7 – Porosity (fractions) and permeability (mD) measurements of the cored interval, colour coded by facies.

The siliciclastic association shows a clear distinction between the sandy chalk and sandstone facies. The sandstones are found in lower porosity and permeabilities values than the sandy chalk. The porosity remains constant while the permeability of most of the sandstones varies between approximately 0.10 – 1 mD.

The following relationships between the core porosity and permeability, both horizontal and vertical, are found:

Core permeability vs. porosity	RMA Formula	R ² value
All measurements	$\kappa_{core} = 10^{(-2.21 + (8.42 \cdot \varphi_{core}))}$	0.37
Marly chalk	$\kappa_{core} = 10^{(-2.12 + (7.90 \cdot \varphi_{core}))}$	0.09
Homogeneous chalk	$\kappa_{core} = 10^{(-2.20 + (8.18 \cdot \varphi_{core}))}$	0.31
Skeletal chalk	$\kappa_{core} = 10^{(-2.65 + (10.57 \cdot \varphi_{core}))}$	0.28
All other facies without pelagic	$\kappa_{core} = 10^{(-2.73 + (9.47 \cdot \varphi_{core}))}$	0.36

4.2.3 Grain density

The grain density of each of the samples were measured and the distribution is represented in Figure 4.8. In this thesis, densities will be displayed by gram/cc (gm/cc) which is equal to gram/cm^3 (g/cm^3). The minimum density of the chalk core measurements is 2.54 gm/cc, the maximum 2.97 gm/cc with an average of 2.70 gm/cc and a standard deviation of 0.03 gm/cc. The average density of a limestone is dependent mineral density of calcite: 2.71 gm/cc.

The highest number of measurements in the homogeneous and skeletal chalk facies density distribution are found in the expected 2.70 – 2.75 bin. The marly chalk peaks at the 2.65 to 2.70 gm/cc. Detrital or hemipelagic clay input distorts the density of the chalk, depending on the clay mineral composition. Clay minerals which are found in the chalk special core analysis (Petrea, 2015 and 2016) are glauconite¹ (2.40 – 2.95 gm/cc), illite¹ (2.79 – 2.80 gm/cc), smectite¹ (2.00 – 3.00 gm/cc), sepiolite¹ (2.00 – 2.20 gm/cc) and chlorite¹ (2.60 – 3.30 gm/cc). The wide range in density distribution is dependent on the composition and the abundance of these clay minerals.

The redepositional association reveals slightly lower density values due to their clay contaminations. Therefore, the association peaks in the same bin as the marly clay, making it likely to assume that most of these debris layers are made up of clayey material.

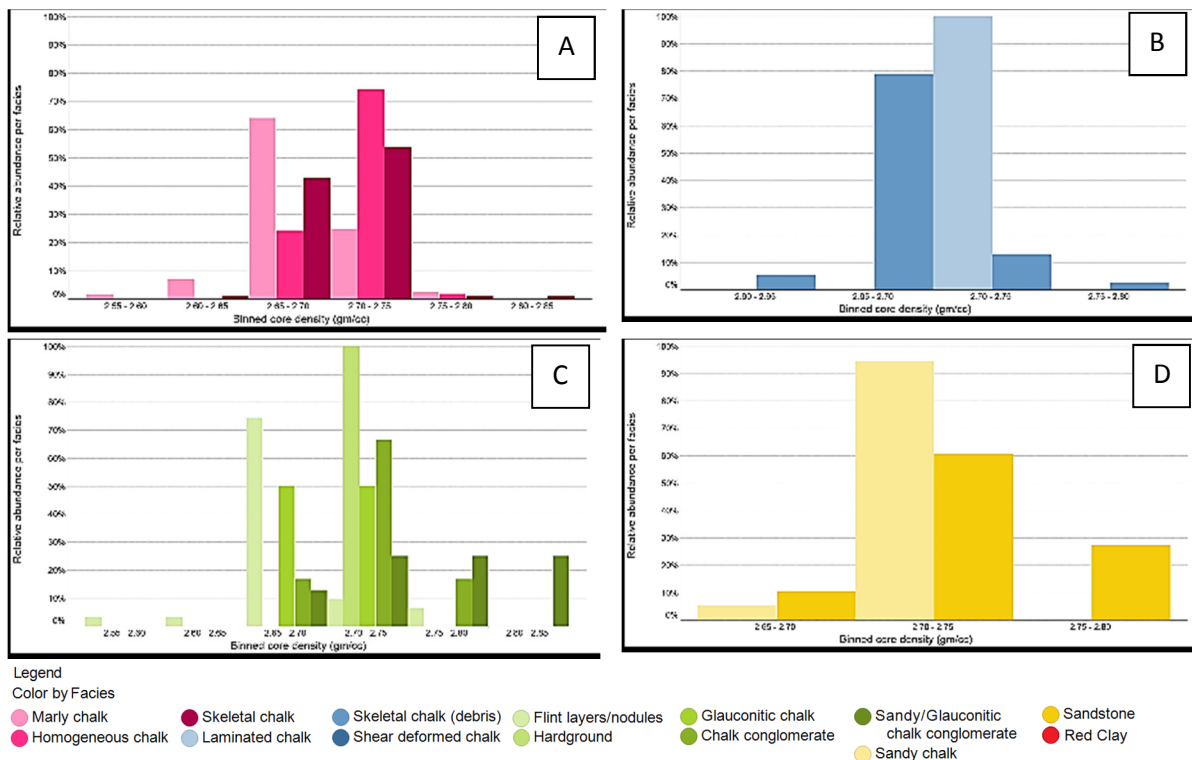


Figure 4.8 – Relative density distribution (gm/cc) per facies of all core measurements. Bins of density per 0.05 gm/cc. Note the x-axis scale is not the same for all trellises. Trellis per association; A: pelagic, B: redepositional, C: secondary alteration and D: siliclastic.

The secondary alteration follows the pelagic chalk distribution, where individual facies differ, as also for the porosity and the permeability. An exception is the glauconitic chalk facies and sandy/glauconitic chalk conglomerate facies, which are found in the higher end of the distribution. This is most likely due to the glauconite mineral density which reveals densities up to 2.95 gm/cc. Flint layers are more likely

¹These values were retrieved from [Mindat](#).

to follow the density of the surrounding rock due to the low thickness range. The hardground facies only consist of one measurement in the F05-04 well, therefore peaking in the 2.70 – 2.75 gm/cc bin.

The sandstones of the F17 wells are expected to have an ideal density of 2.65 gm/cc of the mineral quartz. However, the peak lies in the 2.70 – 2.75 gm/cc bin. This can be explained by the contaminations of chalk and possible influx of detrital clay content in the system. Sandy chalk facies seem to be limited to the bin, while sandstone facies is more widely distributed. This might be due to the higher influx of clay in the system during periods of non-chalk deposition.

4.2.4 Special core analysis

The special core analysis of the chalk comprises whole rock and clay fraction measurements and additional thin section point counting. These measurements were only available for the F14-08, F17-11 and F17-12 cores, therefore limiting their interpretation accuracy. From the clay fraction measurements and point counting, a trend could not be observed.

Figure 4.9 illustrates the relation between CaCO_3 and SiO_2 content in the cores of three wells mentioned above. It is found that there is an approximate linear trend between both contents. In this case, the matching correlation trend is: $\text{CaCO}_3 (\%) = 100 + (-1.35 * \text{SiO}_2 (\%))$. The trendline is force fitted through where 100 % CaCO_3 is matching 0 % SiO_2 . The measurement points are colour coded by the porosity on a scale ranging from low (red) via average (yellow) to high (green). The data reveals that with high CaCO_3 content and low SiO_2 content, the porosity is higher and where the SiO_2 content increases, the porosity decreases.

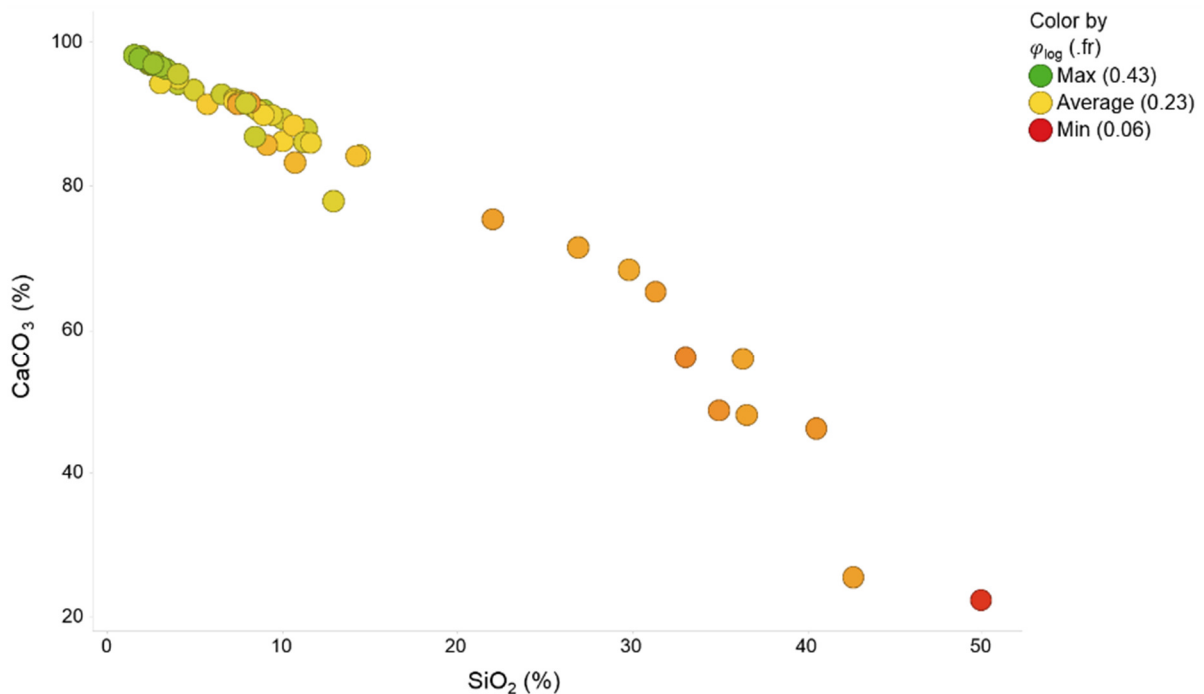


Figure 4.9 – Special core analysis, CaCO_3 vs. SiO_2 content (%). Colour coded with log porosity instead of core porosity due to the larger abundance of log porosity calculations. Note the different axis ranges.

4.3 Facies influence on wireline measurements

An overview of the available well log curves per well are found in Appendix II. Facies influence on the individual wireline logs is explained below.

4.3.1 Bulk density and matrix density

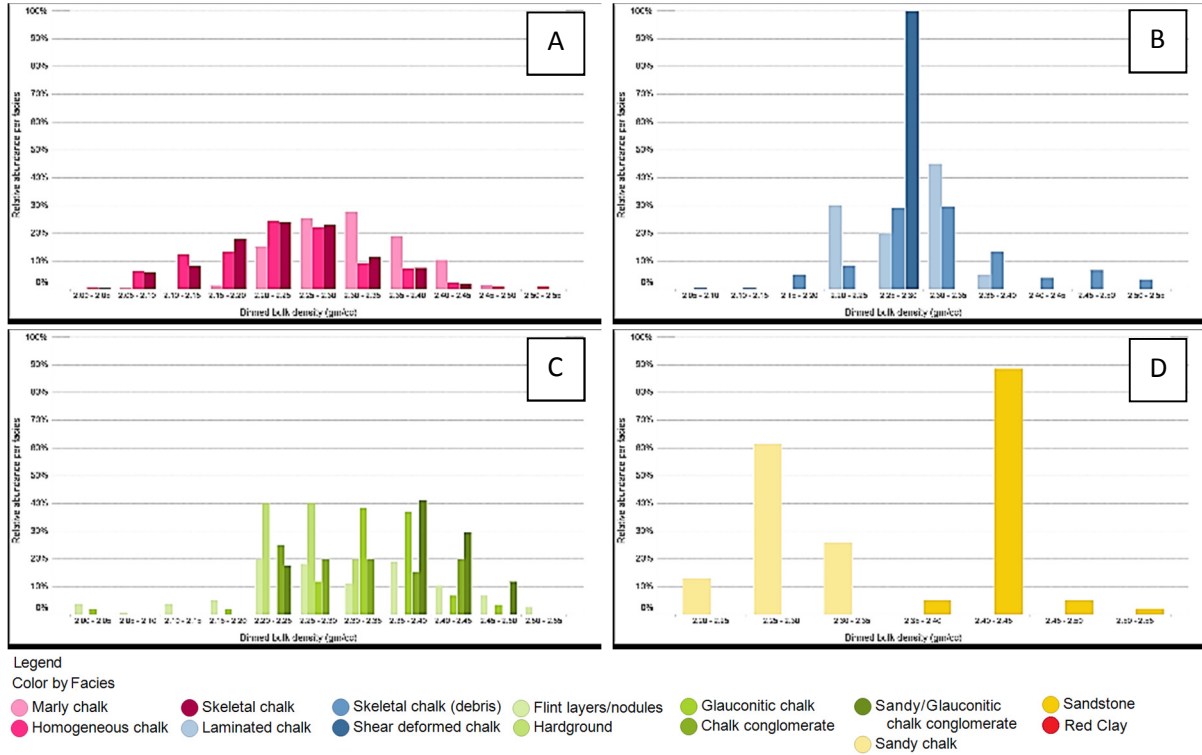


Figure 4.10- Binned bulk density versus the relative abundance per facies. Note the x-axis scale is not the same for all trellises. Trellis per association; A: pelagic, B: redepositional, C: secondary alteration and D: siliciclastic.

Bulk density wireline measurements per facies are shown in Figure 4.10. The distribution illustrates that minor deviations between multiple facies occur. The homogeneous and skeletal chalk both peak in the 2.20 - 2.25 gm/cc bin, while the marly chalk peaks in the 2.30 – 2.35 gm/cc bin. The range where marly chalk bulk density measurements occur is narrower in comparison to the homogeneous and skeletal chalk. The 2.20 – 2.25 gm/cc bin is also where the majority of the redepositional features is situated, where only skeletal chalk (debris) facies is revealing slightly higher density values. The bulk density values for both the secondary alteration association and siliciclastic association have an approximate lower boundary at the 2.20 – 2.25 gm/cc bin, therefore indicating higher bulk densities as a result of these product formations.

In order to compare the bulk density with the grain density, the matrix density was calculated via equation: $\rho_{bulk} = \rho_{fw} \cdot \varphi_{log} + \rho_{matrix} \cdot V_{matrix}$ where ρ_{fw} stands for density of the formation fluid, φ_{log} for wireline log calculated porosity, ρ_{matrix} for matrix density (unknown) and V_{matrix} for volume fraction of the matrix. This matrix density was used to compare the log measurements with the core measurements. Figure 4.11 displays this distribution in the matrix density.

The distribution of the matrix density measurements is similar to the bulk density, with the exception that the measurements are more closely packed in range. In the pelagic association and siliciclastic association, redepositional association and siliciclastic association, the distribution stays approximately the same. Only the shear deformed chalk facies reveals a slightly altered value in comparison to the bulk density, however only one measurement point has been taken.

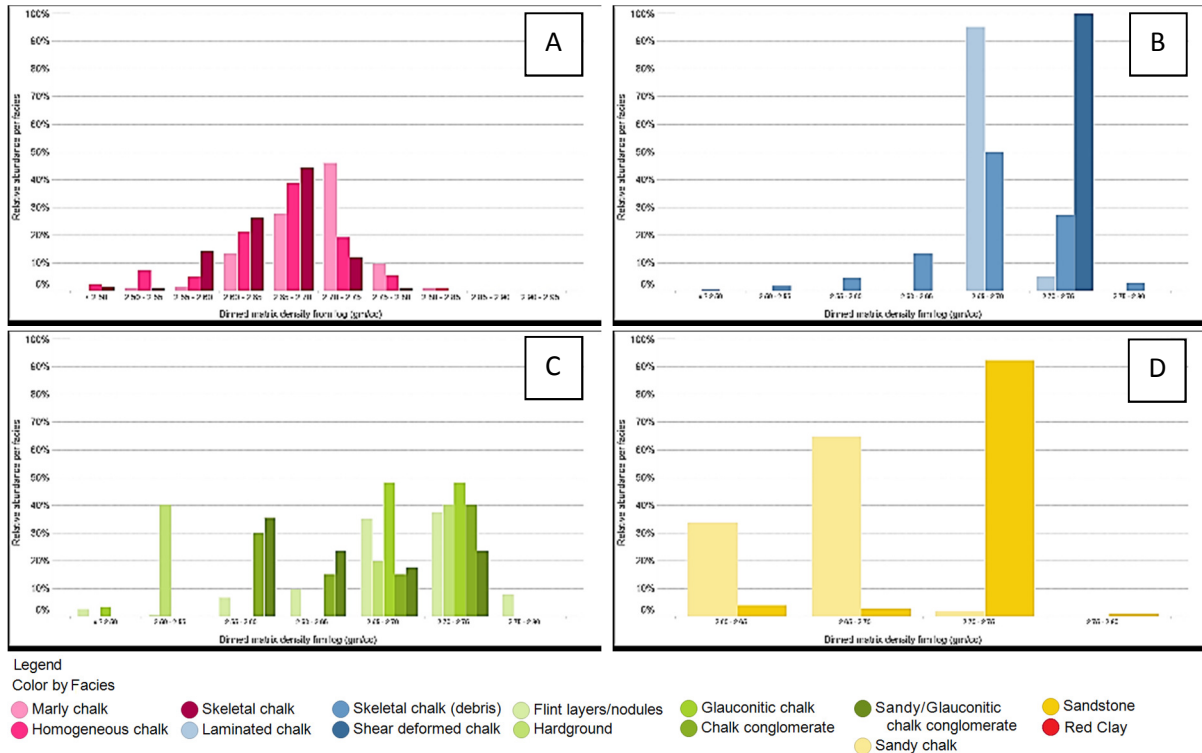


Figure 4.11- Binned matrix density, as calculated from the wireline log, versus the relative abundance per facies. Note the x-axis scale is not the same for all trellises. Trellis per association; A: pelagic, B: redepositional, C: secondary alteration and D: siliciclastic.

The secondary alteration association shows more deviations in the matrix density distribution. Where in the bulk density distribution both the chalk conglomerate and sandy/glauconitic chalk conglomerate show up at the high end of the spectrum, the matrix density appears on the lower end of the matrix density. This is most likely due to the low porosity of these facies in relation to the other facies in the abundance, therefore getting a smaller correction for formation water in the pores.

The matrix density is compared with the grain density of the cores. Most facies show the approximate same patterns, but the grain densities are even closer packed. One exception is found; marly chalk facies shows slightly lower values in the grain densities than the other two facies in the association, while in the matrix density measurements this was the opposite. This can be the result of the overestimation of porosity in the clay as calculated from wireline logs, therefore overestimating the matrix density.

As described above, minor mismatches occur between calculated matrix density and grain density, which is most likely the result of the use of log calculated porosity to calculate the matrix density. Since the porosity calculations has its own margin of error, the matrix density is less reliable than the grain

density measurements. The matrix density measurements is not an indicator for porosity, since the porosity is subtracted from the bulk density in order to calculating the matrix density.

4.3.2 Neutron

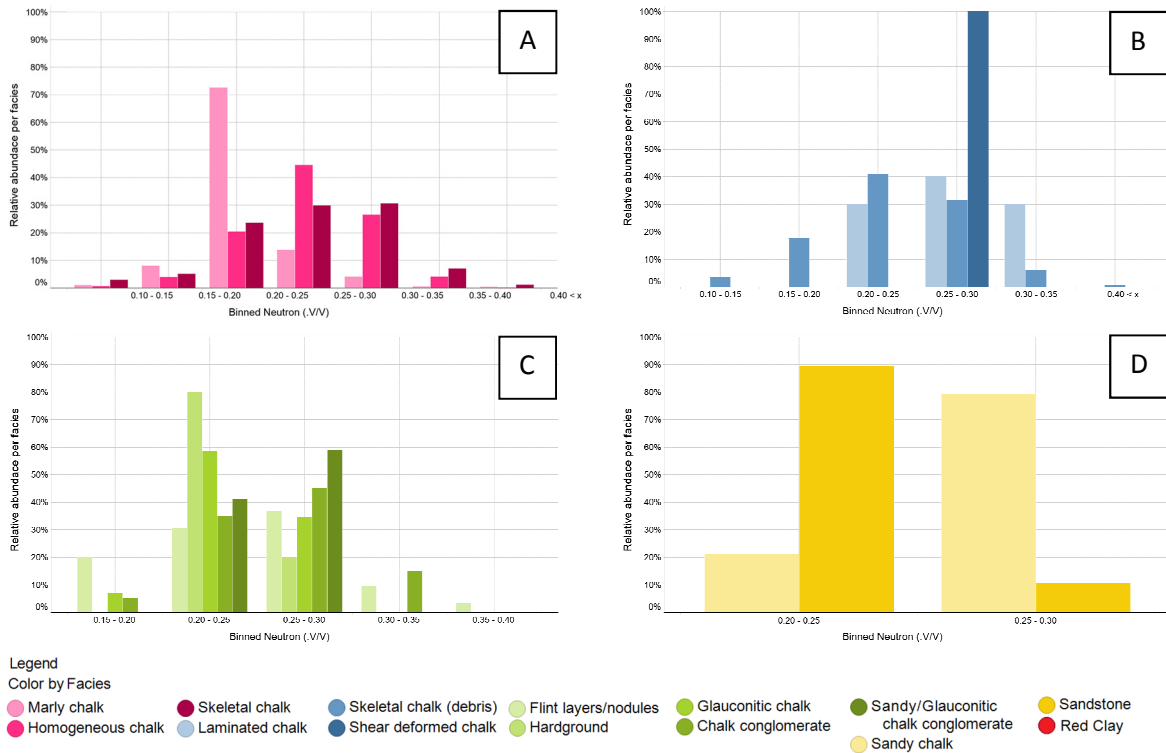


Figure 4.12- Binned neutron measurements versus the relative abundance per facies. Note the x-axis scale is not the same for all trellises. Trellis per association; A: pelagic, B: redepositional, C: secondary alteration and D: siliclastic.

The neutron is thought to be closely linked to the porosity measurements, since the neutron measurement tool detects the hydrogen index which is a direct indicator for porosity. The signature as indicated in Figure 4.12 shows a few trends.

Both the marly chalk and homogeneous chalk facies in the pelagic association show neutron values approximately 5% lower than the log calculated porosity. The facies in the redepositional association and siliclastic association also show lower porosity values than neutron values of approximately 5% difference. The only facies that are overestimated by the neutron is the skeletal chalk facies.

The most significant mismatch between porosity and neutron is found in the sandy/glauconitic chalk facies. This facies peaks in the 15-20% porosity range while the neutron values are found to be focused in the 25-30% range. The only facies that are predicted approximately correct are the skeletal chalk (debris) and the sandy chalk facies.

4.3.3 Gamma Ray

Figure 4.13 illustrates the gamma ray distribution throughout the chalk domain. The measurement points are coloured by facies, however no significant influence on the gamma ray values can be found. This is eclipsed by the effect of differences in measurement equipment, for instance for the F17-11 and F17-12 well, which only have API values higher than 50. This while all the other wells with available gamma ray values limit to approximately 50 API. The F17-10 well does not show deviating gamma ray

values while situated at approximately several hundreds of meters from F17-11 and F17-12. Since the geology most likely does not allow such a difference between these measurements and no difference in measurement tool or calibration can be found, it is suggested that the measurements are deviating due to a geotechnical or borehole issue.

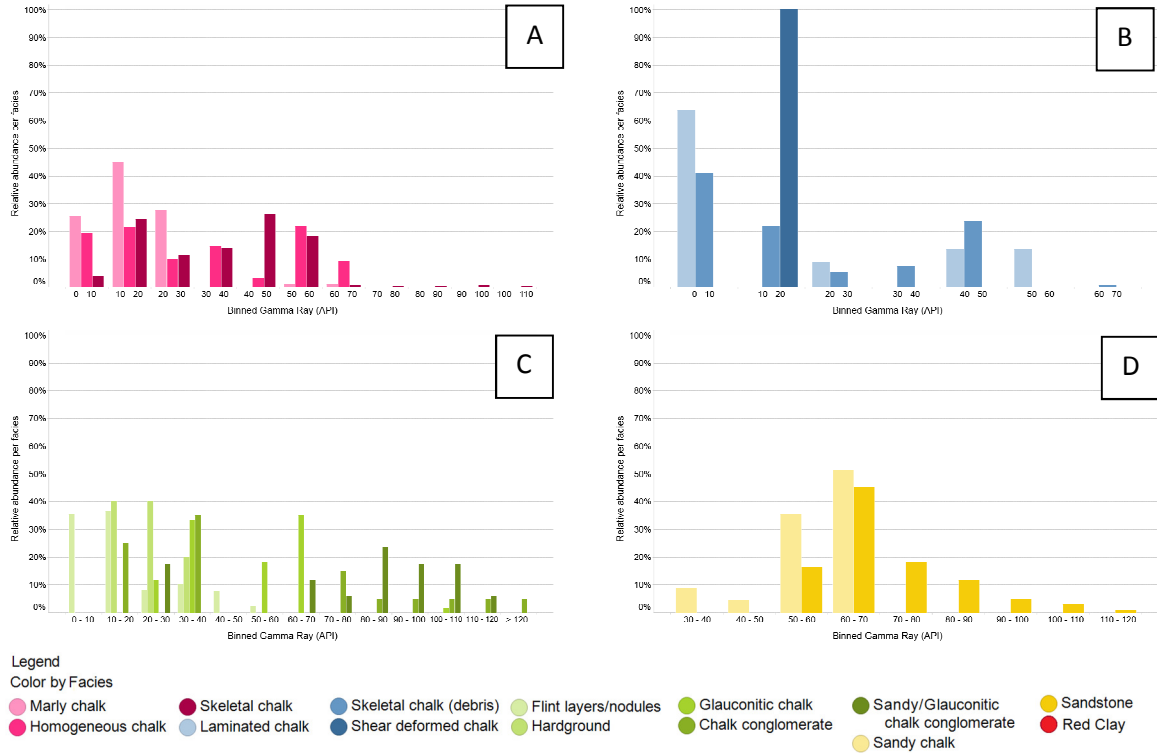


Figure 4.13- Binned gamma ray measurements versus the relative abundance per facies. Note the x-axis scale is not the same for all trellises. Trellis per association; A: pelagic, B: redepositional, C: secondary alteration and D: siliclastic. Values higher than 50 API belong to only the F17-11 and F17-12 wells.

Relative differences in the gamma ray between the pelagic facies are at a minimum. The spread of the marly chalk data is found to be limited while both the homogeneous and skeletal chalk is distributed along the whole range. Another factor is that skeletal chalk generally shows relative higher API values than homogeneous chalk. The association peaks in the 40-50 API bin, where the influence of the F17 wells is not present. Furthermore, marly chalk is expected to have higher gamma ray values than homogeneous and skeletal chalk due to the presence of clay. This is however not the case in the dataset, where marly chalk exhibits lower values.

The influence of skeletal chalk (debris), chalk conglomerate, sandy/glauconitic chalk conglomerate, glauconitic chalk, sandy chalk and sandstone facies relative to the pelagic associations can be seen in the data. These facies all give higher average gamma ray values than the pelagic association even if the higher than 50 API values are filtered.

4.3.4 Artificial intelligence

Several wells with multiple wireline logs were used in order to let neural networks in the program IP predict the facies. The wells used for training are listed in Appendix V. The logs include the neutron, sonic and bulk density log. The program uses neural networks to predict the facies. Training parameters were set to 10 training passes, 1000 epochs per pass and a cross-validation of 30% of the

data. Several of the wells were used for training of the neural network while other wells are left out of the training, therefore making it possible to cross-validate the training results with 30% of the non-trained wells. The gamma ray log was not taken into account since individual influence on facies was not depicted from this log. Only siliclastic association and some secondary alteration facies were depicted by the gamma ray log. Due to this predictability of the siliclastic association and some of the secondary alteration facies on multiple logs, combined with their relative low abundance, it was decided to only predict the limestones in the facies, which were converted to numbers to be used in the program. An overview of the facies accompanying the number are found in below:

Facies number	Facies
1	Marly chalk
2	Homogeneous chalk
3	Skeletal chalk
4	All facies in the redepositional association

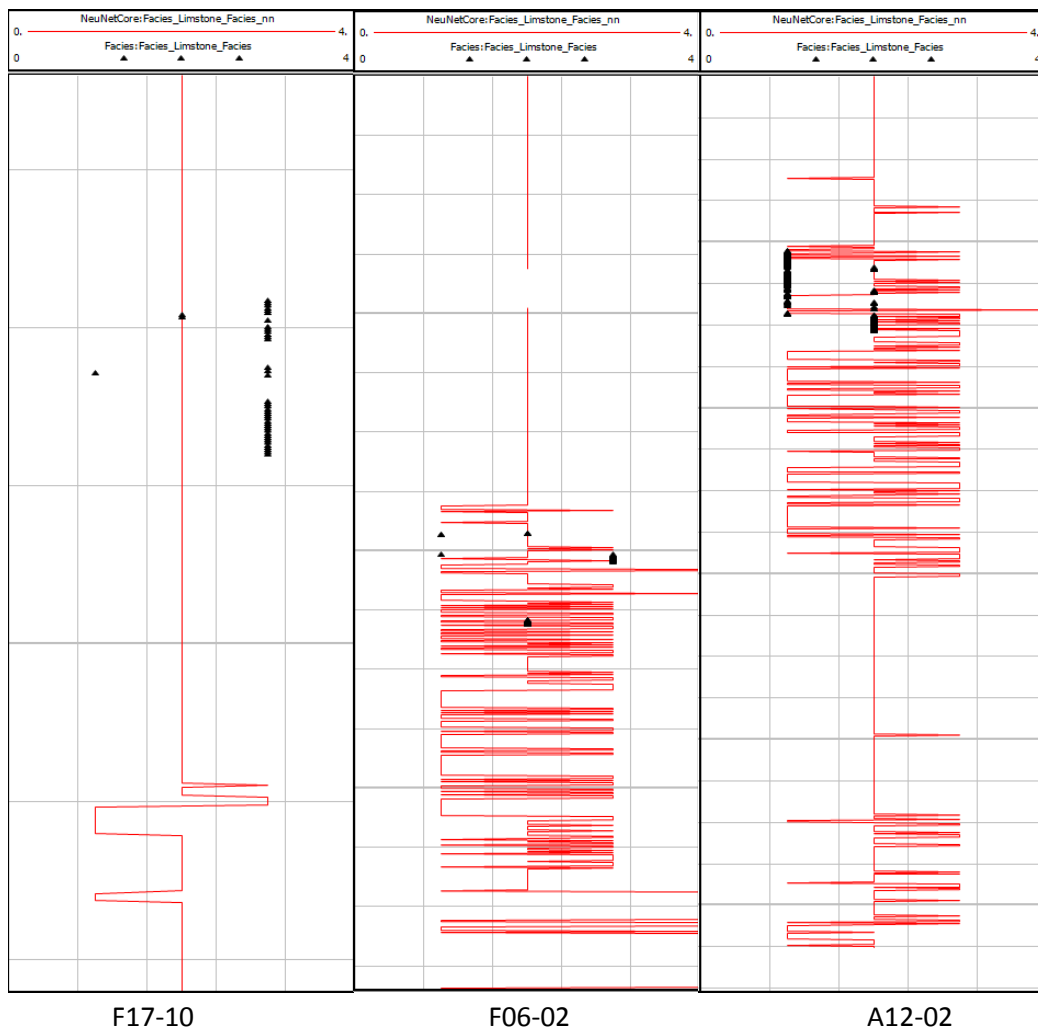


Figure 4.14 – Predicted facies represented by the red line and actual core facies represented by the black triangles from the wells F17-10, F06-02 and A12-02 from left to right. Computed in the program IP.

Skeletal chalk is not picked up by the neural networks, as seen on the left image of Figure 4.14, while marly chalk is also not found by predicted facies as shown in the right figure. This effect is also

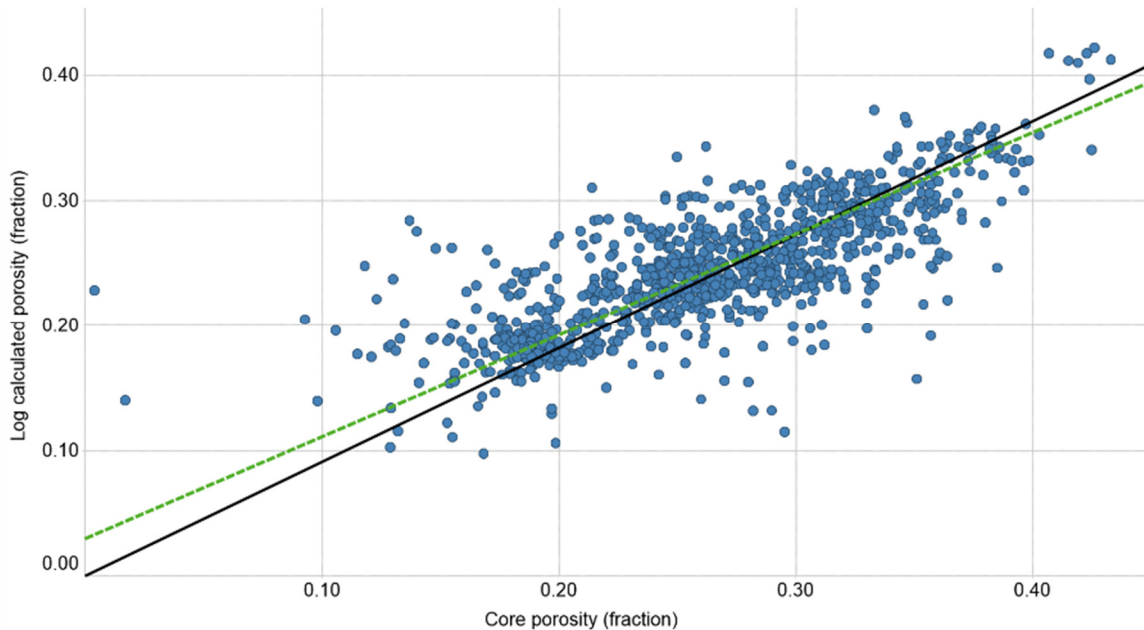
overshadowed by the highly variable amplitudes in short intervals as found in the input logs. Where the input curves show highly irregular surfaces, the facies predictions tend to follow this irregularity, therefore interpreting multiple facies on short notice, while this is not the case in the core data.

4.4 Log calculated porosity

The porosity curve is one of the essential curves for reservoir characterization in the Chalk Group. Section 4.2.1 discusses the influence of facies on the core porosity. Other parameters as depth, spatial position, inversion grade, structural unit and bioturbation grade have their own influence on the porosity of the chalk, which is described in section 4.4.2.

4.4.1 Log porosity vs. core porosity

In an ideal case, the core porosity equals the log calculated porosity. Figure 4.15 reveals that this is not the case, since the porosity correlation represents a deviated trend. A best fit line with a force fit in the origin reveals that the average core porosity is equal to 90.7% of the average log calculated porosity. If it is assumed that both parameters have their own uncertainty, a RMA equation is best suited to explain the situation. The best fitted RMA trend shows an equation where $\varphi_{core} = (1.23 \cdot \varphi_{log}) - 0.04$ with a R^2 of 0.57. No well varies significantly from this trend, therefore the figure shows all data from multiple wells in the same colour, after depth shift of the core data has been applied.



Legend:

— Best fitting line with force fit (0,0) - - - Best RMA Fit

Figure 4.15 – Core porosity versus log calculated porosity. The black line represents the best straight fit line with a forced fit through the origin. The equation of this line is $\varphi_{log} = 0.91 \cdot \varphi_{core}$. The green dashed line represents the best RMA fit with equation is $\varphi_{log} = 0.03 + (0.81 \cdot \varphi_{core})$ with R^2 0.57.

If the individual facies are plotted in this relationship, it is found that some facies follow the ideal trend better than others, which is displayed in Figure 4.16. Where homogeneous and skeletal chalk follow the trend, marly chalk and flint layers/nodules seem to deviate more. The marly chalk seems to have an overestimated log porosity while the log porosity of the flint layers is generally underestimated.

Marly chalk is also found in the deeper depth ranges in the A12 wells. The three pelagic facies, which have the highest abundance of measurements, are separated from the trend to investigate their individual influence on the porosity relationship. These relationships are listed below.

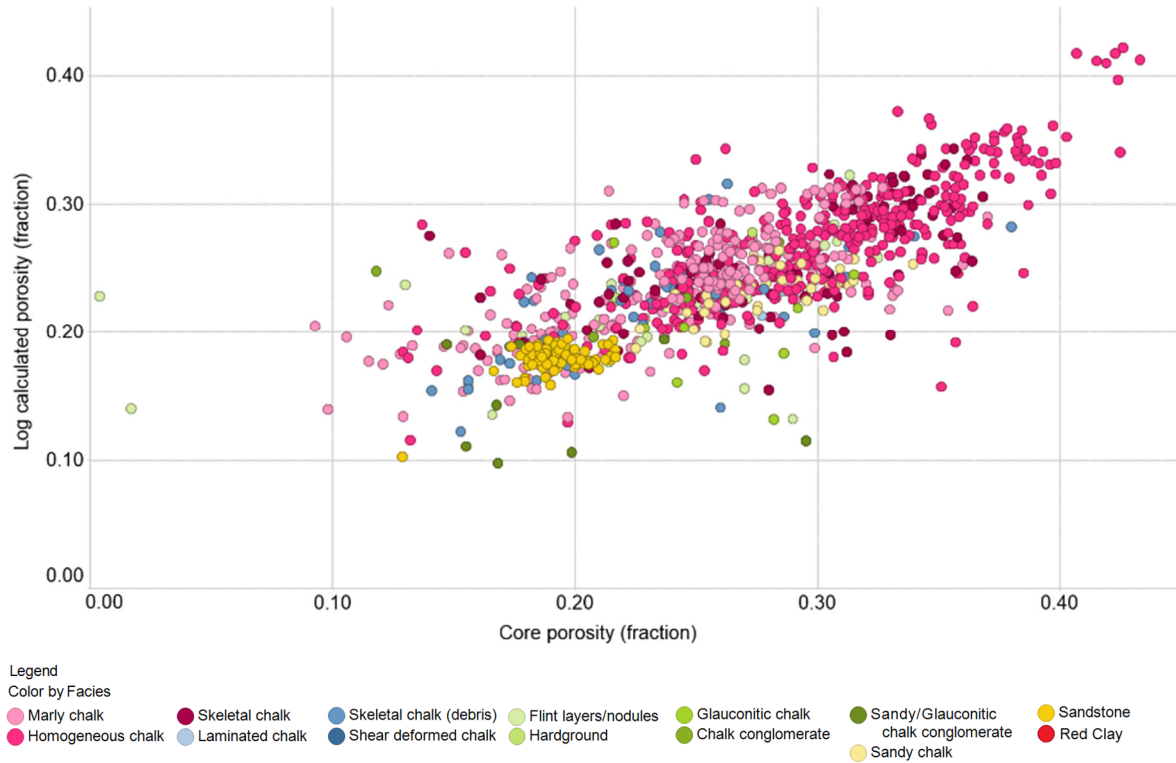


Figure 4.16 - Core porosity versus log calculated porosity colour coded by facies.

Core porosity vs. log porosity	RMA Formula	R ² value
All measurements	$\varphi_{core} = (1.23 \cdot \varphi_{log}) - 0.04$	0.57
Marly chalk	$\varphi_{core} = (1.27 \cdot \varphi_{log}) - 0.06$	0.45
Homogeneous chalk	$\varphi_{core} = (1.19 \cdot \varphi_{log}) - 0.02$	0.57
Skeletal chalk	$\varphi_{core} = (1.35 \cdot \varphi_{log}) - 0.07$	0.17
All other facies without pelagic	$\varphi_{core} = (1.33 \cdot \varphi_{log}) - 0.05$	0.37

The distribution of all log calculated porosity per facies is shown in Figure 4.17. Compared with the core porosity, all facies show the approximate same normal porosity distribution. However, some minor deviations can be found as shown in Figure 4.17.

Where both the marly chalk and homogeneous chalk are slightly underestimated in comparison to the core porosity, the skeletal chalk porosity is more significantly underestimated by the log porosity calculation. This occurs with a magnitude up to 0.10 fraction. Also the secondary alteration and siliciclastic association distribution indicates consistent lower values than the core porosity, in the order of 0.05 magnitude. The relative patterns in the secondary alteration and siliciclastic association are remained, however the log porosity does not seem to show up on the higher side of 25% where the core porosity is not limited on that side.

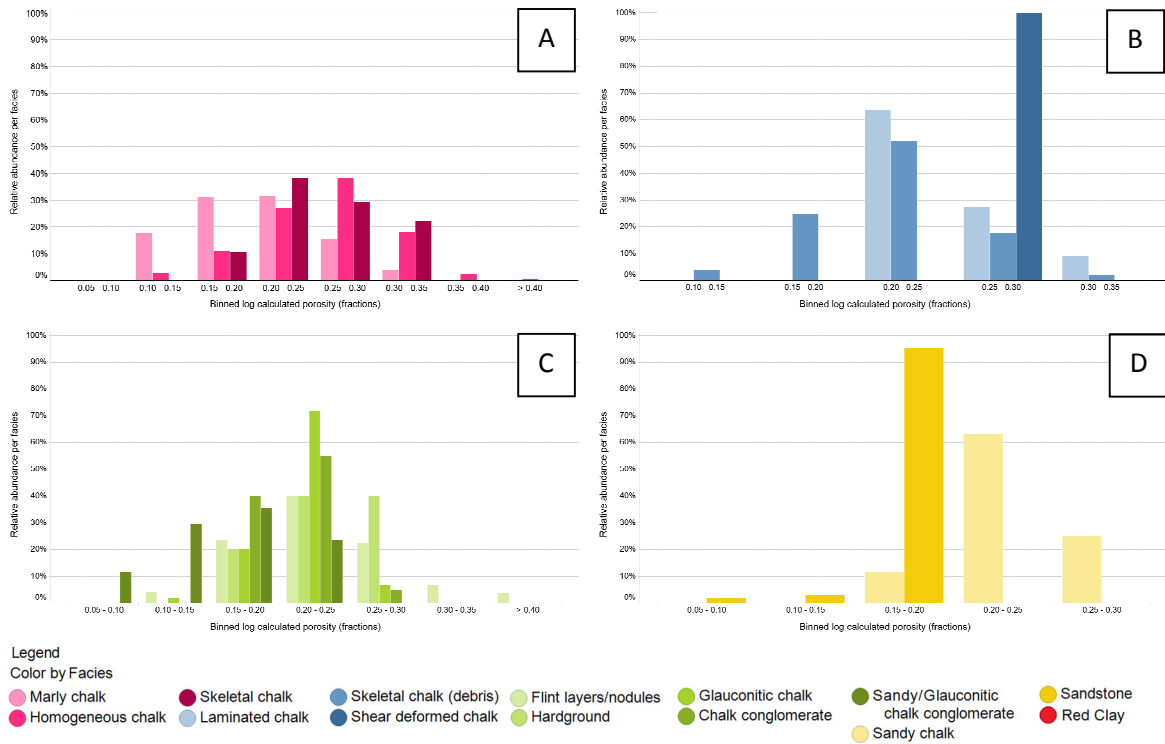


Figure 4.17 – Binned log calculated porosity versus the relative abundance per facies. Note the x-axis scale is not the same for all trellises. Trellis per association; A: pelagic, B: redepositional, C: secondary alteration and D: siliclastic.

4.4.2 Individual wireline effect on log porosity

Bulk density

Figure 4.18 illustrates the wireline bulk density versus the log calculated porosity. Because the density is one of the parameters to calculate the log porosity, there is a trend between the two parameters, where low bulk density equals high porosity and vice versa. Deviation from this trend can be explained by a porosity calculation of the well based solely on neutron, density or sonic. The values with the highest calculated porosities are from K13-A-10, with a porosity calculation based on sonic data.

It is found that lower porosity measurements occur with the same density, which might be explained by the fact that these are gas bearing wells. The density of hydrocarbon bearing chalk is slightly lower than for water wet or dry chalk, therefore suggesting that the porosity is estimated lower. These include F02-A-03 and F02-05. However, this trend is not seen in all hydrocarbon bearing wells as for instance the F17 wells do seem to plot on the observed trend. Due to this possible presence of hydrocarbons, a split in the data seems to occur. At the higher porosities, two individual porosity versus bulk density seem to occur, where lower calculated porosity with same bulk density seems to appear in the hydrocarbon bearing well as described above.

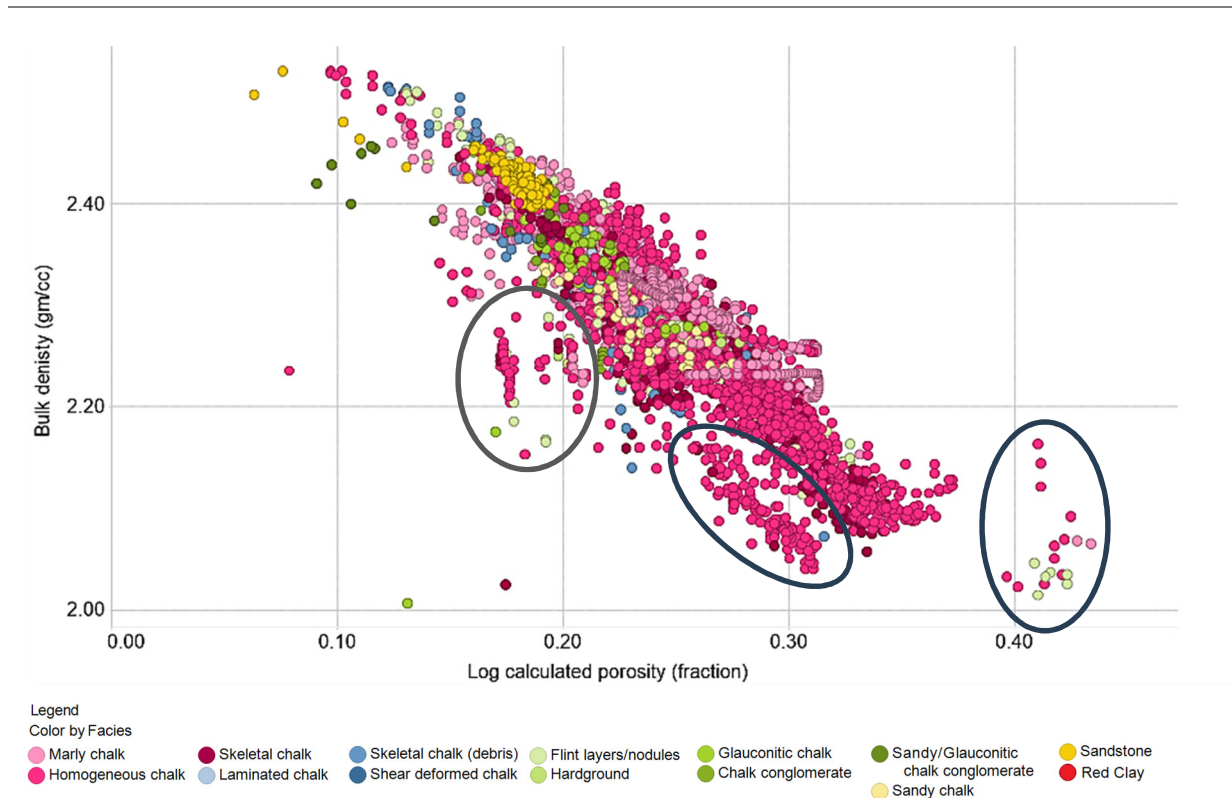


Figure 4.18 – Bulk density from wireline logs vs. log calculated porosity. Colour coding by facies. Left circle: F02-A-03, middle circle: F02-05 and right circle K13-A-10.

If F02-A-03, F02-05 and K13-A-10 are filtered, the three most abundant facies in the chalk cores all show their own porosity – density relationship:

φ_{log} vs. bulk density	RMA Formula	R ² value
All measurements	$\varphi_{log} = 1.46 + (-0.53 \cdot \rho_{bulk})$	0.83
Marly chalk	$\varphi_{log} = 1.72 + (-0.64 \cdot \rho_{bulk})$	0.78
Homogeneous chalk	$\varphi_{log} = 1.42 + (-0.51 \cdot \rho_{bulk})$	0.83
Skeletal chalk	$\varphi_{log} = 1.42 + (-0.52 \cdot \rho_{bulk})$	0.79
All other facies without pelagic	$\varphi_{log} = 1.42 + (-0.51 \cdot \rho_{bulk})$	0.79

This relationship between bulk density and log calculated porosity is expected since the bulk density is a major influence in the porosity calculation via this path, therefore these formulas are only handy when no initial porosity calculation is conducted.

Neutron

The neutron wireline log is another frequently measured log, of which the chalk measurements are displayed in Figure 4.19 against the calculated log porosity. Generally, a higher neutron values equals a higher porosity value. This is due to the fact that the neutron measurement tool does measure the hydrogen index in the chalk, where hydrogen is captured in the pore space.

Two deviating trends can be found in the figure representing the FRA-01-S1 and BRG-01 well. FRA-01-S1 is known from other logs to deviate from certain trends, however the BRG-01 well has not been

mentioned before. The trends both lie at an approximate constant neutron value while the log calculated porosity is varying significantly. Both porosity calculations are primarily based on sonic. Additionally, the BRG-01 neutron log was digitalized since no digital log was yet available. This could account for the differences of these wells.

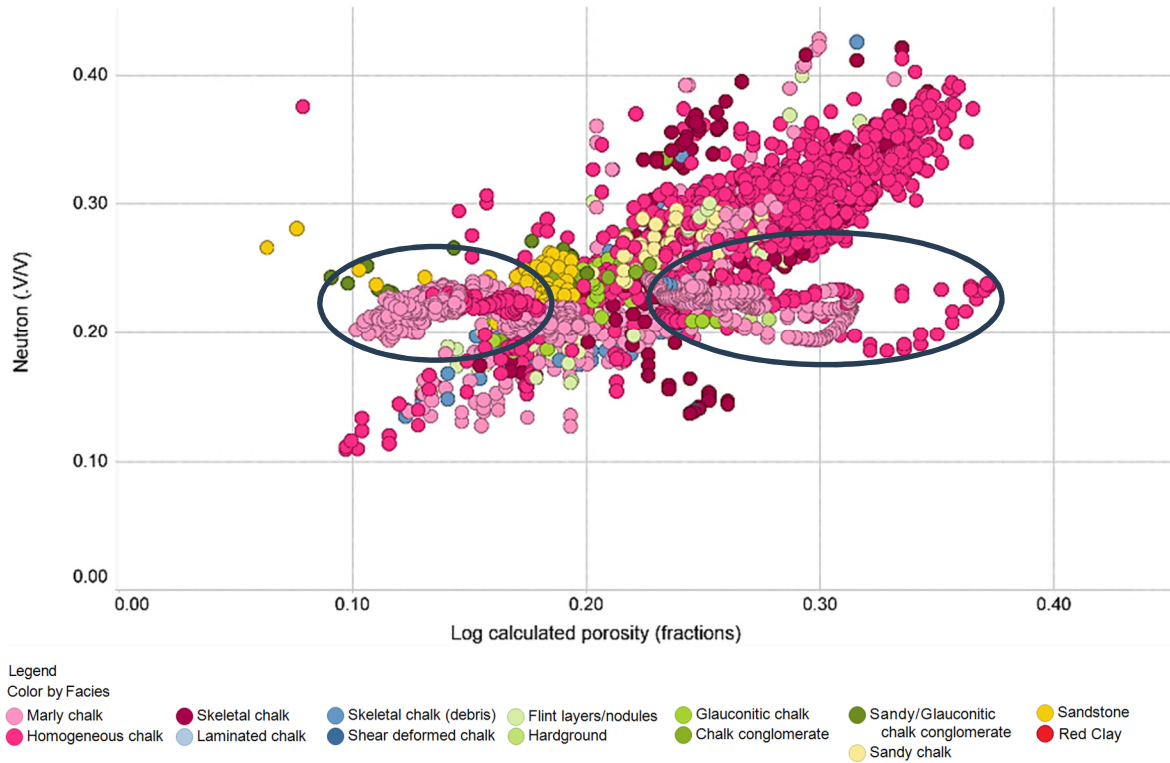


Figure 4.19 – Neutron versus the log calculated porosity colour coded by facies. Left circle: BRG-01, right circle: FRA-01-S1.

If the values from these two wells, FRA-01-S1 and BRG-01, are filtered, the following relationship between neutron and porosity for all facies, the three abundant facies and the rest is found and shown below.

Log porosity vs. neutron	RMA Formula	R ² value
All measurements	$\varphi_{log} = 0.01 + (1.04 \cdot NPFI)$	0.66
Marly chalk	$\varphi_{log} = 0.03 + (0.78 \cdot NPFI)$	0.65
Homogeneous chalk	$\varphi_{log} = -0.03 + (1.03 \cdot NPFI)$	0.68
Skeletal chalk	$\varphi_{log} = 0.05 + (0.74 \cdot NPFI)$	0.43
All other facies without pelagic	$\varphi_{log} = -0.04 + (1.03 \cdot NPFI)$	0.55

For this wireline log, the correlation with the log calculated porosity is less than for the bulk density. This is however not expected since the neutron wireline log is also a log which is used for porosity calculations.

4.4.3 Additional factors influencing log porosity

In this chapter, the influence on individual parameters on the log calculated porosity. The parameters that are investigated are depth, biostratigraphic unit, well position, regional inversion grade and bioturbation grade.

Depth

Most of the wells have a porosity decline curve throughout the chalk interval. However, some specific intervals in certain wells show an increasing porosity with depth. This is the case in the A12-01, A12-02, F06-02 and F17-12 as illustrated in Figure 4.20.

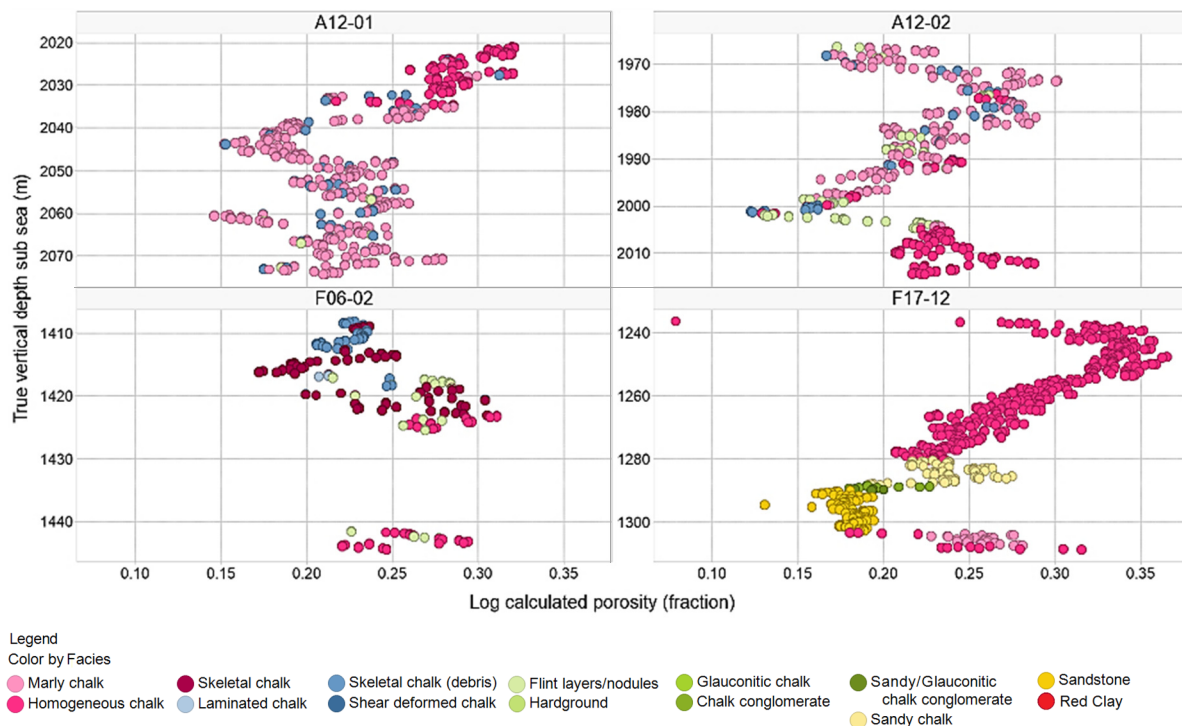


Figure 4.20 – Porosity increase with depth in four wells: A12-01, A12-02, F06-02 and F17-12. Colour coded by facies. Note that the depth scale is different for each visualization.

The A12-01 middle part and A12-02 top half reveal an increase in porosity over these intervals, which both consists of the marly chalk facies with intercallations of skeletal chalk debris facies. These porosity increases can not be explained by either facies or bioturbation grade.

The increase with depth at the bottom of A12-02 and F17-12 can be interpreted as a change from a lower porous to a more porous facies. In the case of A12-02, this is explained by an overall change from marly chalk to homogeneous chalk. This transition coincides with the change from Danian to Maastrichtian biostratigraphy. The F17-12 well discloses a transition from sandy chalk and sandstones to homogeneous chalk.

F06-02 is another complicated porosity increase. The top part is mainly redepositional chalk association which changes with depth to skeletal chalk and homogeneous chalk. It may be that the top part of the skeletal chalk is influenced by diagenetic processes or infill of primary voids by the overriding redepositional unit, therefore changing the porosity of the top skeletal part.

Biostratigraphy

Figure 4.21 presents the porosity measurements in depth, colour coded by biostratigraphy. Several trends can be found in the data.

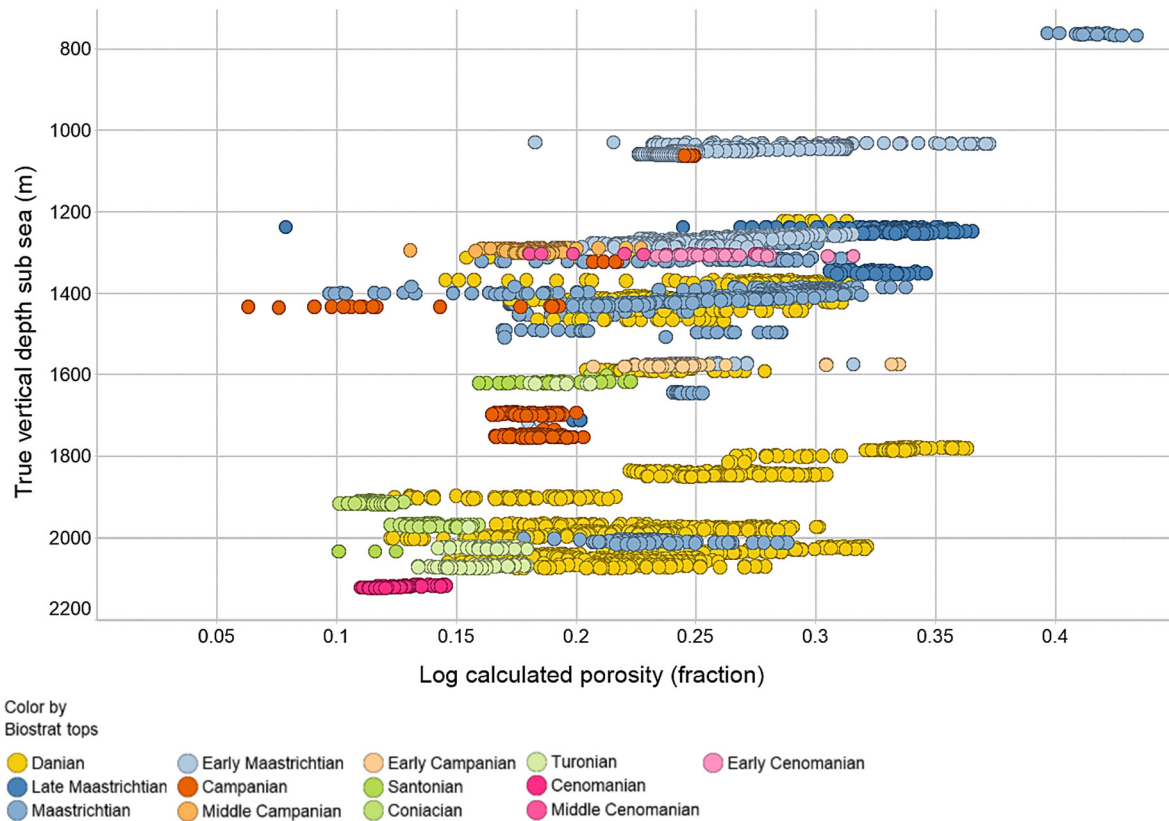


Figure 4.21 – True vertical depth subsea (m) versus log calculated porosity (fraction), colour coded by biostratigraphy.

Danian Chalk reveals a large range in porosity distribution. Furthermore it shows generally higher porosities than the other biostratigraphic units in the deeper depths domains. At depths of approximately 1200 tot 1500 meters, the Danian is only topped off in porosity values by Maastrichtian chalk. The general porosity values seem to decrease rapidly into Campanian. This is not valid for the whole Campanian, while Early Campanian values coincide with Danian and Early Maastrichtian values around approximately 1600 meters depth in F09-02. The oldest chalk ranges from Santonian to Cenomanian, of which the majority is found deeper than 1600 meters. The porosity values for these rocks are significantly lower than those of the Danian and Maastrichtian chalk in the same depth range.

Well position

The position of the well, and thus the cored section is taken from seismic imaging. Where the top of the well is taken is used as a discriminant in this case. Changes in individual well between top and flank of a salt diapir are not taken into account.

The basinal setting well position discloses that the porosity is relatively medium to high above 1100 meters depth and decreasing with depth. This category consists of two wells; BRG-01 and FRA-01-S1. Non-salt related wells are found near salt structures but the chalk does not seem to be influenced by them. This category has only been found in two wells with low to average porosities; F03-03 and F09-02. Where salt structure are present, the porosities seem to be significantly higher. On top of salt

swells, the chalk features significant higher porosities than the basinal setting, as found in the deepest ranges of the chalk. The wells on the flank and top of the salt diapir demonstrate a large variance in the porosity ranges which is most likely explained by individual facies differences. Even though the variance is large, a clear depth trend where porosity is decreasing, is not seen on this level, but only per well.

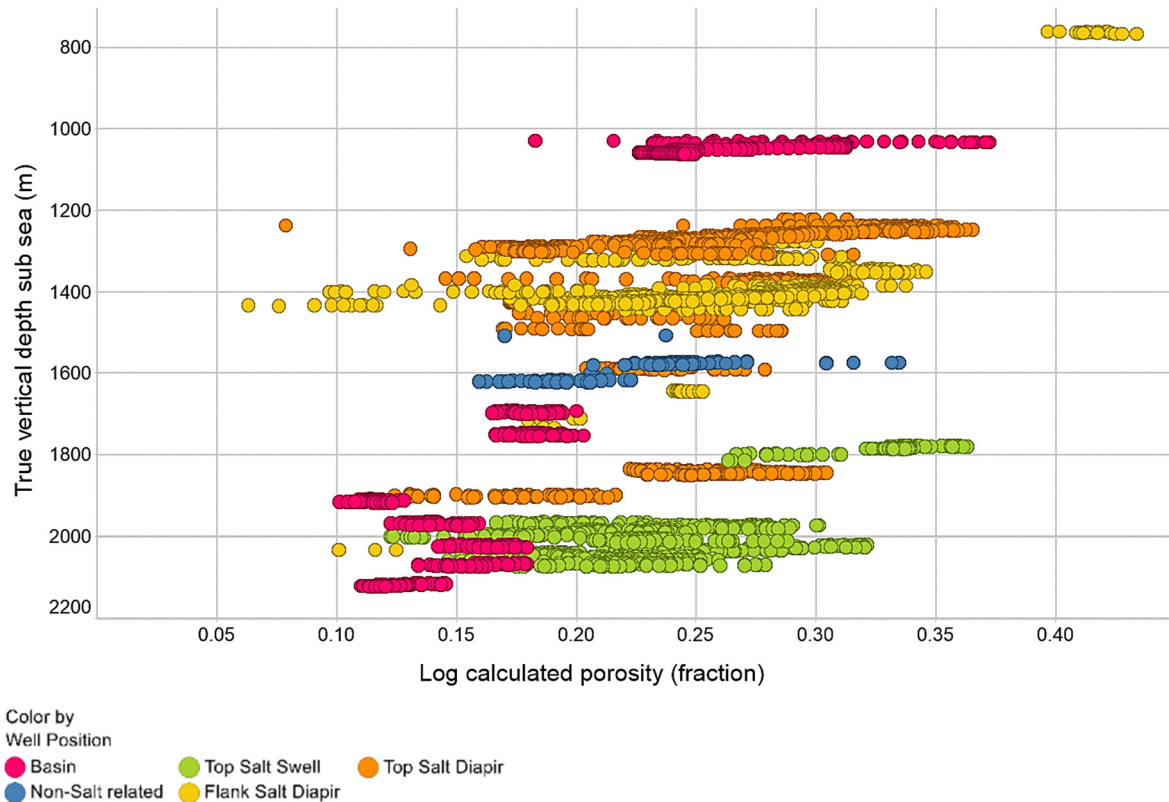


Figure 4.22 - True vertical depth subsea (m) versus log calculated porosity (fraction), colour coded by well position.

Regional inversion grade

A regional inversion grade map (Jager et al., 2007) has been georeferenced over the area to see which wells have undertaken a certain degree of inversion. This inversion coincides with or follows the deposition of the chalk. Most of the wells in the Dutch Central Graben, Vlieland Basin and Texel IJsselmeer High are affected by this inversion grade. Figure 4.23 shows the porosity distribution in depth with a regional inversion grade colour coding.

Wells in the range of 1200 up to 1800 meters have an approximate same porosity range than the deeper wells. If the wells that are situated in inversion areas contain their porosity while being inverted, it is expected that the highest inverted areas have lower porosity than wells at the same depth which have been not to low grade inverted. However, the data does not unveil this relationship since the porosity reveals the same range in comparison to the none to low inverted areas. Therefore, inversion grade itself does not seem to influence the porosity, however it might be suggested that accompanying factors with inversion might enhance the porosity.

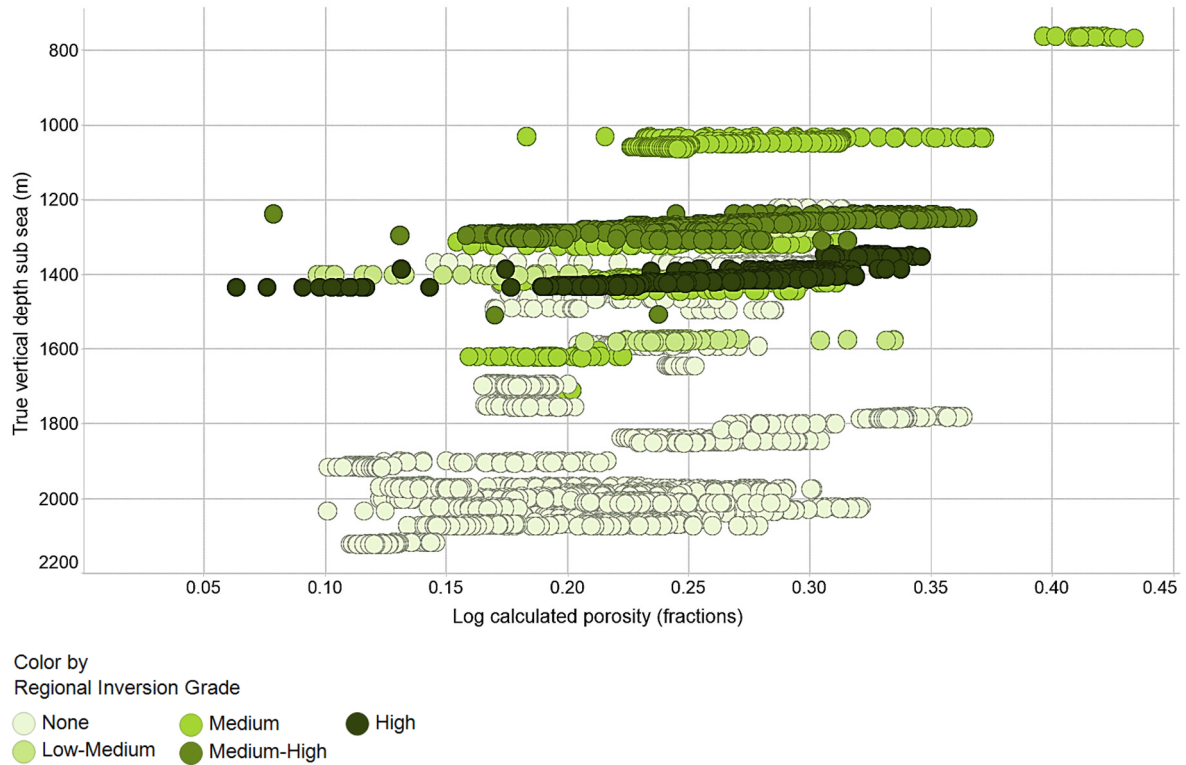


Figure 4.23 – Regional inversion grade as discriminator of log calculated porosity and true vertical depth subsea.

Bioturbation grade

The grade of bioturbation has not been determined in all wells, therefore only a few of the wells are presented here. Figure 4.24 illustrates the bioturbation grade influence on the porosity in F17-10, F17-11 and F17-12. In F17-12 it can be seen that the bioturbation grade changes when going from homogeneous to marly chalk. The none bioturbated marly chalk and lower homogeneous chalk reveal higher porosities than the upper medium bioturbated chalk. However, the homogeneous chalk is situated on top of the chalk section and only has 4 measurements therefore limiting the conclusion.

The deeper measurements are situated in F17-11. Here the bioturbation grade in the skeletal chalk is lower than in the homogeneous chalk beneath. The boundary between those two grades coincides with the boundary of the facies change. At the lower part of the F17-11 well, the bioturbation grade is changed from high to low within the homogeneous chalk. However, this trend seems to be determined by the deeper lying sandstones which lower the porosity of the above lying chalk.

Facies in the pelagic association shows significantly more bioturbation than secondary alteration or siliciclastic input associations. This is due to the fact that the bottom waters are required to be oxygenated in order to allow the fauna to bioturbate the chalk. With siliciclastic input, the oxygenation is not persisted and therefore minor bioturbation is found in those layers.

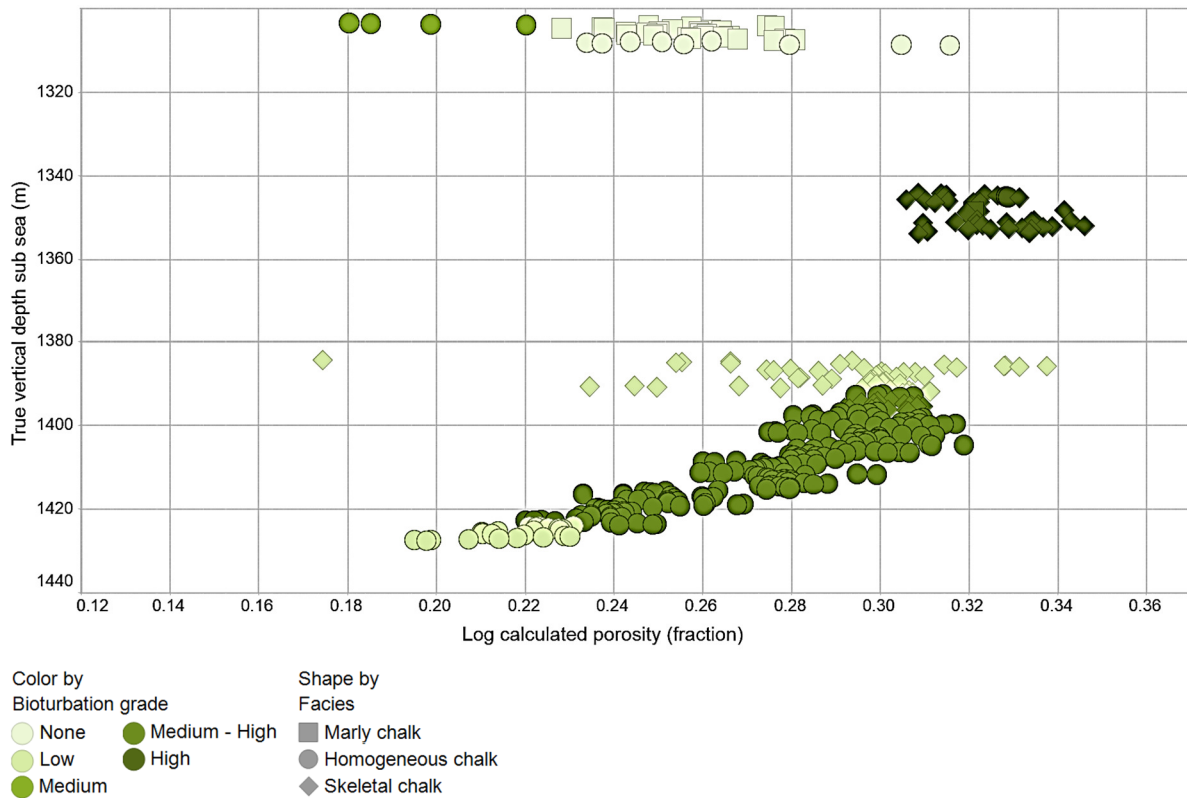


Figure 4.24 – Bioturbation grade (colour coding) in the pelagic association of wells F17-10, F17-11 and F17-12. Shaped by facies.

4.5 Sonic wireline trends

4.5.1 Log calculated porosity

All sonic measurements are displayed against log calculated porosity in Figure 4.25. The general trend is that higher sonic measurements equal higher porosity. This is mainly due to the fact that the larger pore spaces are either filled with water or hydrocarbons, therefore increasing the sonic value. A large variance is found in the data, where some minor deviations can be found. The K13-A-10 well has such high sonic values that these are filtered out of this graph as this will distort the picture.

The sonic measurements of A12-01, F02-05 and BRG-01 are deviating from the others. A12-01 reveals increasing sonic measurements with the same approximate porosity while F02-05 reveals decreasing porosity values with the approximate same sonic measurement. BRG-01 is found on the low side of the spectrum with low sonic measurements with approximate same porosities. The porosity calculation of A12-01 and BRG-01 are based on a neutron sonic combination while F02-05 is based on only bulk density.

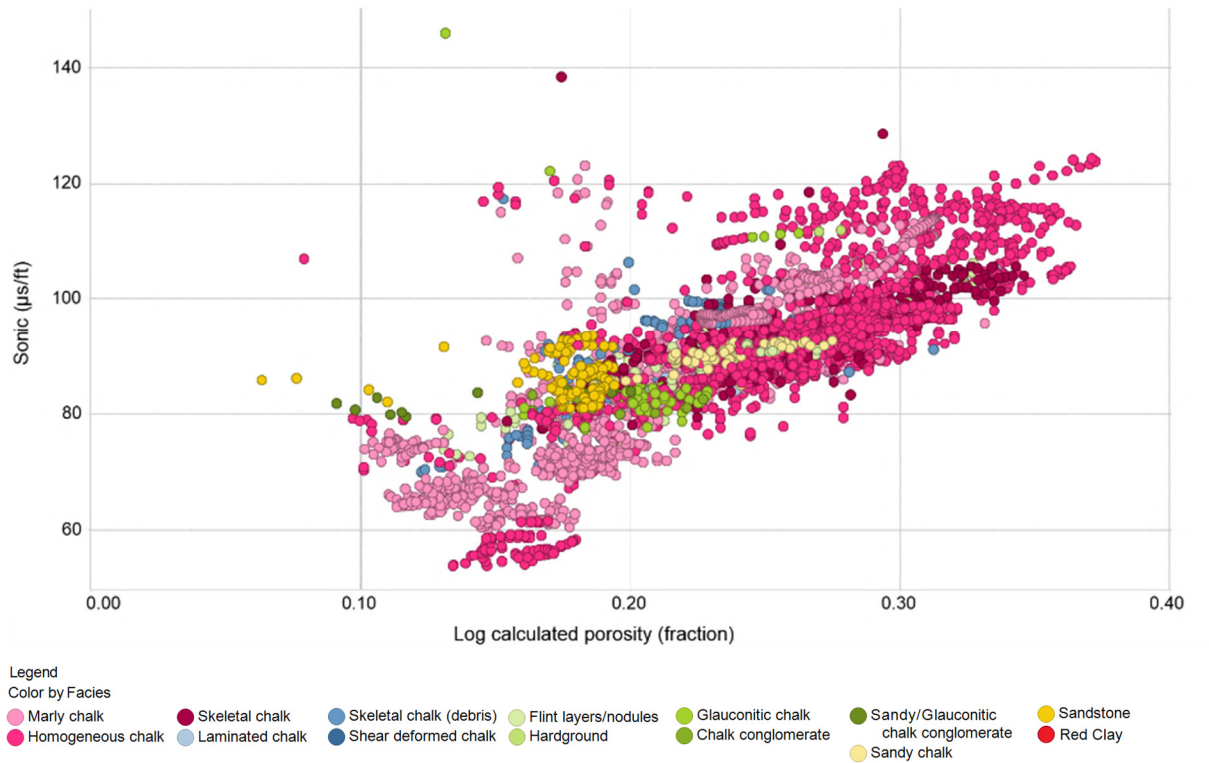


Figure 4.25 – Sonic measurement versus log calculated porosity, colour coded by facies. Note that the K13-A-10 well is not displayed in this figure.

If these three wells, including K13-A-10 are filtered, the following relationships for all facies and for particular facies are found:

Log porosity vs. sonic	RMA Formula	R ² value
All measurements	$\varphi_{log} = -0.21 + (4.87 \cdot 10^{-3} \cdot DT)$	0.77
Marly chalk	$\varphi_{log} = -0.11 + (3.67 \cdot 10^{-3} \cdot DT)$	0.88
Homogeneous chalk	$\varphi_{log} = -0.17 + (4.56 \cdot 10^{-3} \cdot DT)$	0.78
Skeletal chalk	$\varphi_{log} = -0.31 + (6.01 \cdot 10^{-3} \cdot DT)$	0.64
All other facies without pelagic	$\varphi_{log} = -0.27 + (5.43 \cdot 10^{-3} \cdot DT)$	0.63

These equations represent the [Eberhart-Philips](#) relationship (1989).

4.5.2 Facies

Figure 4.26 displays the binned sonic distribution in the Chalk Group. The sonic trend is mostly dependent on the depth of the core with an influence of facies accompanied.

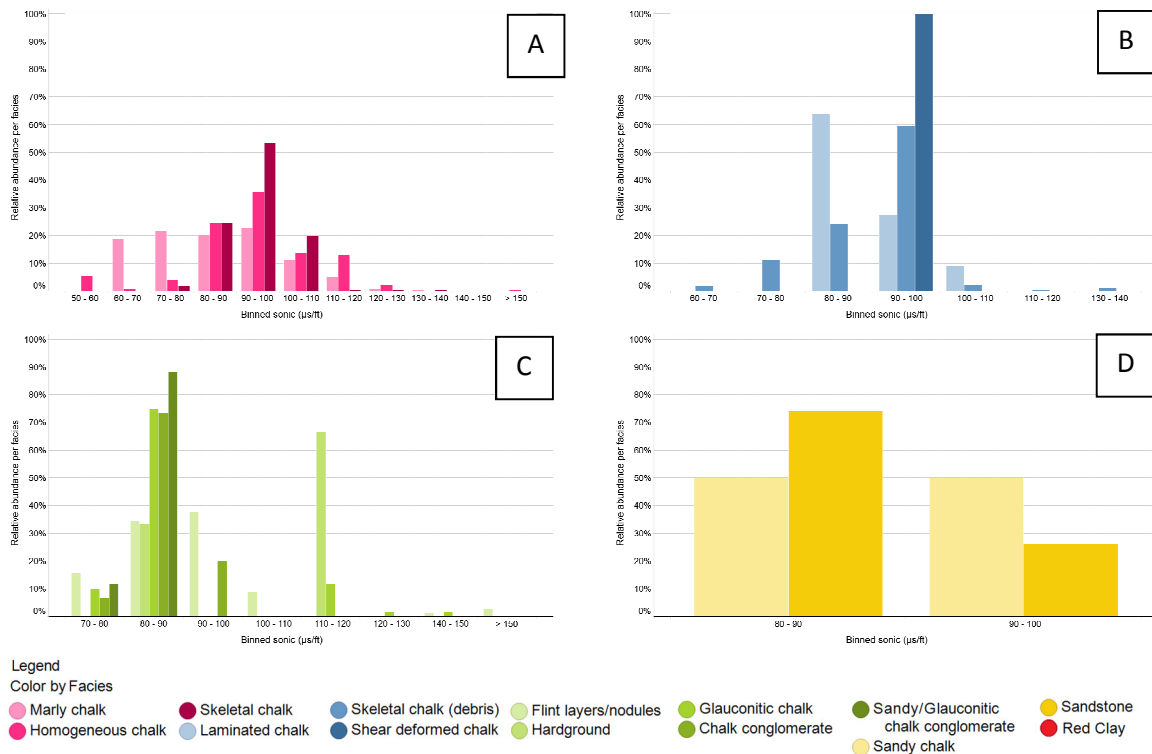


Figure 4.26- Binned sonic measurements versus the relative abundance per facies. Note the x-axis scale is not the same for all trellises. Trellis per association; A: pelagic, B: redepositional, C: secondary alteration and D: siliclastic.

Most of the sonic measurements plot in the 90-100 µs/ft sonic bin. This is especially the case for the pelagic and redepositional association. In the pelagic association, a subdivision between marly chalk and homogeneous / skeletal chalk can be made, where marly chalk shows significant lower sonic values than homogeneous and skeletal chalk. The range of the marly chalk is also much broader than the other two facies. The facies in the redepositional association shows a similar sonic peak, where only the laminated chalk facies is found to have lower sonic values of approximately 80 µs/ft.

Most of the facies in the secondary alteration association and siliclastic association show lower sonic values in comparison to the pelagic association. This is in the order of 10 µs/ft. Only the hardground formation and sandy chalk seem to focus higher in the sonic distribution, where hardground even exceeds the pelagic facies and peaking in the 110-120 µs/ft. This facies has limited measurement points, therefore limiting the validity of this facies, while it is expected that the densely cemented chalk should indicate relative high velocities and thus low sonic values.

The influence of facies on the sonic measurements is explained in section **Error! Reference source not found.** In this section, the influence on the sonic with depth is explained with additional parameters. Sonic measurements are an indicator for seismic wave travel time through a rock, therefore also for seismic velocities. The velocity from sonic travel time is calculated via: $V_{sonic} = \frac{304,800}{DT}$ where V_{sonic} is in meters per second and DT in µs/ft.

4.5.3 Depth

The sonic values are displayed versus depth in Figure 4.27. All available sonic measurements from all available wells are displayed in the figure and no filtering has taken place. The sonic measurements do show a trend with depth where generally the deeper laying chalk has lower sonic measurements and

vice versa. It is important to keep in mind that all the wells show their own decrease of sonic and that this figure shows only the relationship between the different wells.

Several wells deviate from the sonic velocity trend, which are mainly A12-01 and A12-02. They give higher than average sonic velocities in the deepest parts of the chalk sections, while K13-A-10 is the shallowest, giving a broad range of sonic measurements. If these wells are filtered, the best line fit shows a trend where: $DT = 166.36 + (-0.05 \cdot TVDSS)$ which equals $V_{sonic} = 897.80 + (1.73 \cdot TVDSS)$ with a R^2 value of respectively 0.58 and 0.62.

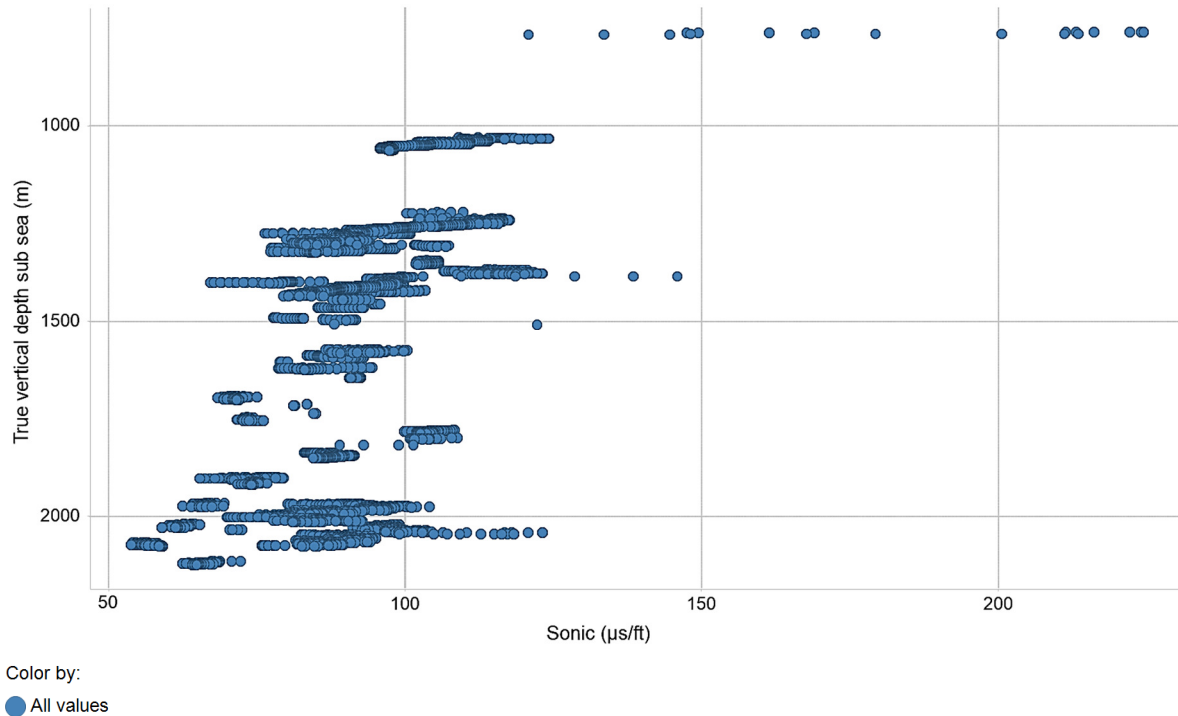


Figure 4.27 - Sonic measurements with increasing depth of all measurements in the cored chalk sections.

Only several wells have enough measurement points to show the individual facies influence on the sonic in those particular wells. These wells include A12-01, A12-02, F17-11 and 17-12. The distribution of sonic measurements in their own depth domain are displayed in Figure 4.28.

The five wells show a minor influence of facies on the sonic, however in most wells this is eclipsed by the sonic-depth relationship. In both A12-02 and F17-12, it is found that after a facies change, the sonic increases significantly with depth. In A12-02, this coincides with a change from marly to homogeneous chalk via a zone of flint layers and skeletal chalk debris layers. In F17-12, the transition occurs at the boundary between sandstone and homogeneous chalk. A12-01 and F17-11 show also facies influence on the sonic, where both top parts reveal an approximate constant sonic with depth, while the facies underneath reveals the expected sonic-depth trend.

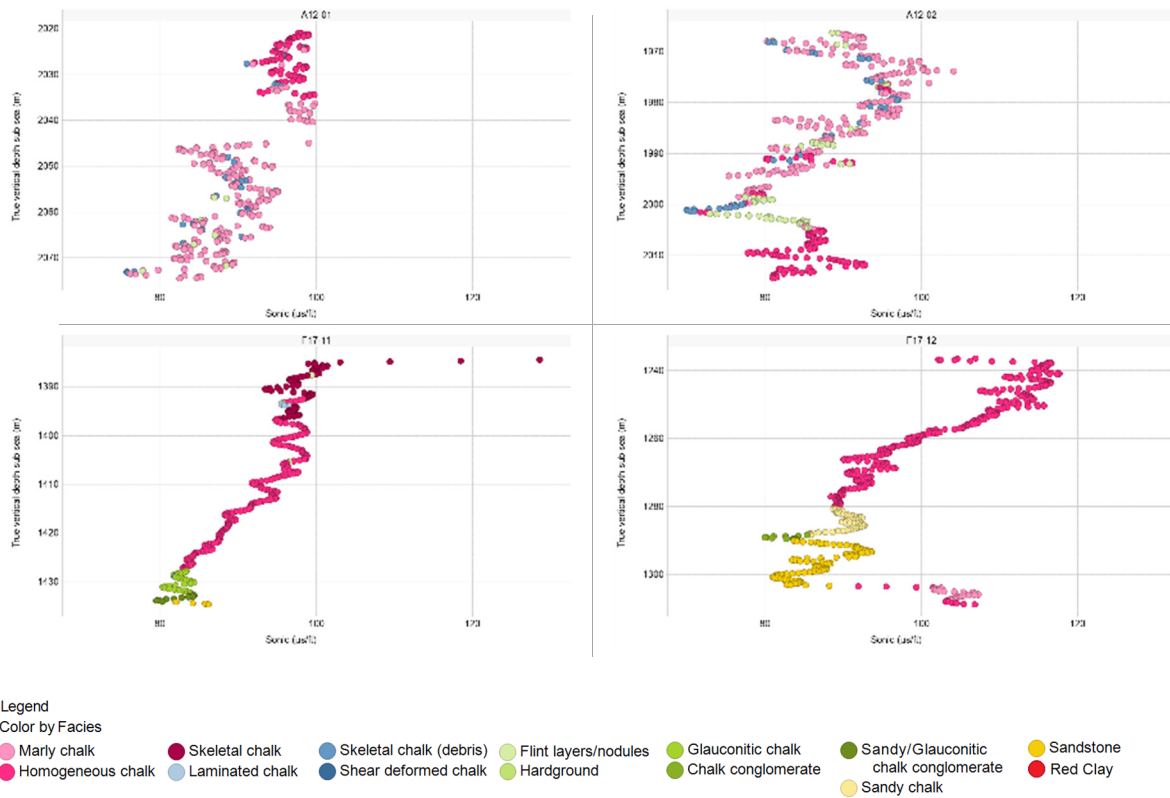


Figure 4.28 – Four different wells with their own sonic – depth relationship, colour coded via facies. Note the different x-axis scales on the visualizations.

4.5.4 Biostratigraphy

Figure 4.29 shows the same sonic distribution, only now colour coded with biostratigraphy. The largest spread in data is found in the Danian section of the velocities, while the other biostratigraphic units follow a narrower trend. This widespread is only the case for the Danian measurements lower than 1700 meters depth.

If the values of the Danian measurements and the K13-A-10 measurements are filtered from the data, the sonic shows the following trend: $DT = 158.14 + (-0.05 \cdot TVDSS)$ which equals $V_{sonic} = 444.53 + (2.09 \cdot TVDSS)$ with an R^2 value of respectively 0.69 and 0.70. Figure 4.30 shows the distribution in the Danian section of the chalk only. The found sonic velocities for the Danian are generally higher than for other biostratigraphic units, however, there is no obvious depth trend in the Danian sonic velocities visible. The sonic velocities, even though ranging significantly, have the same approximate centre of gravity throughout multiple wells, with an average of $92.8 \mu\text{s}/\text{ft}$ which is 3326.5 m/s . The figure shows that in the Danian, the homogeneous chalk has a general higher sonic than the marly chalk. The lowest sonic values come from skeletal chalk and marly chalk intermingled with re depositional features and flint.

Wells that include Danian chalk in the cored interval are generally found in the northern part of the Dutch North Sea. Throughout the Danian, the sonic measurements do not show a focus shift in depth but stay approximately the same.

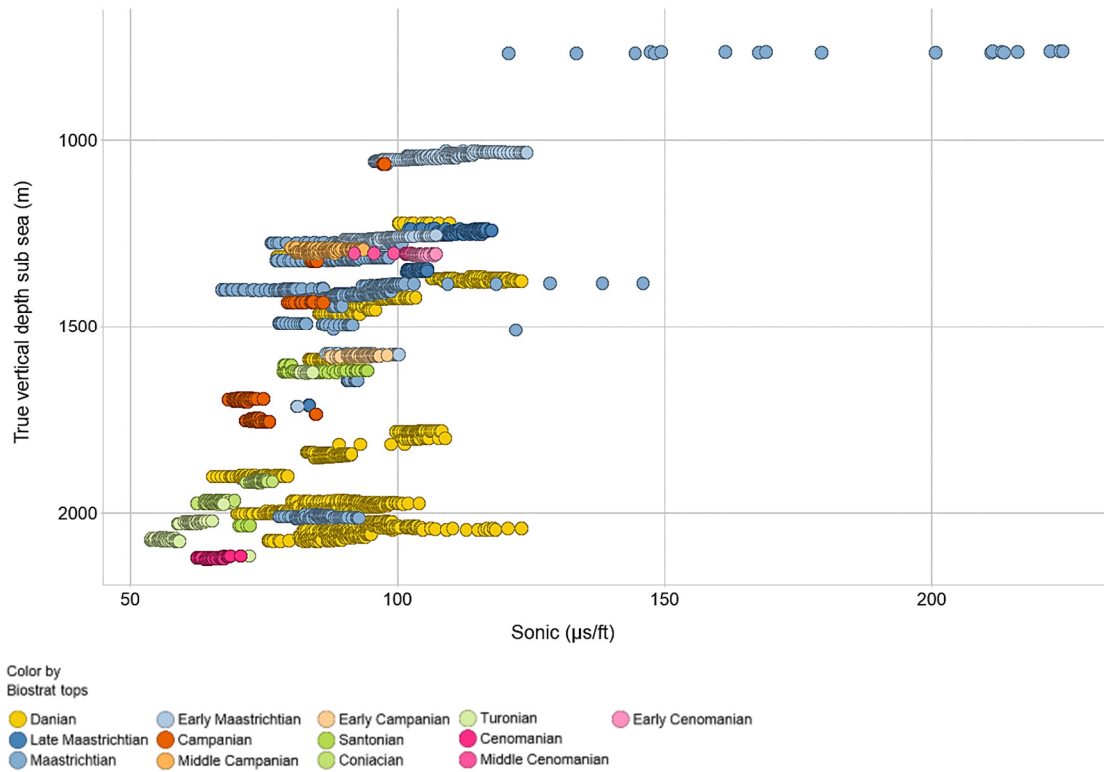


Figure 4.29 - Sonic wireline measurements with increasing depth downwards. Colour coding by biostratigraphy.

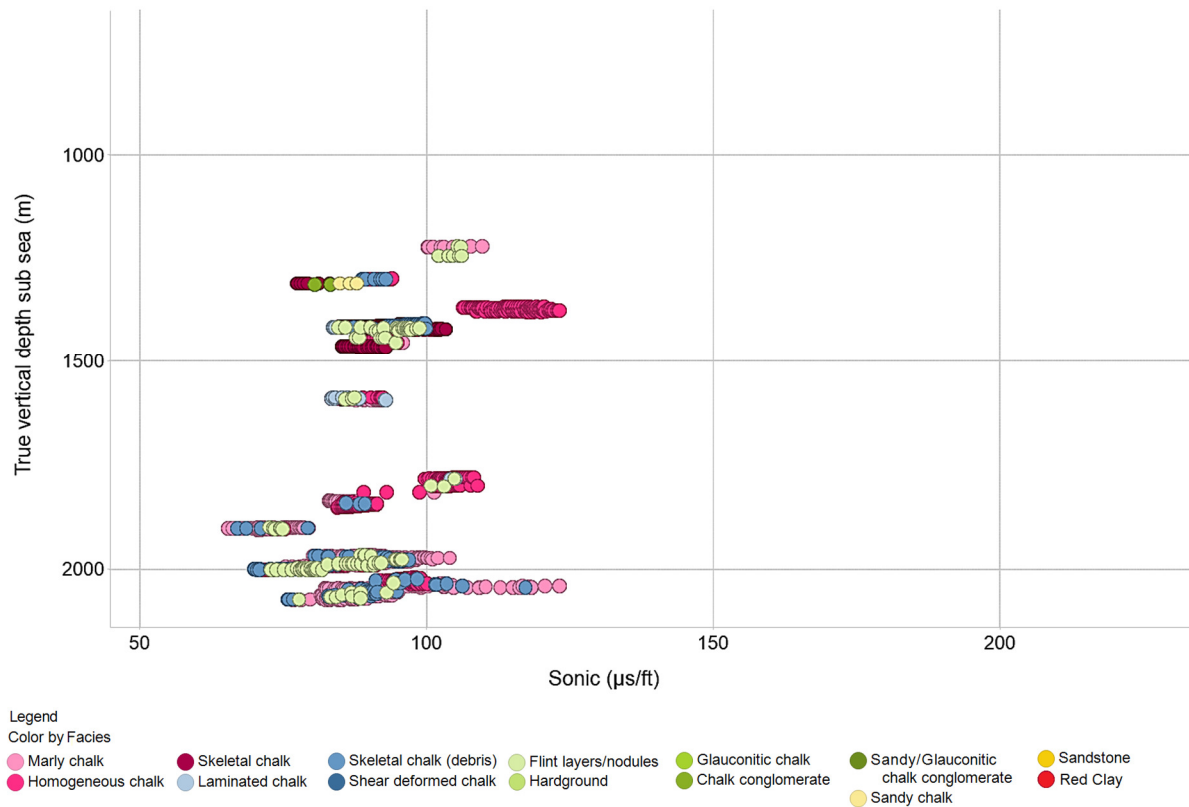


Figure 4.30 - Sonic wireline measurements with increasing depth downwards. Only Danian measurements are displayed. Colour coding by facies.

These biostratigraphic units are captured in three different formations as indicated in section 2.1.3. Where the Ekofisk formation comprises the Danian chalk, the Ommelanden everything from the

Turonian up to Maastrichtian and the Texel formation comprises the Cenomanian chalk. If the Ekofisk formation is filtered from the data, together with the K13-A-10 well and the Maastrichtian A12-02, the data shows the following sonic depth trends:

Sonic vs. depth	RMA Formula	R ² value
All measurements	$DT = 161.23 + (-0.05 \cdot TVDSS)$	0.76
	$V_{sonic} = 307.38 + (2.22 \cdot TVDSS)$	0.80
Marly chalk	$DT = 147.04 + (-0.04 \cdot TVDSS)$	0.90
	$V_{sonic} = 999.22 + (1.80 \cdot TVDSS)$	0.90
Homogeneous chalk	$DT = 179.04 + (-0.06 \cdot TVDSS)$	0.74
	$V_{sonic} = -585.96 + (2.84 \cdot TVDSS)$	0.81
Skeletal chalk	$DT = 207.88 + (-0.08 \cdot TVDSS)$	0.07
	$V_{sonic} = -284.37 + (2.46 \cdot TVDSS)$	0.07
All other facies without pelagic	$DT = 168.82 + (-0.06 \cdot TVDSS)$	0.11
	$V_{sonic} = 754.62 + (2.03 \cdot TVDSS)$	0.11

DT is expressed in $\mu\text{s}/\text{ft}$, V_{sonic} is expressed in meters per second while TVDSS is expressed in meters.

The trend above explains that the marly chalk and homogenous chalk facies show a fairly good correlation with depth. The correlations are significantly higher than the other facies. The skeletal chalk has only a correlation of 7% and all other facies combined 11%. It must be held in mind that the abundances of these facies are lower than for the marly and homogeneous chalk.

5. Discussion

5.1 Improved facies model

Several uncertainties arise while improving the facies model of the chalk. These uncertainties are listed below.

- The redepositional and secondary alteration association both consists of relative small layers. In a core domain, of approximately 15 centimetres in diameter, these layers can be easily miss-picked or miss-interpreted.
- The described shear deformed chalk can also be found on ten-of-meter scale ([Kennedy, 1987](#)) and therefore not be distinguishable in the cored intervals.
- With the presence of relative small layers, convolution of measurements can occur, therefore limiting the interpretation of these layers.
- Thorough bioturbation can destroy depositional and diagenetic features, therefore making it impossible to distinguish it on a core domain.
- Several authors recognized sheet slides in the Chalk Group on seismic ([Kennedy, 1987](#), [van der Molen, 2004](#)). These features are lithified sheets which slide into new positions, therefore remaining their former characteristics, even though they are redeposited. Furthermore, skeletal chalk with low transportation distance might occur as in place skeletal chalk while there are no indications of redeposition.
- Marly laminations with low amount of bioclasts can be interpreted as marly solution seams as well as laminated chalk, even though their depositional processes and probably petrophysical properties are different.
- Glauconite forms as an in situ process, but redeposition of the grains can also occur if the chalk is not sufficiently cemented. When glauconite grains are recovered, no indication of redeposition might be found.
- Conglomerates can be formed due to several different processes as indicated in the facies model, which all can have their own petrophysical signature.

Even though most of the cores are positioned on structural highs, which is related to petroleum exploration, the 'undisturbed chalk' is not cored frequently. It is expected that the undisturbed chalk is similar to the pelagic chalk as mentioned in the facies model (e.g. [Kennedy, 1987](#)). The pelagic association regards an abundance of approximately 85 % in the cored section. Therefore, it is believed that this model and its results are applicable to the undisturbed chalk section. It must be kept in mind that this regards mainly the primary sedimentary structures and that alteration of the products is not taken care of, e.g. fracturing through salt movement.

Volcanic clay

Elf Petroleum claims that the red clay layer found in the F06-02 well is of volcanic origin. Thin section made for this thesis questions that statement, since no evidence for volcanic clay is found in the section. The thin section consists of mainly bioclastic material and glauconitic grains in a reddish matrix as shown in respectively Figure 5.1 A and B. The matrix is too fine grained to be interpreted on microscale, therefore the origin of the matrix is not fully understood.

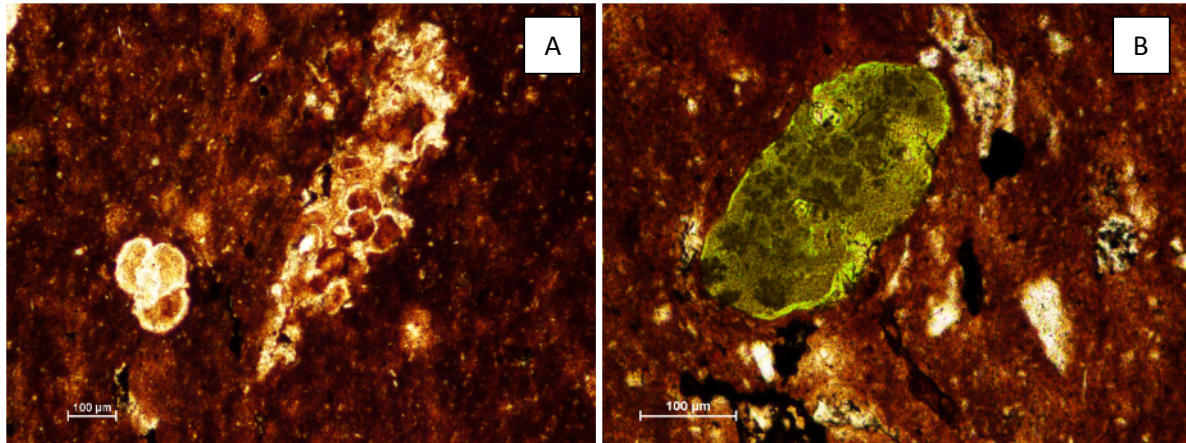


Figure 5.1 – **A:** Recrystallized planktonic foraminifera debris in a reddish matrix. Bioclasts recognized as being foraminifera, even though ostracod debris is also a significant component in the thin section. **B:** Glauconitic grain in red matrix with possible kaolinite (whitish mineral in the lower right corner). Whole rock has a floatstone Dunham classification.

The presence of clay minerals as glauconite and kaolinite, combined with the presence of probable planktonic foraminifera and ostracods in the thin sections are two main indicators that the depositional environment of most of the clays is marine.

Similar products have been found in England and described by [Whitham \(1991\)](#) and [Mitchell \(1995\)](#), where significant occurrences of red chalk intermingled with red clay beds, known as the Hunstanton Formation, are found. These red clay beds are rich in fossil debris as for instance ammonites, belemnites, ostracods and foraminifera. An important main difference between these depositions is that the Hunstanton Formation is deposited in the early Cretaceous Albian, while the chalk in the F06-02 well is believed to be of Danian age. However, the processes forming these layers might be similar.

5.2 Chalk facies petrophysics

It must be kept in mind that all analysis in this paragraph are done on petrophysical core samples. The core sampling is a selective process which is done once to multiple times per meter in consistent and representative layers. Therefore, interpreting the whole core domain from only these samples is uncertain. However, since this is the only data available for a petrophysical analysis, it is used to discriminate between the facies. The same problem accounts for the wireline data, where the regular interval between two measurements is up to 10 cm. Therefore, it must be held in mind that these measurements give a partial representation of the layers, making it complex to interpret the whole domain.

Pelagic association

From the pelagic association, it is seen that both the porosity and permeability of the chalk decreases with an increasing marl content is found in basinal settings as in the Step Graben and the Vlieland Basin, especially focusing on the Maastrichtian and Danian. [Røgen et al. \(2002\)](#) states that with increasing clay content, the specific surface area of both clay and calcite increase, therefore making it more likely for the chalk to recrystallize. Recrystallization coincides with fluid flow, therefore filling of voids and pathways can occur lowering both the porosity and the permeability. Additionally, claystone is known that it can act as a seal rock, with significant low porosities.

The skeletal chalk and homogeneous chalk both follow cannot be petrophysically distinguished in most wells, however some wells find better porosity and permeability for the skeletal chalk facies. An explanation is found in the susceptibility to dissolve skeletal grains as indicated by the thin sections from F17-11, increasing both the porosity and permeability if the fluids can escape. Furthermore, the skeletal chalk was deposited in areas with relative low chalk deposition, therefore the chalk might not have filled the open pore space completely and cementation could not occur due to the absence of overlying chalk. [Mapwood \(1975\)](#) states that the framework of chalk stiffens during early compaction and therefore preservation of these pores is likely.

Some pelagic facies show consistently lower porosity and permeability values than average. These facies are mainly deposited in the vicinity of the Campanian – Maastrichtian biostratigraphy boundary and intermingled with redepositional associated facies. They can fill in gaps and destroy the porosity and permeability of the pelagic association significantly. It is suggested that a certain part of the homogeneous and skeletal chalk is a redeposited facies form and that it has not been recognized as being so in the facies reports, therefore increasing the matrix clay content and lowering the porosity.

Since no clear indications were found for the influence of bioturbation, no direct interpretation can be made. The data presented above suggests that thorough bioturbation is negatively influencing the petrophysical signature of the chalk, however this statement is debatable.

Redepositional association

Even though the porosity is significantly lower than pelagic association, the permeability of the associations stays approximately the same. The core observations from HRL-02 presented in section 4.1.2 gives indications that the permeability of the system is indeed higher than the surrounding chalk. Most of the measurements come from the skeletal chalk debris facies only.

Secondary Alteration association

The main processes creating the secondary alterations include cementation, recrystallization and erosion. Cementation has a direct negative impact on the porosity by filling the available pore space ([Moore, 1989](#)), while the erosional process does not necessarily lower the porosity. Cementation related processes include the formation of flint in the chalk, of which the impact on the core porosity is not directly recognizable since not all of the flint layers are sampled from cores. Some of the flint layers that have been sampled and measured show significant lower porosities. This combined with the oil up to contact in F06-02 suggests that some of the flint layers have a large extent, but also drastic impact on the porosity and permeability of the system. They thus may form local seals and barriers to hydrocarbon migration.

Erosional processes are thought to create conglomeratic products in the chalk ([Kennedy, 1987](#)). In this dataset it is found that the conglomerate show relative low porosity. This is accounted for by the low matrix abundance combined with crystalline and bioclastic grains ([Petrea, 2016](#)). Another accompanied factor is that cementation of the conglomerates can coincide with the erosional processes during periods of non-deposition and a temporary stop of the chalk fabric. Cementation and recrystallization can also occur during these periods ([Scholle et al., 1998](#)). Glauconite and hardground formation are two other facies in this association. Both facies show low to intermediate porosity and

permeabilities. This is most likely dependent on the amount of cementation and/or glauconite grains in the chalk. [Diaz et al. \(2009\)](#) suggests that glauconite formation in sandstones destroys both the permeability and porosity, therefore it is assumed that the effects for chalk are the same.

Siliciclastic association

The siliciclastic association shows both low porosity and permeability. The facies is found in multiple wells in the Dutch Central Graben, but has not yet been found outside of this structural unit. The porosity in these siliciclastics is likely to come from microporosity in the chalk matrix ([Punternvold et al., 2009](#)), since no intercrystalline porosity is found. Low matrix abundance has been found in the thin sections, therefore correlating with a lower porosity. The relationship between point counted matrix abundance and porosity is illustrated in Figure 5.2. The point counting analysis has only been carried out for F17-11 and F17-12. Figure 5.3 presents a thin section of a sandstone in between the chalk. The sandstone consists of a low matrix (M) with multiple bioclasts and crystals of quartz (Q).

Sandy chalk has lower quartz abundance, therefore giving more space for chalk matrix. Microporosity in the matrix is most abundant ([Petrea, 2016](#)), therefore higher matrix abundance provides higher porosity relative to sandstones. The sandy chalk has been found in the Campanian, Maastrichtian and Danian in the F05-04, F14-08 and F17-12 wells. The linear trend in the CaCO_3 and SiO_2 content described in section 4.2.4 indicates that SiO_2 is the most important chalk contaminator in these wells.

5.3 Facies influence on wireline data

5.3.1 Wireline logs

All wireline measurements are not influenced directly by facies since repeated overlap between facies occurs, therefore making it impossible to distinguish between facies and associations based on wireline measurements. This is partly explained by the scaling factor as described in section 5.2 above. Minor facies influence on the wireline measurements are found and listed below. Neural networks were not sufficient to interpret the facies from the logs, which is a conformation that direct facies influence on wireline logs is not available. The exception is the siliciclastic association.

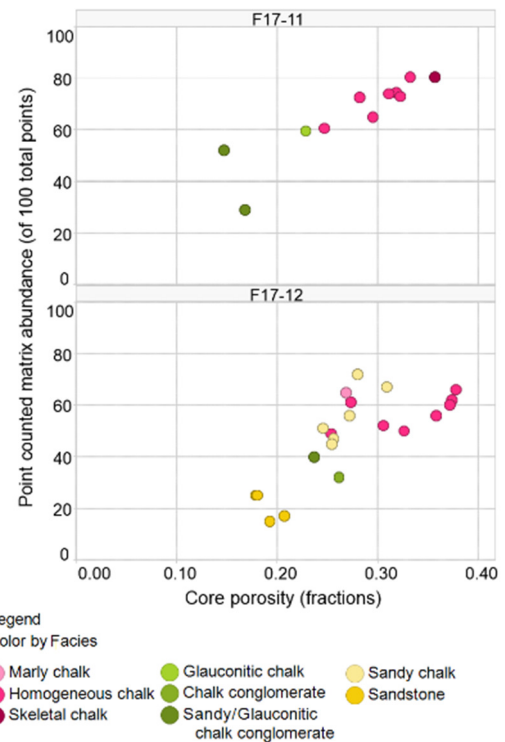


Figure 5.2 - Point counted matrix abundance in relation to the core porosity (fractions).

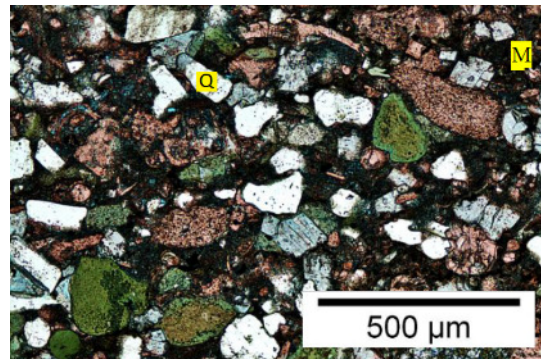


Figure 5.3 - Thin section from well F17-12, plug number: PP 116 and core depth 1439.53 m. Glauconitic rich sandstone with quartz (Q) and micritic matrix (M). From [Petrea, 2016](#).

Bulk density

Influx of detrital material as clay or quartz tend to increase the bulk density gradually where higher amount of detrital material equals higher bulk densities. This process is related to the porosity decrease accompanying this influx. Values found lower than 2.20 gm/cc are highly likely to be from either homogeneous or skeletal chalk. The thickness of the layers in the redepositional and secondary alteration association is also a limiting factor in the bulk density value, where layers of limiting thickness show densities close to the surrounding pelagic chalk. The same relations are found in the matrix density, only closer packed. Some gas bearing wells are found to impact the bulk density negatively, whilst other gas bearing wells do not find this trend.

Compared to the grain densities, only marly chalk reveals deviating values compared to bulk densities. The majority of marly chalk matrix densities are found to be higher than homogeneous or marly chalk, while the grain densities show the opposite. This effect cannot be enhanced by the fact that the porosity of the marly chalk is significantly lower than the other pelagic rocks, since the matrix density is corrected for this effect. High grain density values for argillaceous chalk are confirmed by [Gennaro et al. \(2013b\)](#) in the Danian Ekofisk field. No consistent explanation can be found for the observed difference. Therefore, it is suggested that clay compositions are different for both datasets.

Neutron

Where marl/clay content the neutron values normally increase, it is found that in this dataset, the marly and clay content as well as glauconitic and sand content, decrease the neutron values. Bioclast content tends to increase the neutron value. This is seen in the pelagic association but not in the redepositional association, indicating that detrital material has a higher influence on neutron values than the skeletal content. Most likely the primary and secondary porosity of the skeletal chalk gets filled in by detrital material. Both secondary alteration and siliciclastic association facies are limited to neutron values between 0.20-0.30 API.

Neutron values are not consistent to estimate the porosity, since most of the neutron values are underestimating the porosity. Only the log calculated porosity of the skeletal chalk is overestimated by the neutron. These neutron values are more likely to represent the core porosity. If all the neutron values are compared to the core porosity, the distribution is more alike. Neutron values are only closer packed and do not display both exceptionally low or high values.

Gamma Ray

Clean chalk is expected to reflect low gamma ray values due to the lack of radioactive minerals. Glauconite is a mineral consisting of potassium, therefore it increasing the gamma ray values which is reflected by data above. This is confirmed by the fact that most sandstones and sandy chalks in the chalk primarily consist of glauconite and quartz.

It is expected that marly chalk shows relative higher values of gamma ray (API) than for instance homogeneous chalk, however no significant higher values are found. This might be the consequence of the hemipelagic origin of the clay, lacking radioactive isotopes due to lack of heavy minerals from terrestrial origin.

The influx of detrital material is regulated by the distance to the main land and erosional material influx. It is found that wells closer to the paleo-shoreline have higher gamma ray values than wells in the northern parts of the study area. Furthermore, in the middle of the Dutch Central Graben the chalk was exposed during multiple phases in the Late Cretaceous, coinciding with the inversion phases (e.g. [Japsen, 1998](#)). Therefore, influx of detrital material might have occurred, raising the gamma ray values in the graben itself.

Artificial intelligence

With the neural network toolbox of Interactive Petrophysics and optimization of the input parameters and sensitivity of the toolbox, it can be concluded that the facies could not have been depicted from the wireline logs with the help of this toolbox. This is with the current input and output parameters, whereas different parameters might give better indications.

5.3.2 Porosity calculation

The log porosity shows a relationship with core porosity where $\varphi_{log} = 0.91 \cdot \varphi_{core}$ with a spread in the data covered by an R^2 of 0.57. This is most likely the correction factor where the core porosity must be corrected for the expansion that occurs between reservoir and surface conditions. The data reveals that the bulk density is the best correlated with the log porosity, followed respectively by sonic and neutron. This relationship is for all facies together, where individual facies show different relationships.

Comparing the results of the porosity calculations with the wireline logs, it can be found that the bulk density wireline log is the best estimator for the log calculated porosity, with an overall correlation for all facies of 83%. This is followed by the sonic wireline log with a correlation of 77% and afterwards by the neutron with a correlation of 66%.

Minor deviations in the porosity calculation can occur, in comparison to the measured core porosity. Due to these deviations, the porosity reliability in particular intervals and particular wells is questionable. Geological reasons for interpreting inaccurate porosity are found in possible fractured zones and contaminated chalk measurements with for instance clay. The fracturing and contaminations in the chalk have a direct influence on the neutron, sonic and density log. The influence of clay is found in the deviations in the sonic log of A12-01, where the chalk shows a transition from homogeneous to marly chalk. After the transition, the sonic values seem to stabilize again. Since no abnormal caliper measurements were found and the core does not show significant deviations from surroundings, a measurement tool error is most likely. Facies in the secondary alteration and siliciclastic associations tend to show higher gamma ray values in the dataset, while the clay content is not necessarily higher. Since the porosity calculation uses a clay volume estimation from this gamma ray measurement, the porosity calculation might be underestimated for these particular layers. Other deviations come from measurement tool issues and errors, as for instance in the Franeker well. The wireline logs from this well represents a line shaped tool, where most likely only point measurement where taken and interpolated in between.

5.3.3 Additional discriminators

Depth

Porosity is decreasing with depth as expected by the compaction in the chalk which has a negative impact on the porosity (e.g. [Mallon et al., 2002](#)). However, in some wells this porosity increases with depth, therefore suggesting higher porous facies. If the porosity change in a certain well cannot be explained by facies, it can only be suggested that the changes are the result of fluxes in depositional rates ([Scholle et al., 1998](#)), where higher depositional rate equals higher porosity preservation. Another factor might be that the layers are distorted by bioturbation. The decrease of porosity with depth is best described by the sonic wireline measurement.

Biostratigraphy

The Campanian coincides with a major inversion phase ([van der Voet, 2015](#)) and erosion of these inversion highs, therefore it is likely that in these phases the gamma ray values are higher than those of chalk of other biostratigraphic units. This is confirmed by the data in the wells that reached Campanian. Values of the Early Campanian do not tend to deviate since the inversion phases began in the middle Campanian. During these periods of low to non chalk deposition, cementation, recrystallization and influx of detrital material occurs. These all have influence on well logs as gamma ray, density, neutron and sonic.

Maastrichtian and Danian chalk have better average porosities than all other biostratigraphic units which is expressed on wireline logs with relative low bulk densities, high neutron and high sonic. Due to the consistent deviation of Danian chalk on multiple logs, it is suggested that the chalk of this age is represented by some lithology change in comparison to the older chalk. Multiple authors also show that there are composition variations in the chalk as for instance [Mapstone \(1975\)](#).

Well position

Well position is of minor influence on all the wireline logs in the Chalk. If wells are situated on top of a salt swell or diapir, fracturing of the chalk may occur, therefore enhancing both the porosity and the permeability of the system (e.g. [Price, 1987](#)). This has a direct impact on the sonic, neutron and density measurements. This is however not the case in the dataset presented here. Influx of detrital material during salt movement during deposition of the chalk may result in an increase of gamma ray values.

Regional inversion grade

Regional inversion grade is likely to follow the well position influence on chalk, since upward movement via inversion may cause the same effect as for a salt swell or diapir, therefore enhancing the porosity and permeability due to fracturing. However fracturing due to inversion grade seems less likely than through salt movement since the uplift is not locally focussed and therefore dividing the stress over a larger spatial extent makes fracturing less likely. There is a high uncertainty in the exact determination of this grade since salt movement during times of deposition makes it difficult to separate the effect of inversion or salt movement.

Bioturbation grade

Bioturbation is not of a major influence on the porosity in this well, it is more likely that the facies does have an influence on the porosity of the system and on the bioturbation grade. In most wells, the chalk is thoroughly bioturbated over the whole interval, therefore making it difficult to compare with non-

bioturbated chalk. Non-bioturbated chalk also coincides with periods of non-chalk deposition as for instance in the Campanian, giving it an even more biased picture of the influence of bioturbation.

5.4 Sonic wireline trends

The velocity trend depicted from seismic wireline measurements, is influenced by several parameters; depth, facies and biostratigraphic unit. A general depth trend is found, being the main parameters influencing the sonic wireline log, although several deviations from this trend can be found. It must be noted that all wells have their individual depth trend and that the presented formulas are averaged over all wells.

While the majority of pelagic and redepositional association sonic measurements focus around 90-100 $\mu\text{s}/\text{ft}$, it is found that both the secondary alteration and siliciclastics focus on the lower end, caused by lower porosity. The decrease of the sonic is expected with processes as cementation or recrystallization, lowering the porosity and therefore lowering the sonic. Detrital input is also found to have consistent lower sonic measurements, therefore indicating that these products have less porosity than the pelagic facies.

The sonic measurements of Danian chalk seem to focus on the high side, where all other biostratigraphic units are following the trend. If the Danian values, above also presented as Ekofisk Formation, are filtered from the data, combined with the spatial outlier K13-A-10 and A12-02, the following relationship can be applied: $DT = 161.23 + (-0.05 \cdot TVDSS)$ with an R^2 of 0.76 without regarding any facies. For the homogeneous and marly chalk, this correlation with depth is even higher, therefore indicating that if only these two facies are present, the velocity-depth relationship can be determined with good accuracy.

The Danian chalk itself does not show a specific depth trend and stays more or less constant throughout depth, around an average of 92.8 $\mu\text{s}/\text{ft}$. Individual facies influence on the sonic in the Danian can be found, where marly chalk show consistent lower sonic values than homogeneous and skeletal chalk. Values for secondary alteration and siliciclastic influx are also generally lower than the values for pelagic chalk. The same patterns are observed for all other data, where the influx of marly content in the system generally lowers the sonic measurements even more. The lower sonic travel time of clay contaminated sandstones is described by [Han et al. \(1986\)](#), which is also confirmed for the chalk here.

6. Conclusion

Homogeneous chalk exhibits a broad range of porosities of which the majority is found in the 30-35% core porosity and 25-30% log porosity ranges. Bioclast content has a positive influence on porosity with depth. Marl content tends to decrease the porosity of the system, as for glauconite and siliclastic content. The marly chalk is found in great quantities in the Step Graben, Vlieland Basin, Elbow Spit, and Texel-IJsselmeer High. Homogeneous and skeletal chalk illustrates a large porosity value variance. The highest porosities are situated in Danian and Maastrichtian chalk, while the older biostratigraphic units have lower porosities. The permeability of the homogeneous chalk is found to be relatively medium too high on the flank and on top of the salt diapir in Danian and Late Maastrichtian homogeneous chalk. Skeletal chalk, if not redeposited, has a positive influence on the reservoir properties and is found mainly in the Dutch Central Graben. Danian measurements for porosity and sonic are generally higher than other biostratigraphic units. Together with observations by other authors, it is thought that Danian chalk acts different than the older chalk. Most processes which create secondary alteration or siliclastic association are found to be porosity decreasing, with a main focus of cementation in for instance sandstones and conglomerates.

A decrease in porosity is found with increasing depth. Wells on top of salt structures are found to have higher porosity, however this trend is partly overprinted by the facies. The same accounts for the regional inversion grade influence on porosity. Bioturbation grade itself was found to have a minor influence on the porosity.

Facies influence on wireline logs is limited due to the wide spatial distribution of the cores and the overlap between different facies. The density, neutron and sonic measurements are mainly influencing the calculated porosity of the chalk. The porosity, as described above is mainly related to facies. Where low bulk density, high neutron and high sonic equal high porosity and high bulk density, low neutron and low sonic equal low porosity. Core calculated porosity was found to be 91% of the chalk core porosity, for all facies. Only wireline log which have less impact on the gamma ray values is the gamma ray log, which is overshadowed by multiple well calibration issues. If these measurements are taken as correct, the marly chalk cannot be distinguished base on only this log even though clay minerals are present. Only notable gamma ray influences come from detrital influx into the chalk; e.g. redepositional and siliclastic association.

Depth trends on sonic velocities are found to be influenced by depth, facies and biostratigraphic age. The Ekofisk formation, of Danian age, shows a constant value throughout depth; average 92.8 $\mu\text{s}/\text{ft}$. Another outlier is K13-A-10, being significantly shallower than other wells and A12-02 Maastrichtian values. If these are filtered, the chalk consisting of all facies shows a depth trend where $V_{sonic} = 307.38 + (2.22 \cdot TVDSS)$ with a correlation coefficient of 0.80. Marly chalk and homogeneous chalk are the two facies that can be best predicted while all other facies tend to have lower correlation coefficients. These two facies are also believed to make up the most significant amount of undisturbed chalk, where most of these cores are focused on disturbed chalk by salt movement or inversion during or after deposition.

Recommendations

- Coring of parts of the chalk interval where the chalk is not influenced by salt tectonics or inversion to provide a better understanding of the undisturbed behaviour of the chalk.
- Include core and field observations from other countries in the model to better understand the physical behaviour of the chalk.
- Biostratigraphy of wells that drill through the chalk, but do not have chalk as a primary objective, might contribute to giving more insight into the distribution of the biostratigraphic units and their influence on wireline logs.
- Neural network predictability of different formations or biostratigraphic units may be possible with more input parameters.
- Look at a combination of several wireline logs in order to depict facies and not at these parameters individually.
- Sonic velocity prediction is kept to a basis in this thesis, therefore it can be used as input for several other studies on the chalk as for instance calculating the V_0k function of several intervals.

7. Acknowledgement

I would like to thank EBN for enabling me to participate in and contribute to the Chalk study and giving me insight in a typical E&P company environment. In particular, I thank my daily supervisor Nora Heijnen for helping me with different aspects of the study, giving new insights in petroleum geology and for the extensive discussions that helped forming the end product. Other EBN employees that helped forming my final thesis are Jan Lutgert, Eveline Roosendaal, Abdul Hamid, Guido Hoetz and Maarten Jan Brolsma. I would also like to thank my fellow student interns for their criticism, advice on different aspects of the study as well as the pleasant work atmosphere.

From the VU Amsterdam I would like to thank my supervisor John Reijmer and my second supervisor Bernd Andeweg, John for all the interim discussions, geological input and final feedback on the thesis and presentations and Bernd with the assessment of the thesis.

At last I want to thank Jurgis Klaudius and Senergy for providing me with a student license of the program Interactive Petrophysics during my internship.

8. References

- Anderskov, K., & Surlyk, F. (2011). Upper Cretaceous chalk facies and depositional history recorded in the Mona-1 core, Mona Ridge, Danish North Sea. *Geological Survey of Denmark and Greenland Bulletin*, vol. 25, pp. 3-60.
- Archie, G. E. (1952). Classification of carbonate reservoir rocks and petrophysical considerations: *AAPG Bulletin*, vol. 36 (2), pp. 218–298.
- Bailey, H. W., Gale, A. S., Mortimore, R. N., Swiecicki, A. & Wood, C. J. (1984). Biostratigraphical criteria for the recognition of the Coniacian to Maastrichtian stage boundaries in the Chalk of north-west Europe, with particular reference to southern England. *Bulletin of the Geological Society of Denmark*, vol. 33 (1), pp. 31-39.
- Bohonak, J.A. (2004). RMA: Software for Reduced Major Axis regression v. 1.17. Retrieved from <http://www.bio.sdsu.edu/pub/andy/RMA.html>
- Bramwell, N. P., Caillet, G., Meciani, L., Judge, N., Green, M., & Adam, P. (1999). Chalk exploration, the search for a subtle trap. *Geological Society, London, Petroleum Geology Conference series*, vol. 5, pp. 911-937.
- Biondi, P. (1998), Sedimentology of Well F06-02, Block F6, the Netherlands Offshore. Sedimentary Geology Department, Elf EP, 92078- Paris La Défense Cedex. (Confidential).
- Brasher, J. E., & Vagle, K. R. (1996). Influence of lithofacies and diagenesis on Norwegian North Sea chalk reservoirs. *AAPG bulletin*, vol. 80 (5), pp. 746-768.
- Caldeira, K., & Rampino, M. R. (1991). The Mid-Cretaceous Super Plume, carbon dioxide, and global warming. *Geophysical Research Letters*, vol. 18 (6), pp. 987-990.
- Diaz, E., Prasad, M., Mavko, G., & Dvorkin, J. (2003). Effect of glauconite on the elastic properties, porosity, and permeability of reservoir rocks. *The Leading Edge*, vol. 22 (1), pp. 42-45.
- Downing, R.A., Price, M. & Jones, G.P. (eds.). *The Hydrogeology of the Chalk of North-West Europe*, Clarendon Press. pp. 14–35.
- Eberhart-Phillips, D., Han, D. H., & Zoback, M. D. (1989). Empirical relationships among seismic velocity, effective pressure, porosity, and clay content in sandstone. *Geophysics*, vol. 54 (1), pp. 82-89.
- Gennaro, M., Wonham, J. P., Gawthorpe, R., & Sælen, G. (2013a). Seismic stratigraphy of the Chalk Group in the Norwegian Central Graben, North Sea. *Marine and Petroleum Geology*, vol. 45, pp. 236-266.
- Gennaro, M., Wonham, J. P., Sælen, G., Walgenwitz, F., Caline, B., & Faÿ-Gomord, O. (2013b). Characterization of dense zones within the Danian chalks of the Ekofisk Field, Norwegian North Sea. *Petroleum Geoscience*, vol. 19 (1), pp. 39-64.

- Hancock, J. M. (1993). Sea-level changes around the Cenomanian-Turonian boundary. *Cretaceous Research*, vol. 14 (4), pp. 553-562.
- Hallam, A., & Sellwood, B. W. (1976). Middle Mesozoic sedimentation in relation to tectonics in the British area. *The journal of Geology*, pp. 301-321.
- Hays, J. D., & Pitman, W. C. (1973). Lithospheric plate motion, sea level changes and climatic and ecological consequences. *Nature*, vol. 246 (5427), pp. 18-22.
- Ineson J.R., Bjerager, M., Kristensen, L. (2014). Upper Cretaceous – Danian chalk of the Netherlands subsurface. Geological Survey of Denmark and Greenland internal report. (Confidential).
- Jager, J. de (2007). Geological development. *Geology of the Netherlands*, pp. 5-26.
- Japsen, P. (1998). Regional velocity-depth anomalies, North Sea Chalk: a record of overpressure and Neogene uplift and erosion. *AAPG bulletin*, vol. 82 (11), pp. 2031-2074.
- Kennedy, W. J. (1987). Late Cretaceous and Early Palaeocene Chalk Group Sedimentation in the Greater Ekofisk Area, North Sea Central Graben. *Bulletin Des Centres de Recherches Exploration-Production Elf-Aquitaine* vol. 11 (1).
- Kombrink, H., Doornenbal, J. C., Duin, E. J. T., Den Dulk, M., ten Veen, J. H., & Witmans, N. (2012). New insights into the geological structure of the Netherlands; results of a detailed mapping project. *Netherlands Journal of Geosciences*, vol. 91 (4), pp. 419-446.
- Lutgert, J. (2016). [RMA Regression Excel calculation workbook].
- Maliva, R. G., & Siever, R. (1989). Nodular chert formation in carbonate rocks. *The Journal of Geology*, pp. 421-433.
- Mallon, A. J., & Swarbrick, R. E. (2002). A compaction trend for non-reservoir North Sea Chalk. *Marine and Petroleum Geology*, vol. 19 (5), pp. 527-539.
- Mapstone, N. B. (1975). Diagenetic history of a North Sea chalk. *Sedimentology*, vol. 22(4), pp. 601-614.
- Mitchell, S. F. (1995). Lithostratigraphy and biostratigraphy of the Hunstanton Formation (Red Chalk, Cretaceous) succession at Speeton, North Yorkshire, England. *Proceedings of the Yorkshire Geological and Polytechnic Society*, vol. 50 (4), pp. 285-303.
- Molen, A. S. V. D. (2004). Sedimentary development, seismic stratigraphy and burial compaction of the Chalk Group in the Netherlands North Sea area. PhD. thesis, Utrecht University.
- Moore, C. H., 1989, *Carbonate Diagenesis and Porosity*: Amsterdam, Elsevier, 338 p.
- Paasche, E. (2001). A review of the coccolithophorid *Emiliania huxleyi* (Prymnesiophyceae), with particular reference to growth, coccolith formation, and calcification-photosynthesis interactions. *Phycologia*, vol. 40 (6), pp. 503-529.

-
- Petrea, C.C. (2015). Sedimentology, fracture description, petrography and reservoir quality of cored interval in Well F17-11, Dutch offshore. Panterra and Wintershall. (Confidential).
- Petrea, C.C. (2016). Fracture Description, Sedimentology, Petrography and Reservoir Quality of cores 1 to 12 (Chalk Group) in Well F17-12, Dutch offshore. Panterra and Wintershall. (Confidential).
- Price, M. (1987). Fluid flow in the Chalk of England. Geological Society, London, Special Publications, vol. 34 (1), pp. 141-156.
- Punternold, T., Strand, S., & Austad, T. (2009). Coinjection of seawater and produced water to improve oil recovery from fractured North Sea chalk oil reservoirs. *Energy & fuels*, vol. 23 (5), pp. 2527-2536.
- Raymer, L. L., Hunt, E. R., & Gardner, J. S. (1980). An improved sonic transit time-to-porosity transform. 1980 Annual Logging Symposium, Society of Petrophysicists and Well-Log Analysts, pp. 1–12.
- Røgen, B., & Fabricius, I. L. (2002). Influence of clay and silica on permeability and capillary entry pressure of chalk reservoirs in the North Sea. *Petroleum Geoscience*, vol. 8(3), pp. 287-293.
- Rohatgi, A. (2015). WebPlotDigitizer. Retrieved from <http://arohatgi.info/WebPlotDigitizer>.
- Schlanger, S. O., Arthur, M. A., Jenkyns, H. C., & Scholle, P. A. (1987). The Cenomanian-Turonian Oceanic Anoxic Event, I. Stratigraphy and distribution of organic carbon-rich beds and the marine $\delta^{13}C$ excursion. Geological Society, London, Special Publications, vol. 26 (1), pp. 371-399.
- Schlumberger (2009). Log interpretation charts. Texas, United States: Schlumberger.
- Scholle, P. A., Albrechtsen, T., & Tirsgaard, H. (1998). Formation and diagenesis of bedding cycles in uppermost Cretaceous chalks of the Dan Field, Danish North Sea. *Sedimentology*, vol. 45 (2), pp. 223-243.
- Van Adrichem Boogaert, H. A., & Kouwe, W. F. P. (1994). Stratigraphic nomenclature: section H–Upper Cretaceous and Danian (Chalk Group). *Mededelingen Rijks Geologische Dienst*, pp. 50.
- Van der Voet, E. (2015). Geological evolution of the Chalk Group in the northern Dutch North Sea. VU University Amsterdam and EBN B.V., Utrecht, Netherlands.

Appendix I

Core measurement overview and the minima, averages and maxima of these measurements sorted per well.

Used abbreviations: PHI: porosity, K_h: horizontal permeability, K_v: vertical permeability, RHO: density, Comp.: composition analysis, PC: point counting, Biot.: bioturbation and Biostr.: biostratigraphy. Cells filled with a number are representative of number of measurements per well and cells marked with an X are available curves while empty boxes are absent curves.

Well	PHI	K_h	K_v	RHO	Comp.	PC	Facies	Biot.	Biostr.
A12-01	77	77					X	X	X
A12-02	149	78		149			X	X	X
A18-02-S1	72	12		72			X	X	X
B13-01	8	7		8			X	X	X
B13-02	7			7			X		X
B17-02							X	X	X
B17-03							X		X
E18-07							X		X
F02-A-03	5	4		5			X	X	X
F02-03							X	X	X
F02-05	44	44			X		X	X	X
F02-06	57	56		57			X	X	X
F03-03	23	11		23			X	X	X
F05-04	42	42		42			X	X	X
F06-02	44	30	5	40			X	X	X
F09-01	31		15				X	X	X
F09-02	18	17	14	18			X	X	X
F14-08	3	3			X	X	X		X
F17-10	15	8	8	15			X	X	X
F17-11	80	79		80	X	X	X	X	X
F17-12	258	248	49	283	X	X	X	X	X
K13-A-10	8	2	1	8			X	X	X
L01-02	2	1	1	2			X	X	X
L02-03							X		X
FRA-01-S1	110	110					X	X	X
BRG-01							X	X	X
Total	1053	829	93	809					

Porosity distribution in the associations and facies. φ Symbol used for porosity.

Association	Facies	Min. φ (.fr)	Avg. φ (.fr)	Max. φ (.fr)	# measurements
Pelagic		0.09	0.28	0.43	738
	Marly chalk	0.09	0.24	0.37	261
	Homogeneous chalk	0.13	0.30	0.43	388
	Skeletal chalk	0.14	0.29	0.37	89
Redepositional		0.14	0.23	0.38	48
	Laminated chalk	0.28	0.28	0.29	2
	Skeletal chalk (debris)	0.14	0.23	0.38	46
	Shear deformed chalk	-	-	-	0
Secondary Alteration		0.00	0.23	0.33	60
	Flint layers/nodules	0.00	0.23	0.33	36
	Hardground	0.22	0.25	0.27	2
	Glauconitic chalk	0.22	0.26	0.32	8
	Chalk conglomerate	0.12	0.22	0.28	5
	Sandy/glauconitic ck. conglo.	0.15	0.20	0.30	9
Siliciclastic		0.13	0.23	0.34	134
	Sandy Chalk	0.23	0.28	0.34	39
	Sandstone	0.13	0.19	0.22	65

Permeability distribution in the associations and facies. κ Symbol used for permeability.

Association	Facies	Min. κ (mD)	Avg. κ (mD)	Max. κ (mD)	# measurements
Pelagic		0.05	2.35	42.76	586
	Marly chalk	0.06	0.98	9.96	192
	Homogeneous chalk	0.05	2.73	42.76	317
	Skeletal chalk	0.06	4.18	32.83	77
Redepositional		0.07	1.36	5.92	23
	Laminated chalk	1.41	1.41	1.41	1
	Skeletal chalk (debris)	0.07	1.36	5.92	22
	Shear deformed chalk	-	-	-	0
Secondary Alteration		0.10	1.93	16.49	38
	Flint layers/nodules	0.18	2.67	16.49	15
	Hardground	1.00	1.77	2.53	2
	Glauconitic chalk	0.36	1.98	5.73	8
	Chalk conglomerate	0.10	0.73	1.39	5
	Sandy/glauconitic ck. conglo.	0.15	1.28	3.25	8
Siliciclastic		0.08	0.83	9.13	103
	Sandy Chalk	0.11	1.48	9.13	38
	Sandstone	0.08	0.45	4.21	65

Grain density distribution in the associations and facies. ρ Symbol used for densities.

Association	Facies	Min. ρ (gm/cc)	Avg. ρ (gm/cc)	Max. ρ (gm/cc)	# meas- urments
Pelagic		2.56	2.70	2.83	541
	Marly chalk	2.56	2.68	2.78	125
	Homogeneous chalk	2.65	2.71	2.80	332
	Skeletal chalk	2.64	2.70	2.83	84
Redepositional		2.62	2.68	2.77	39
	Laminated chalk	2.72	2.72	2.72	1
	Skeletal chalk (debris)	2.62	2.68	2.77	38
	Shear deformed chalk	-	-	-	0
Secondary Alteration		2.54	2.70	2.90	52
	Flint layers/nodules	2.54	2.68	2.76	31
	Hardground	2.70	2.70	2.70	1
	Glaucconitic chalk	2.70	2.71	2.73	6
	Chalk conglomerate	2.70	2.72	2.75	6
	Sandy/glaucconitic ck. conglo.	2.70	2.79	2.90	8
Siliciclastic		2.68	2.73	2.90	103
	Sandy Chalk	2.68	2.72	2.73	37
	Sandstone	2.69	2.73	2.90	66

Appendix II

Overview of all the well log data available, sorted per well. These measurements are used in section 4.2.4.

Well	GR	DT	RHOB	NPHI	BS	CAL	RESS	RESM	RESD
A12-01	X	X	½	X	X	X	X		X
A12-02	X	X	X	X	X	X	X		X
A18-02-S1	X	X	X	X	X	X	X		X
B13-01	X	X			X	X	X	X	X
B13-02	X	X	X	X	X	X	X		X
B17-02	X	X	X	X	X	X	X		X
B17-03	X	X	X	X	X	X	X		X
E18-07	X	X			X	X			
F02-A-03	X		X	X	X				
F02-03	X	X	X	X					
F02-05	X	X	X	X	X	X	X		X
F02-06	X	X	X	X	X	X	X		X
F03-03	X	X	X		X	X	X		X
F05-04	X	X	X	X	X	X	X	X	X
F06-02	X	X	X	X	X	X	X		X
F09-01	X	X	X	X	X	X	X		X
F09-02	X	X	X	X	X	X	X		X
F14-08	X		X		X		X	X	X
F17-10	X	X	X	X	X	X	X	X	X
F17-11	X	X	X	X	X	X	X	X	X
F17-12	X	X	X	X	X	X	X	X	X
K13-A-10	X	X	X		X				X
L01-02	X	X	X	X	X	X			X
L02-03	X	X	X	X	X	X			X
FRA-01-S1	X	X	X	X	X	X	X		X
BRG-01	X	X		X			X		

Used abbreviations are: GR: gamma ray, DT: sonic, RHOB: bulk density, NPHI: neutron, BS: bitsize, CAL: caliper, RESS: shallow resistivity, RESM: medium resistivity and RESD: deep resistivity. Boxes marked with an X are available curves while empty boxes are absent curves.

Appendix III

Wireline porosity calculations input model settings. Individual input parameters are discussed in section 3.3.

Well	Vclay method	Phi/S _w method	Remarks
A12-01	Gamma Ray	Neutron Sonic	Neutron Density Phi calculation in upper half Danian.
A12-02	Gamma Ray	Neutron Density	Unclear boundary Danian-Maastrichtian.
A18-02-S1	Gamma Ray	Neutron Density	
B13-01	Gamma Ray	Sonic	
B13-02	Gamma Ray	Neutron Density	
B17-02	Gamma Ray	Sonic	Neutron Density Phi calculation in Danian. No core data.
B17-03	Gamma Ray	Neutron Density	
E18-07	Gamma Ray ½	Sonic	Half gamma ray available.
F02-A-03	Gamma Ray	Neutron Density	
F02-03	Gamma Ray	Neutron Density	Neutron and density stop in Campanian.
F02-05	Gamma Ray	Density	
F02-06	Gamma Ray	Neutron Density	
F03-03	Gamma Ray	Density	
F05-04	Gamma Ray	Neutron Density	
F06-02	Gamma Ray	Neutron Density	
F09-01	Gamma Ray	Neutron Density	
F09-02	Gamma Ray	Neutron Density	
F14-08	Gamma Ray	Density	
F17-10	Gamma Ray	Neutron Density	
F17-11	Gamma Ray	Neutron Density	
F17-12	Gamma Ray	Neutron Density	
K13-A-10	Gamma Ray	Sonic	Sonic better suited for porosity prediction.
L01-02	Gamma Ray	Neutron Density	
L02-03	Gamma Ray	Density	
FRA-01-S1	Gamma Ray	Sonic	
BRG-01	Gamma Ray	Neutron Sonic	Logs were digitalized with software (Rohatgi, 2015).

Appendix IV

Core depth shift in meters, applied to each individual core in Interactive Petrophysics.

<i>Well</i>	<i>Interval top</i>	<i>Interval bottom</i>	<i>Core depth Shift</i>	<i>Remarks</i>
A12-01	2055.10	2108.80	+ 0.15	
A12-02	2006.00	2033.20	- 0.35	
	2033.50	2052.00	+ 2.10	
A18-02-S1	1874.10	1889.10	+ 2.50	
	1943.00	1950.70	- 4.57	
B13-01	-	-	-	No depth shift needed.
B13-02	-	-	-	No depth shift needed.
B17-02	-	-	-	No core data available.
B17-03	-	-	-	No core data available.
E18-07	-	-	-	No core data available.
F02-A-03	-	-	-	No depth shift needed.
	-	-	-	No depth shift needed.
F02-03	-	-	-	No core data available.
F02-05	-	-	-	No depth shift needed.
	1454.00	1459.00	- 1.68	
F02-06	-	-	-	No depth shift needed.
	1500.00	1503.05	+ 1.89	
	1530.20	1532.20	- 0.64	
F03-03	-	-	-	
	1656.00	1661.70	- 3.84	
F05-04	-	-	-	No depth shift needed.
	1350.00	1361.90	+ 0.73	
F06-02	1447.00	1464.40	+ 1.22	
	1480.00	1482.90	+ 1.71	
F09-01	1310.70	1315.74	-	Fragmented and sidewall samples.
	1435.00	1439.80	-	Fragmented and sidewall samples.
F09-02	1603.00	1612.00	+ 1.22	
F14-08	-	-	-	Not enough core data available.
F17-10	1378.00	1380.70	+ 0.15	
	1383.00	1383.60	- 0.56	
	1386.00	1388.15	- 1.45	
F17-11	1419	1445.29	+ 0.66	
	1457.00	1469.90	+ 0.34	
F17-12	-	-	-	No depth shift needed.
K13-A-10	-	-	-	No depth shift needed.
L01-02	-	-	-	No depth shift needed.
L02-03	-	-	-	No core data available.
FRA-01-S1	1038.00	1065.00	- 0.61	
	1065.00	1074.00	- 3.16	
BRG-01	-	-	-	No core data available.

Appendix V

Input wells, curve to predict and input curves for the neural network toolbox in IP.

Well	Curve to predict	Input curve 1	Input curve 2	Input curve 3	Used for training
A12-01	Facies (Limestones only, see section 4.3.5).	Neutron wireline log	Bulk density wireline log	Sonic wireline log	
A12-02					X
A18-02-S1					X
F02-03					
F02-06					
F05-04					X
F06-02					X
F17-10					
F17-11					X
F17-12					X

Appendix VI

IP overview of porosity calculations in comparison to wireline logs, facies and biostratigraphy zonation and core data. The data is raw and thus not corrected for core depth shift.

